Development and Applications of Foam-Based ELISA: An Innovation in Biosensing Platform

By

BOFENG PAN

DISSERTATION

Submitted in partial satisfaction of the requirements for the degree of

DOCTOR OF PHILOSOPHY

in

Agricultural and Environmental Chemistry

in the

OFFICE OF GRADUATE STUDIES

of the

UNIVERSITY OF CALIFORNIA

DAVIS

Approved

_____

Gang Sun, Chair

_____

Kit S. Lam

_____

Dean J. Tantillo

Committee in Charge

2024

Acknowledgments for the Use of Copyrighted Materials

This dissertation includes material extracted from the following published materials.

1) Pan, B., Zhao, C., Norwood, M., Wang, M., Liu, G., & Sun, G. (2023). Highly Sensitive Naked Eye Detectable Colorimetric Biosensors Made from Macroporous Framework Melamine Foams for Onsite and Simultaneous Detection of Multiple Environmental Hazards in Flowing Through Sensing Systems. *Advanced Sensor Research*, *3*(1), 2300080.

2) Pan, B., El-Moghazy, A. Y., Norwood, M., Nitin Nitin, & Sun, G. (2024). Rapid and Ultrasensitive Colorimetric Biosensors for Onsite Detection of *Escherichia coli* O157:H7 in Fluids. *ACS Sensors*, *9*(2), 912–922.

3) Pan, B., He, Q., Yu, X., De Choch, D., Lam, K. S., Hammock, B. D., & Sun, G. (2024). Versatility and Stability of Melamine Foam Based Biosensors (f-ELISA) Using Antibodies, Nanobodies, and Peptides as Sensing Probes. *Talanta*, *279*, 126634–126634.

These published contents have been slightly modified and reproduced here with the permission of the copyright holders.

ACKNOWLEDGMENTS

I would like to express my deepest gratitude to my advisor, Dr. Gang Sun, for his invaluable guidance, patience, and support throughout my research journey. Dr. Sun has been a mentor to me since my senior year as an undergraduate, playing a crucial role in helping me complete my undergraduate thesis, earn my master's degree, and navigate the challenges of this dissertation. His expertise, insightful feedback, and steadfast belief in my abilities allowed me to shape the direction and ensure the success of my research. During times of difficulty and struggle, Dr. Sun has always been there to provide guidance, help me persevere, and foster my academic growth. I am truly fortunate to have the opportunity to work under his exceptional mentorship, which has a profound impact on my academic and personal development.

I am also immensely thankful to my QE committee members, Prof. Kit Lam, Prof. Dean Tantillo, Prof. Ning Pan, Prof. Peter Green, and Prof. Charlie Li, whose expertise and thoughtful critiques have significantly contributed to the refinement of this work. Their suggestions and rigorous review were essential in enhancing the quality and impact of my research. I would like to extend special thanks to Prof. Dean Tantillo and Prof. Kit Lam for their dedicated service as members of my dissertation committee.

I am deeply grateful to my lab mates in Dr. Gang Sun's group, who have provided invaluable support, friendship, and a collaborative spirit that greatly enriched my research experience. Peixin Tang and Zheng Zhang offered numerous constructive

suggestions on organic and polymer chemistry, while Yue Ma, Jiahan Zou, and Noha Amaly Mohammed Hassan Abdelbaky helped me better understand the protocols of various experiments and assays. I would also like to express my gratitude to Cunyi Zhao and Yang Si, who encouraged me to embark on this academic journey. Building on their extensive expertise, I was able to pursue my research and investigation in the biosensor field. Furthermore, I am deeply appreciative of the significant assistance provided by Makela Norwood and Dylan De Choch, whose insightful ideas and contributions to my work were invaluable. Without their efforts, I would have struggled to complete this dissertation with such efficiency and quality.

My sincere gratitude extends to all my collaborators, without whom this work would not have been possible. I would like to express my sincere appreciation to Dr. Xingjian Yu and the other lab members from Dr. Lam's group, Ms. Minyuan Wang from Dr. Liu's Lab, and Dr. Ahmed El-Moghazy from Dr. Nitin's group, and Dr. Qiyi He from Dr. Hammock group for their invaluable expertise, support, and contributions throughout our collaborative projects. Their insights, dedication, and willingness to help have greatly contributed to the success of our shared research endeavors and have enriched my work.

Besides, I would like to acknowledge the Graduate Studies and Agricultural and Environmental Chemistry Graduate Group at the University of California, Davis, for providing me with a graduate admission fellowship and the Jastro Shields Research Award. These financial support opportunities have been essential in enabling me to

pursue my doctoral studies and dedicate myself fully to my research endeavors. Furthermore, I am sincerely grateful for the financial support received from the National Institute of Environmental Health Sciences, which has been crucial in funding my research.

Lastly, I would like to express my deepest gratitude to my family and friends for their steadfast support and encouragement throughout my academic pursuits over the past few years. I am particularly thankful to Dr. Haoqian Miao, Dr. Huitao Ling, Dr. Zheng Zhang, and Dr. Yichen Li, whose companionship and shared moments of joy have added so much color to my life and helped me persevere through challenging times in Davis. I am especially grateful to my mother, Gao Jing, my father, Jingsheng Pan, my grandmother, Huiying Fan, and my grandfather, Jinjun Pan, whose constant encouragement and unconditional love have been the pillars of my resilience and success. I would also like to extend a special thank you to my fiancée, Xuying Liu, whose unwavering support, understanding, and companionship have been invaluable to me throughout this journey. The love, care, and support from my family and loved ones have been the driving force behind my perseverance and dedication to my research, and I am forever indebted to them for their selfless sacrifices and for always believing in me.

Development and Applications of Foam-Based ELISA: An Innovation in Biosensing Platform

ABSTRACT

Enzyme-linked Immunosorbent Assay (ELISA) serves as a fundamental tool for the selective and sensitive detection of various analytes, including antibodies, pesticides, antibiotics, proteins, and pathogens, playing a crucial role in biomedical diagnosis, chemical quality control, and the detection of hazardous chemicals in foods and environments. Despite its widespread use, conventional ELISA faces limitations such as high costs, limited scalability and flexibility for personal use, challenges in simultaneously examining multi-target chemicals at low concentrations, and reliance on specialized instrumentation and trained personnel. In response to these challenges, paper-based ELISA (p-ELISA) emerged as an alternative, using fibrous and microporous platforms to offer increased surface area, reduced cost, and ease of use. However, the inherent heterogeneous structure of paper and fibrous membranes, particularly in the vertical direction, impedes the penetration of large biomolecules, leading to less biomolecule incorporation and, consequently, reduced sensitivity and inhomogeneous colorimetric signals. Addressing these deficiencies, this dissertation introduces a novel biosensing platform based on chemically modified melamine foam (MF) with a three-dimensional (3D) reticulated macroporous structure. Our study has proven that this foam-based ELISA (f-ELISA) platform to be rapid, sensitive, additive, and volume-responsive, showcasing its versatility across various ELISA

methodologies, including direct, competitive, and sandwich ELISA. Moreover, the platform's adaptability to varied ligands, such as antibodies, nanobodies, and peptides, alongside its capability to accurately detect a wide range of targets, including biomarkers, antibiotics, environmental toxicants, pathogens, etc., underscores a substantial improvement upon conventional and paper-based ELISA techniques.

Specifically, Chapter 1 summarizes the background information on current detection techniques and applications of melamine foam in varied fields. In Chapter 2, a novel, highly sensitive, naked-eye detectable colorimetric biosensor was developed based on chemically modified melamine foam (MF). This platform is designed for the rapid, on-site detection of various environmental hazards and toxicants in fluid systems. Using the unique three-dimensional reticulated macroporous structure of MF, this platform enables the fast and efficient transfer of biomolecules, ensuring enhanced sensitivity and broad applicability across multiple detection methods, including direct, competitive, and sandwich ELISA. This advancement of f-ELISA technology demonstrates significant improvements over traditional and paper-based ELISA methods, offering an alternative solution for environmental monitoring and potential healthcare applications.

In Chapter 3, the application of f-ELISA in the detection of bacterial cells could further demonstrate the advantages of the macroporous features offered by the chemically modified MF as mentioned in Chapter 2. In essence, this study paves the way for a rapid, sensitive, and volume-flexible biosensing platform, using *E. coli*

O157:H7 as a proof of concept, which holds promise for the rapid and ultrasensitive detection of various pathogenic bacteria in real-world applications.

In Chapter 4, the study elaborates on refining the foam-based ELISA (f-ELISA) platform developed in Chapter 2 and Chapter 3, showcasing its expanded versatility and efficacy for onsite detection applications. Through different chemical modifications to melamine foam, the research developed a macroporous 3D substrate that effectively binds various ligands, including antibodies, nanobodies, and peptides. This study highlights the platform's adaptability, affordability, and user-friendly design, making it a versatile and effective tool in diagnostics, offering broader applications, and improving detection processes in various fields. Lastly, Chapter 5 summarizes the invention of the f-ELISA system and its applications under different scenarios.

List of Figures

Scheme 2.1. Mechanism of NHS@MF based (a) direct ELISA, (b) sandwich ELISA, and (c) competitive ELISA.

Figure 2.4. Optical images and the calibration curve of membranes in the detection of SARS-CoV-2 spike protein RBD using (a) direct ELISA approach and (b) Sandwich ELISA. (c) optical image and the calibration curve of membranes treated by varied concentrations of CAP using a competitive ELISA approach. All data are presented as mean ± SD, with n = 3 independent experiments.

Figure 2.5. Effect of the sample volume in color signal intensities of (a) direct ELISA, (b) Sandwich ELISA, and (c) Competitive ELISA. All data are presented as mean ± SD, with n = 3 independent experiments.

Figure 2.6. (a) Schematic illustration of the mechanism of simultaneous multiple on-site targets detection. (b) Photograph demonstrated the fast-flow device driven by a syringe pump. (c) Optical image and ΔRGB values of membranes treated by the mixture of varied concentrations of CAP and CPS using a competitive ELISA approach. All data are presented as mean ± SD, with n = 3 independent experiments.

Figure S2.1. Chemical structure of melamine foam and SEM-EDS results

S5. Calibration curves of FITC-dextran, HIgG, NHS group, and an antibody conjugated with fluor Alexa 647.

Figure S2.2. Calibration curves for (a) HIgG, (b) FITC-dextran, (c) NHS, and (d) an antibody conjugated with Alexa 647.

Figure S2.3. Immobilized antibody amounts on NHS@MF, NHS@NF, and nitrocellulose paper (NP) from 1 mg/L of 100 μL of antibody solution. Data are

presented as mean ± SD, with n = 3 independent experiments. *P < 0.05 (two-tailed Student's t-test).

Figure S2.4. Specificity of the assay. (a) Images of the NHS@MF membranes with different treatments after the addition of TMB substrate: 100 μL SP-RBD-His (2 mg/L); 200 μL BSA (3%); 100 μL SP-RBD-His (2 mg/L), and then 200 μL BSA (3%); 200 μL BSA (3%) and then 100 μL Ab-HIS-HRP (1 mg/L); 100 μL Ab-HIS-HRP (1 mg/L); 100 μL SP-RBD-His (2 mg/L), 200 μL BSA (3%), and then 100 μL Ab-HIS-HRP (1 mg/L). (b) The bar diagram for the ΔRGB observed from the images. Data are presented as mean ± SD, with n = 3 independent experiments.

Figure S2.5. Blocking optimization. Optical images and the intensity of colorimetric signals of 1%, 3%, 5% BSA treated membranes and 1%, 3%, 5% skim milk treated membranes. Data are presented as mean ± SD, with n = 3 independent experiments.

Figure S2.6. Optical image of sensing test of NHS@MF after the material was exposed to different concentrations of CAP. (without image crop)

Figure 3.1. (a) Scheme of the used side-by-side chamber; (b) the correlation between diffusion time and concentration of *E. coli* O157:H7 diffused through NF, NP, and MF in different thicknesses. (c) Vertical flow test of *E. coli* O157:H7 solution (at 10^4 CFU/mL concentration) through various materials: NF, NP, and MF with different thicknesses, with each material positioned at the base of a syringe. (d) The unspecific adsorption of *E. coli* onto the tested materials after buffer wash. (NF thickness =0.21mm; NP thickness =0.18mm). Data are shown as mean ± SD, based on n = 3 independent experiments. *LOD =Limit of detection.

Figure 3.2. Schematic illustration of preparation and use of foam-based sandwich ELISA (f-ELISA). (a) Immobilizing antibodies and capturing bacteria; (b) Adding HRP-labeled secondary antibody and enzymatic substrate TMB to generate color signals, and obtaining images using a smartphone.

Figure 3.3. SEM images of (a) Pristine MF, (b) NHS@MF after incubation with *E. coli* O157:H7 solution (10^5 CFU/mL); (c) Ab@NHS@MF incubated with *E. coli* O157:H7 solution (10^5 CFU/mL); (d) Ab@NHS@MF after incubation with *E. coli* O157:H7 solution (10^3 CFU/mL). Fluorescent microscopic images of (e) NHS@MF and (f) Ab@NHS@MF, after incubation with *E. coli* O157:H7 solution at a concentration of 10^7 CFU/mL. Data are shown as mean ± SD, based on n = 3 independent experiments. ***P < 0.001 (two-tailed Student's t-test).

Figure 3.4. (a) Optical images and the calibration curve of the MF media in the detection of *E. coli* O157:H7. (b) Linear equation for the colorimetric assay was fitted to be y= 0.0749x+ 26.499 (R^2= 0.989) between 50 and 10^3 CFU/mL. Data are shown as mean ± SD, based on n = 3 independent experiments.

Figure 3.5. (a) Calibration curves generated using varying sample volumes for the detection of *E. coli* O157:H7. (b) Influence of sample volume on the colorimetric signal intensities in the f-ELISA method. Data are shown as mean ± SD, based on n = 3 independent experiments.

Figure 3.6. Optical images and the colorimetric signals before and after 1h enrichment of *E. coli* O157:H7 at various concentrations. Data are shown as mean ± SD, based on n = 3 independent experiments. **P < 0.01 (two-tailed Student's t-test).

Figure 3.7. Selectivity of f-ELISA toward *E. coli* O157:H7 detection in comparison with other bacteria strains, including *Pseudomonas fluorescens, Listeria innocua, Listeria monocytogenes, Salmonella enterica* and *E. coli* BL21. The concentration of each bacteria strain used in this experiment is 10^5 CFU/mL. Data are shown as mean ± SD, based on n = 3 independent experiments. ***P < 0.001 (two-tailed Student's t-test).

Figure 3.8. (a) The scheme illustrated the sensing of *E. coli* O157:H7 in agricultural water and the photograph showcased a rapid-flow device operated by a syringe pump. (b) Optical images and ΔRGB values of membranes treated by different concentrations of *E. coli* O157:H7 in spiked samples, sterilized Agwater, and non-sterilized Agwater. (c) Whole plate images of bacterial cultures upon exposure to non-sterilized agricultural water. Data are shown as mean ± SD, based on n = 3 independent experiments.

Figure S3.1. Calibration curve for *E. coli* O157:H7 at the wavelength of 600 nm.

Figure S3.2. Photograph demonstrating the liquid filtering test using syringes and vials.

Figure S3.3. Chemical structure of melamine foam

Figure S3.4. (a) Reaction of MF with DSC and proteins and (b) FTIR results of MF and NHS@MF.

Figure S3.5. Optimization of (a) the reaction time between HRP and TMB substrate; (b) the concentration anti-*E. coli* O157:H7 antibodies used for immobilization; (c) the concentration of Anti-*E. coli* O157:H7 antibodies conjugated with HRP used as the secondary antibody in f-ELISA.

Figure S3.6. Specificity of the assay. Images of the NHS@MF membranes with different treatments after the addition of TMB substrate: 100 µL Ab-*E. coli* (5 mg/L), 200 µL skimmed milk (SKM) (3%), 200 µL *E. coli* O157:H7 (10^7 CFU/mL), and 100 µL Ab-*E. coli*-HRP (2 mg/L) were used accordingly. The bar diagram for the ΔRGB was observed from the images. Data are presented as mean ± SD, with n = 3 independent experiments.

Figure S3.7. Optical image and ΔRGB values of membranes treated by different concentrations of *E. coli* O157:H7 in spiked milk samples. Data are presented as mean ± SD, with n = 3 independent experiments.

Figure S3.8. Long-Term Stability Assessment. The Ab@NHS@MF membranes were prepared by using 10% sucrose as a stabilizer followed by freeze-drying. They were stored at a consistent temperature of 4°C and assessed over a period of 90 days. Data are presented as mean ± SD, with n = 3 independent experiments. *C = Control group

Figure 4.1. (a) Optical view of a commercial MF and standardized membranes with a thickness of 1 mm and diameter of 5 mm. (b) Schematic illustration of the reagent modification and the following ligand immobilization. (c) Reaction of MF with DSC, CDI, and CC, and ligands with free amino group. (d) ATR-FTIR results of MF after different modifications. (e) SEM images of MF, NHS@MF, CDI@MF, and CC@MF. (f) Water contact angle results of MF, NHS@MF, CDI@MF, and CC@MF.

Figure 4.2. (a) Schematic illustration of Ab-HRP immobilization; optical images and colorimetric comparison results among different MF membranes. (b) Quantification of antibodies immobilized on different MF membranes via BCA assay kit. (c) A diagram

of the antibodies as immunoprobes in f-ELISA for human IgG. (d) Optical images and the calibration curve of f-ELISA by using Ab-HIgG as the capture antibody. (e) Selectivity of f-ELISA toward HIgG detection in comparison with rabbit IgG (RIgG), goat IgG (GIgG), mouse IgG (MIgG), and Human serum albumin (HSA). The concentration of each protein used in the selectivity assay is 1 mg/L. The data are presented as the mean ± standard deviation (SD) from three independent experiments. Statistical significance was determined using a two-tailed Student's t-test. *P < 0.05, ***P < 0.001. *LOD = limit of detection.

Figure 4.3. (a) Schematic illustration of biotinylated nanobody (Bt-Nb) immobilization and the use of SA-HRP as the signal development tracer. (b) Optical images and colorimetric comparison results among different MF membranes. (c) Quantification of nanobodies immobilized on different MF membranes via BCA assay kit. (d) A diagram of the nanobodies as immunoprobes in f-ELISA for human mEH. (e) Optical images and the calibration curve of f-ELISA by using Nb-mEH as the capture ligand. (f) Selectivity of f-ELISA toward human mEH detection in comparison with rat mEH, human sEH, EH3, EH4, and denatured human mEH. The concentration of each epoxide hydrolase used in the selectivity assay is 1 mg/L. The data are presented as the mean ± standard deviation (SD) from three independent experiments. Statistical significance was determined using a two-tailed Student's t-test. *P < 0.05, ***P < 0.001. *LOD = limit of detection.

Figure 4.4. (a) Schematic illustration of biotinylated L10-2 peptide (Bt-L10-2) immobilization and the use of streptavidin with Alexa 647 conjugation as the signal

development tracer. (b) Optical images captured from Bio-Rad imaging system and fluorescence results among different MF membranes. (c) Quantification of peptides immobilized on different MF membranes via pierce quantitative fluorometric peptide assay. (d) A diagram of the peptides as immunoprobes in f-ELISA for SARS-CoV-2 spike protein with His tag (S-protein-His). (e) Schematic illustration of L10-2 and peptides with 1-3 AEEA linkers. One AEEA linker was added to the N-terminus of L10-2a, two with L10-2b, and three with L10-2c. (f) Optical images and the colorimetric results of f-ELISA by using peptides with different numbers of linkers as illustrated above. (g) Optical images and the calibration curve of f-ELISA by using L10-2c peptide as the capture antibody. The data are presented as the mean ± standard deviation (SD) from three independent experiments. Statistical significance was determined using a two-tailed Student's t-test. *P < 0.05. *LOD = limit of detection.

Figure 4.5. Comparison of the colorimetric signal (%) of Ab@CC@MF, Nb@CC@MF, and Pt@NHS@MF over a 30-day storage period at different storage temperatures: (a) 4°C and (b) 25°C (room temperature, RT). The membranes were used to detect HIgG (5 mg/L), mEH (5 mg/L), and S-protein-His (5 mg/L), respectively, using the f-ELISA assay at specific time points during the storage period. The colorimetric signal (%) represents the percentage of the initial signal intensity retained at each time point. The data are presented as the mean ± standard deviation (SD) from three independent experiments.

Figure S4.1. Calibration curves for (a) antibody, (b) nanobody, and (c) peptide

Figure S4.2. Chemical structure of the melamine foam.

Figure S4.3. SEM images of (a) antibodies-immobilized CC@MF (Ab@CC@MF), (b) nanobodies-immobilized CC@MF (Nb@CC@MF), and (c) peptides-immobilized NHS@MF (Pt@NHS@MF).

Figure S4.4. Specificity of the assay. Images of the NHS@MF membranes with different treatments after adding TMB substrate: 100 μL Ab-HIgG (5 mg/L), 200 μL skimmed milk (SKM) (3%), 200 μL HIgG (1 mg/L), and 100 μL Ab-HIgG-HRP (1 mg/L) were used accordingly. The bar diagram for the ΔRGB was observed from the images. Data are presented as mean ± SD, with n = 3 independent experiments.

Figure S4.5. Chemical structure and mass spectrometry of L10-2.

Figure S4.6. Chemical structure and mass spectrometry of L10-2a.

Figure S4.7. Chemical structure and mass spectrometry of L10-2b.

Figure S4.8. Chemical structure and mass spectrometry of L10-2c.

Figure S4.9. Quantification of varied peptides immobilized on NHS@MF membranes via pierce quantitative fluorometric peptide assay.

Table of Contents

Chapter 1. Introduction

Abstract

My Ph.D. study delves into the development and application of a novel foam-based ELISA (f-ELISA) for detecting a broad range of analytes, emphasizing the innovative use of melamine foam (MF) to enhance biosensing efficacy. The introduction and literature review highlight the advantages and limitations of traditional detection techniques, including Polymerase Chain Reaction (PCR), Cell Flow Cytometry, Bacteria Culture Plates. The introduction also emphasizes the strengths and limitations of the Enzyme-Linked Immunosorbent Assay (ELISA) along with the critical role of approaches, platforms, and ligands in the efficiency of immunoassay-based biosensors. To address the need for a detection method that is rapid, easy to use, visually distinguishable, highly sensitive, and specific for on-site detection of environmental pollutants and health bioinformatics, the f-ELISA system has been invented. Besides, in this introductory section, MFs' properties and applications in various fields are discussed to highlight the suitability of MF as a potential biosensor platform. Furthermore, the introduction highlights f-ELISA's potential to revolutionize diagnostic methodologies across diverse fields for real-world applications.

1.1 Detection Techniques

1.1.1 Polymerase Chain Reaction (PCR)

Polymerase Chain Reaction (PCR) is a revolutionary method that was invented in 1983 by Kary Mullis who was awarded the Novel Prize in Chemistry in 1993 based on this discovery[1]. PCR enables the amplification of specific DNA sequences from minute quantities of DNA, making it possible to study genetic material with unprecedented precision and efficiency. This technique relies on thermal cyclings, consisting of repeated heating and cooling cycles to denature DNA, anneals primers to target sequences, and extends these primers to create millions to billions of copies of the desired DNA segment[2,3]. The versatility and sensitivity of PCR have led to its widespread application across various fields of science and medicine. In addition, PCR has evolved significantly since its inception, leading to the development of various types of PCR, each tailored to specific applications and research needs. Reverse Transcription PCR (RT-PCR) is a technique used to detect and measure the expression of RNA[4]. It is particularly valuable in virology for identifying RNA viruses and in gene expression studies. RT-PCR involves two main steps: first, reverse transcription converts RNA into complementary DNA (cDNA) using the enzyme reverse transcriptase; then, this cDNA is amplified using traditional PCR. This method allows researchers to study gene expression levels and to detect RNA viruses, offering insights into viral load and the activity of specific genes[5]. Quantitative PCR, also known as Real-Time PCR (qPCR), is an advanced form of PCR that allows for

the real-time monitoring of DNA amplification. This is achieved by using fluorescent dyes or probes that bind to the DNA, with the intensity of the fluorescence increasing as the DNA is amplified. qPCR enables the quantification of the starting amount of DNA, making it a powerful tool for measuring gene expression levels, detecting pathogens, and performing precise genetic analysis. The real-time aspect of qPCR provides a dynamic view of the amplification process, enhancing both the accuracy and reliability of the measurements[6]. Digital PCR (dPCR) is a refinement of PCR that provides absolute quantification of nucleic acid samples without the need for calibration curves, unlike qPCR[7]. In dPCR, the sample is partitioned into many individuals, parallel PCR reactions; some containing the target molecule (positive), and others not (negative). Following amplification, the number of positive reactions is counted and used to calculate the absolute number of target molecules in the sample. This method offers high precision and sensitivity and is particularly useful for detecting low abundance targets, quantifying viral loads, and validating next-generation sequencing data[8]. These variations enhance PCR's utility and have become a cornerstone in diagnostic procedures for detecting pathogens in infectious diseases, identifying genetic disorders, and forensically analyzing DNA in criminal investigations[9,10]. Additionally, PCR plays a crucial role in research and development, facilitating gene cloning, sequencing, and functional analysis of genes. Its ability to detect and quantify specific DNA or RNA sequences has also made it invaluable in the fields of genomics, clinical diagnostics, evolutionary biology, environmental science, etc. In the context of clinical diagnostics, PCR is widely used for the rapid

detection of infectious agents, including bacteria and viruses[11]. For example, it plays a critical role in diagnosing viral infections such as HIV, hepatitis, and more recently, SARS-CoV-2, the virus responsible for COVID-19[12,13,14]. By targeting specific genetic markers of these pathogens, PCR can provide accurate and early detection, which is crucial for timely treatment and containment efforts. The presence of SARS-CoV-2 in respiratory specimens was detected by real-time Reverse transcription polymerase chain reaction (RT-PCR) amplification of SARS-CoV-2 open reading frame 1ab (ORF1ab), nucleocapsid protein (NP) genes fragments, as mentioned in previous published paper[15]. Following guidelines in the Clinical Laboratory Standards Institute (CLSI) document EP17-A, the lowest concentration level with a detection rate of 95% for positive results was taken as the limit of detection (LOD) for each assay. The LOD of different commercialized kits of RT-PCR is ranging from 242 copies/mL to 7744 copies/mL[16]. Overall, since its authorization in February 2020, the PCR test has remained the gold standard for COVID-19 diagnosis due to its accuracy and reliability.

1.1.2 Flow Cytometry

Flow cytometry is an important technology for the detailed analysis of cellular properties, combining advanced optical and electronic systems for high-throughput examination of cells and particles[17]. This technique uses light scattering and fluorescence to analyze the physical and chemical characteristics of individual cells in a fluid stream. As a start of sample preparation, cells or particles are suspended in a

fluid and injected into the flow cytometer instrument. As each cell passes through a laser beam, it scatters light and, if labeled with fluorescent dyes, emits light at specific wavelengths, revealing intricate details about cell size, internal complexity, and the presence of specific molecular markers[18]. Flow cytometry's real-time data acquisition allows for the simultaneous multiparametric analysis of thousands of particles per second, making it a potent tool in fields ranging from immunology and cancer research to plant biology and infectious disease diagnostics[19,20]. Its applications extend from fundamental research, aiding in the deciphering of cellular functions and phenotypes, to clinical analysis where it is crucial for diagnosing various diseases, including cancer, AIDS, COVID-19, etc[21,22,23]. For example, Tamai et al. analyzed the expression of carcinoembryonic antigen (CEA) in 26 gastric carcinomas, of which six were ascites specimens, using flow cytometry, which can detect both membranous and cytoplasmic CEA, and additionally provided quantitative data[24]. The technology's capacity for rapid and comprehensive analysis renders it invaluable for diagnosis through the quantification of specific biomarkers related to various diseases.

1.1.3 Bacteriological Culture Methods

A microbiological culture, also known as a microbial culture, is a technique used to cultivate and multiply microorganisms under controlled laboratory conditions[25]. This method involves providing a suitable environment, such as a predetermined culture medium, for the microorganisms to grow and reproduce. Microbial cultures serve as fundamental and essential tools in molecular biology research and diagnostic

procedures[26]. The term "culture" can refer to the process of growing microorganisms. These cultures are employed to identify the type of microorganism present, determine its abundance in the sample under investigation, or achieve both objectives simultaneously. Microbial cultures are among the primary diagnostic methods in microbiology and are used to determine the cause of infectious diseases by allowing the pathogen to multiply in a specific medium[27]. Cultures are used to isolate and identify the specific microorganism responsible for an infection. For example, in the case of a suspected bacterial infection, a sample (such as blood, urine, or a swab from an infected site) is inoculated onto a culture medium. The microorganisms present in the sample will grow and form colonies, which can then be identified through various biochemical and molecular tests. One common example is a throat culture, where a sample is obtained by swabbing the back of the throat and transferring it to a medium to screen for harmful microorganisms like Streptococcus pyogenes, which is responsible for strep throat[28]. Another example involves testing for *Escherichia coli* (*E. coli*) O157:H7, a particular strain of *E. coli* that can cause severe foodborne illness. In this case, a sample might be taken from suspect food items or fecal matter and placed onto a specific medium designed to identify and facilitate the growth of *E. coli* O157:H7, enabling the detection of this pathogen[29]. Similarly, for identifying Salmonella infections, which are common causes of food poisoning, a stool sample is collected and spread onto a selective medium tailored to encourage the growth of Salmonella species[30]. This method facilitates the detection of these pathogens, which are responsible for symptoms ranging from diarrhea to severe gastroenteritis[31]. The

word "culture" is commonly used in an informal sense to describe the process of selectively cultivating a particular strain or species of microorganism in a laboratory environment. Frequently, it is necessary to obtain a pure (or axenic) culture, which consists of a population of cells or multicellular organisms growing in isolation, without the presence of any other species or types. A pure culture may originate from a single cell or organism, in which case the cells are genetic clones of one another. To solidify the culture medium and provide a semi-solid or solid surface for microbial growth, a gelling agent is often used. Agar, a gelatinous substance derived from certain seaweed species, is a common choice for this purpose[32]. As a more cost-effective alternative, guar gum can be employed, particularly for the isolation and maintenance of thermophiles[33].

Overall, microbial cultures are indispensable tools in research laboratories, enabling the study of microorganisms' physiology, genetics, pathogenicity, and the development of new antimicrobial agents, vaccines, and diagnostic tests.

1.1.4 Immunoassay Biosensors

Typically, most immunoassay biosensors are based on the same principle as ELISA techniques, which involves antigen-antibody interactions for the detection and quantification of specific biomolecules[34]. Immunoassay biosensors represent a technological advancement that integrates the ELISA principle with biosensor technology to provide rapid, sensitive, and often real-time analysis. In these immunoassay biosensors, the immunochemical reaction is coupled with a platform

that allows for the immobilization and flow of reagents, as well as a transducer that converts the biological interaction into a measurable optical or electronic signal. This integrated system enables the detection and analysis of specific biomolecular interactions, enabling accurate and sensitive diagnostic capabilities[35].

The platform component provides a surface or matrix where the necessary reagents, such as antibodies or other ligands, can be immobilized. This immobilization step ensures that the target analytes present in the sample can bind specifically to the capture reagents. Additionally, the platform facilitates the controlled flow and exposure of the sample to the immobilized reagents, allowing for efficient binding interactions.

Coupled with the platform is a transducer, which serves as the detection component of the system. The transducer converts the biological interactions, such as the binding of analytes to the immobilized reagents, into a measurable signal. This signal can take various forms, including optical signals (e.g., color, fluorescence, absorbance, or chemiluminescence) or electronic signals (e.g., electrochemical or impedance changes)[36,37].

Immunoassay biosensors combine the specificity of immunochemical reactions with the sensitivity of various transducers to detect and quantify target biomolecules or biomarkers in a sample. These biosensors utilize different ELISA formats, such as direct, indirect, sandwich, or competitive, depending on the target analyte and the desired sensitivity and specificity. The immunochemical reaction takes place on a

platform that allows for the immobilization of reagents (e.g., antibodies or antigens) and the flow of the sample. The interaction between the target analyte and the immobilized reagents generates a signal, which is then converted by a transducer into a measurable output.

This integrated approach offers several advantages over traditional ELISA, including:

1. Portability: Immunoassay biosensors can be designed as portable devices for on-site testing.
2. Lower limits of detection: The use of sensitive transducers enables the detection of low concentrations of target analytes.
3. Faster analysis times: The integration of the immunochemical reaction and signal detection allows for rapid analysis compared to traditional ELISA.
4. Miniaturization and multiplexing: Immunoassay biosensors can be miniaturized and designed to detect multiple analytes simultaneously[38].

These advantages make immunoassay biosensors a powerful tool for diagnosing and monitoring a wide range of targets, such as disease biomarkers, environmental contaminants, foodborne pathogens, antibiotics, and biological threat agents[39].

1.1.4.1 Types of ELISA

The Enzyme-Linked Immunosorbent Assay (ELISA) is a widely used analytical biochemistry technique that leverages the specificity of antibody-antigen interactions to detect and quantify target molecules in a sample. It is a solid-phase immunoassay

that combines the principles of selective antibody binding with enzymatic amplification and colorimetric or fluorescent detection[40]. The ELISA technique involves immobilizing one component of the antibody-antigen reaction (either the antigen or the antibody) onto a solid surface, typically a 96-well plate. The sample containing the target molecule is then introduced, and any binding that occurs between the immobilized component and the target is detected through a series of steps involving enzyme-labeled antibodies or antigens. The presence of the enzyme label results in a colorimetric or fluorescent signal, the intensity of which is proportional to the concentration of the target molecule in the sample[41].

ELISA assays can be configured in different formats, including direct, indirect, sandwich, and competitive, depending on the specific requirements of the analysis and the nature of the target molecule[42].

Direct ELISA: Introduced in 1971 by Engvall, Perlmann, Van Weemen, and Schuurs, the direct ELISA method is suitable for quantifying high molecular weight antigens. The plate surface is coated with the target antigen or antibody. An enzyme-conjugated antibody or antigen enables detection. After incubation and washing to remove unbound components, a substrate is added, producing a colored or fluorescent signal proportional to the antigen or antibody concentration[43].

Indirect ELISA: Developed in 1978 by Lindström and Wager, inspired by the direct method, the indirect ELISA measures antibodies against a coated antigen. The fundamental principle of indirect ELISA involves immobilizing the target antigen

onto a solid surface, typically a microplate well. The sample containing the primary antibodies of interest is then added. If present, these antibodies will bind to the immobilized antigen. To detect this antigen-antibody complex, a secondary antibody, which is conjugated to an enzyme and directed against the species of the primary antibody, is introduced. Upon addition of a substrate for the enzyme, a colorimetric or fluorescent change occurs, indicating the presence of the primary antibodies. The intensity of the color change is proportional to the amount of antibody in the sample, allowing for quantification[44].

Competitive ELISA: Developed in 1976 by Yorde et al., the competitive ELISA measures antigens or antibodies by their competition with enzyme-labeled counterparts for binding to immobilized antibodies or antigens, respectively. The sample and enzyme-labeled component are added simultaneously, competing for limited binding sites. After washing and substrate addition, the signal intensity is inversely proportional to the analyte concentration in the sample. Normally, competitive ELISA is generally more suitable for detecting and quantifying smaller targets or analytes compared to other ELISA formats[45].

Sandwich ELISA: The Sandwich ELISA was first developed in 1977 by Kato et al. The process begins with the coating of a microplate well with a capture antibody specific to the target antigen. After incubation, the sample containing the antigen is added, allowing the antigen to bind to the capture antibody. Following a washing step to remove unbound substances, a detection antibody is added, which binds to a

different epitope on the target antigen, forming a sandwich complex. The detection antibody is either directly conjugated to an enzyme or recognized by a secondary enzyme-conjugated antibody. Upon adding a chromogenic substrate, the enzyme catalyzes a color change, the intensity of which is directly proportional to the amount of antigen present in the sample[46].

The various types of ELISAs differ in their format, sensitivity, and suitability for detecting specific targets. The direct ELISA, the simplest format, has lower sensitivity compared to the indirect ELISA, which detects antibodies using a primary antibody from the sample and an enzyme-labeled secondary antibody. The sandwich ELISA, highly sensitive and specific for multi-epitope antigens, employs capture and detection antibodies. The competitive ELISA, suitable for small molecules or single-epitope antigens, relies on competition between sample and enzyme-labeled antigens for binding to immobilized antibodies, resulting in an inversely proportional signal. While direct and indirect ELISAs are better suited for qualitative analysis, sandwich and competitive ELISAs enable quantitation, with the choice depending on the target, its size and epitope availability, the required sensitivity, and the availability of suitable antibodies. In the field of immunoassay biosensors, all the different types of ELISAs – direct, indirect, sandwich, and competitive – have been successfully integrated and utilized in real-world applications across a wide range of studies[47]. The versatility of ELISA formats has allowed researchers and developers to adapt these immunoassay techniques to various biosensor platforms, utilizing the specific advantages of each format to meet the unique requirements of their target analytes and applications.

1.1.4.2 Types of platforms

One classic platform is the 96-well plate, which serves as a fundamental platform for conducting enzyme-linked immunosorbent assays (ELISA), a versatile and widely used technique for detecting and quantifying substances, ranging from toxicants to disease related proteins and pathogens. The configuration of the 96-well plate, with its array of small wells, allows for high-throughput screening, making it an invaluable tool in both research and diagnostic settings[48]. The plates are usually made from polystyrene for colorimetric assays due to its clarity and low fluorescence, or polypropylene for storage or assays requiring thermal cycling due to its higher chemical and thermal resistance. The interaction between the polystyrene plate and the antibody is primarily non-covalent. Physical adsorption is the most straightforward method of attaching antibodies to the plate. It relies on hydrophobic interactions between the polystyrene surface and hydrophobic regions of the antibodies. While this method is simple and does not require chemical modification of the antibody or the surface, it might not provide the strongest or most oriented attachment. Besides, positively or negatively charged groups on the plate surface or the antibody can attract oppositely charged groups, contributing to the adherence of the antibody to the plate as well[49]. While non-covalent bonds are convenient for coating plates, it is crucial to ensure that the attachment is stable under assay conditions and that it does not interfere with the antibody's antigen-binding activity. After coating the plate with antibodies, blocking steps are typically performed to cover any remaining unbound sites on the plate surface. This prevents nonspecific

binding of assay components, which could otherwise contribute to background signal[50]. In addition, 96-well plates have different types corresponding to various applications. Flat-bottom wells are ideal for optical measurements, such as those used in ELISA, absorbance spectroscopy, and cell-based assays where visual inspection under a microscope is required. Round-bottom wells are better suited for mixing and applications involving cell culture, as they facilitate easier resuspension of pellets[51]. V-bottom wells are designed to concentrate samples into a smaller volume, making them useful for precipitation assays or when collecting samples post-reaction[52].

In conclusion, the 96-well plate, with its adaptability and capacity for high-throughput analysis, has become an indispensable tool in the ELISA methods, supporting a wide range of applications from basic research to clinical diagnostics, ensuring precise and reliable quantification of analytes in various sample types.

Despite the advantages of 96-well plate, certain limitations exist with this conventional ELISA sensing platform. These include relatively high cost, lack of scalability and flexibility for personal use and simultaneous examinations of multi-target chemicals in very low concentrations, as well as dependence on specialized instrumentation. As an alternative, paper-based ELISA (p-ELISA) is using fibrous and microporous platforms with the advantages of increased surface areas of fibers, reduced cost, ease of use, improved detection sensitivity, and results that are distinguishable to the naked eye[53].

Cellulose paper, a fibrous and microporous material, serves as an ideal substrate for p-

ELISA due to its high protein-binding capacity and uniform pore structure. This material can effectively immobilize proteins, including antibodies and antigens, through non-specific adsorption, providing a stable matrix for immunoassay development. The fibrous nature of nitrocellulose paper provides a large surface area for biomolecule immobilization, enhancing the assay's sensitivity by facilitating more extensive interactions between target molecules and detection reagents. Besides, compared to traditional solid-phase supports, nitrocellulose paper is significantly less expensive, making p-ELISA an economically viable option, particularly in resource-limited settings[54]. When fabricating sensors, one of the most commonly utilized paper substrates is Whatman No. 1 chromatography paper. This type of paper offers several desirable properties, including a smooth surface texture and consistent quality on both sides. Its medium flow rate and thickness of 0.18 mm make it compatible with printing using commercial machines. Notably, Whatman No. 1 chromatography paper comprises 98% α-cellulose, without the addition of strengthening agents, whitening agents, or other additives. This high purity reduces the potential for interference, making it a suitable choice for sensor fabrication[55].

To further enhance the sensitivity of p-ELISA, nanofibers have been chosen as a promising platform. Compared with conventional biosensor systems, nanofiber biosensors offer several merits, including high sensitivity, proper mass transfer, convenient operation process and less false positive or negative rate. These merits can be attributed to the unique properties of the nanofibers, including their exceptionally ultra-high specific surface area, high porosity, portability and flexibility for surface

modification[56]. The significantly large surface area offered by the nanofibers enhances antibody binding capacity, which in turn improves sensitivity. In the context of ELISA's operating principles, nanofiber biosensors exhibit a more intense signal for analytes at the same concentration compared to traditional biosensors, thereby achieving remarkably high sensitivity. Previous studies have demonstrated that by utilizing nanofibrous membranes made from poly(vinyl alcohol-co-ethylene) (PVA-co-PE) as a substrate, significant sensitivity in detecting key substances has been achieved. Specifically, chloramphenicol (CAP), a crucial antibiotic, was detectable at a limit of detection (LOD) of 0.1 ng/mL, and the SARS-CoV-2 spike protein was identifiable at a 2 ng/mL level[57,58].

Many biosensors incorporate a variety of other materials into their platforms, such as magnetic beads, gold nanoparticles, hydrogels, graphene, carbon nanotubes, quantum dots, pyromellitic dianhydride (PMDA), metal-organic frameworks (MOFs), and conductive polymers. These materials, as detailed in the subsequent Table 1.1, are chosen for their distinct properties, which are important in enhancing performance and expanding the application range of biosensing technologies.

Table 1.1. Comparison of different types of platforms

Material	Properties	Applications	References
Magnetic Beads	Easy separation, manipulation with magnetic fields	Sample preparation, purification, magnetic biosensors	59
Gold Nanoparticles	Optical properties, surface plasmon resonance (SPR)	Optical biosensors, SERS-based sensing, drug delivery	60
Hydrogels	High water content, biocompatibility	Cell culture platforms, tissue engineering	61
Graphene	High conductivity, large surface area	Electrochemical biosensors, biosensing transistors	62
Carbon Nanotubes	Excellent conductivity, high aspect ratio	Electrochemical biosensors, nanoelectronic biosensors	63
Quantum Dots	Size-dependent fluorescence	Fluorescent biosensors, imaging, diagnostic assays	64
polydimethylsiloxane (PDMS)	Biocompatibility, optical transparency, low non-specific binding	Materials for microfluidic immunoassays	65
MOFs (Metal-Organic Frameworks)	High porosity, tunable structures	Chemical sensing, gas sensing, enzyme immobilization	66
Conductive Polymers	Electrical conductivity, biocompatibility	Electrochemical biosensors, flexible biosensing platforms	67

1.1.4.3 Types of ligands

Immunoassays are highly sensitive and specific analytical techniques used for the detection and quantification of target analytes in a sample. The success of an immunoassay mainly depends on the specific binding interaction between a ligand

and its target. Ligands are molecules that bind specifically to their target analytes, forming the basis of the detection system in immunoassays. Over the years, various types of ligands have been developed and employed in immunoassays, each with its own unique characteristics, advantages, and limitations.

Antibodies are the most widely used ligands in immunoassays. These Y-shaped proteins are produced by the immune system and consist of two heavy chains and two light chains. The variable regions of the heavy and light chains form the antigen-binding site, which allows antibodies to bind to their target antigen with high affinity and specificity. Antibodies can be polyclonal, recognizing multiple epitopes on an antigen, or monoclonal, recognizing a single epitope[68]. They are used in various immunoassay formats, such as ELISA, Western blot, and immunohistochemistry, and have been the gold standard in immunoassays for decades[69].

Nanobodies, also known as single-domain antibodies, are derived from the variable domain of heavy-chain (VHH) antibodies found in camelids[70]. They are smaller than conventional antibodies, with a molecular weight of around 15 kDa, and consist of a single monomeric variable antibody domain. Nanobodies have several advantages over traditional antibodies, including higher stability, better solubility, and easier production in microbial systems. They can penetrate tissues more easily due to their small size and have high affinity and specificity for their targets. Nanobodies are increasingly being used in immunoassays, especially for the detection in situations where conventional antibodies may not be suitable[71].

Peptides are short chains of amino acids, typically ranging from 2 to 50 residues, that can be designed to bind specifically to a target antigen. They are smaller than antibodies and nanobodies, and can be synthesized chemically, making them cost-effective and easier to produce and modify. Peptides can be designed using various approaches, such as rational design based on the structure of the target antigen, and one bead one compound (OBOC) combinatorial library method. They can be used as ligands in immunoassays[72]. However, peptides may have lower affinity and specificity compared to antibodies and might be more susceptible to degradation[73].

Aptamers are short, single-stranded oligonucleotides (DNA or RNA) that can fold into specific three-dimensional structures and bind to their targets with high affinity and specificity[74]. They are selected through an in vitro process called SELEX (Systematic Evolution of Ligands by Exponential Enrichment), which involves iterative rounds of selection and amplification. Aptamers can be designed to bind to a wide range of targets, including proteins, small molecules, and even whole cells[75]. They offer several advantages over antibodies, such as chemical synthesis, reproducibility, stability, and the ability to be easily modified for various applications. Aptamers are increasingly being used in immunoassays as an alternative to antibodies, particularly in situations where antibodies may not be available or suitable[76].

The choice of ligand for an immunoassay depends on various factors, including the nature of the target analyte, the desired sensitivity and specificity, the assay format, and the available resources. Each type of ligand has its own strengths and weaknesses,

and researchers continue to develop and optimize these ligands to improve the performance of immunoassays.

1.2 Melamine Foams and Their Applications

Melamine foam is a unique material known for its combination of low weight, open-cell structure, good thermal insulation properties, high sound absorption capacity, abrasiveness, flame resistance, and constant physical properties over a wide temperature range. It is made from melamine resin, a thermoset polymer derived from melamine and formaldehyde, through a process that results in a foam with a network of interconnected, and flexible strands[77]. Due to the unique properties of MF as mentioned above, there are a wide range of applications, such as oil/water separation, adsorbents for ion dyes, electrochemical electrodes, and other applications in fire resistance, water disinfection, and catalytic reactions[78].

Melamine foam (MF) is naturally hydrophilic, requiring modifications to be suitable for separating oil and water. Several approaches were employed to convert hydrophilic MF into a hydrophobic sponge: 1) Turning MF into hydrophobic carbon foam through direct carbonization. This maintains the 3D porous structure with good mechanical properties. Factors like carbonization temperature, heating rate, and duration impact the resulting sorbent properties. Higher temperatures can lead to increased water absorption, reducing oil/water separation performance[79]. 2) Coating the MF surface with hydrophobic monomers followed by gelation or polymerization. This introduces water-repelling functional groups but often involves use of costly

monomers, toxic solvents, or additional treatments like hydrothermal, UV, or microwave[80]. 3) Treating MF with HCl to create protonated MF with excellent antifouling and oil/water separation abilities.[81] 4) Coating nanomaterials like graphene oxide (GO) or metal-organic frameworks (MOFs) on MF[82]. In this case, MF's bulk structure and high mechanical properties prevent nanoparticle agglomeration and ease the use and recovery. GO is often used for its hydrophobicity. Long-term stability is a concern due to potential nanoparticle detachment.

Among these, direct carbonization is simplest but results in low surface area and reduced mechanical strength. Polymerization effectively creates hydrophobicity but frequently uses expensive or toxic reagents. Acid treatment is straightforward but not environmentally friendly. Nanoparticle coatings provide excellent hydrophobicity but may have limited durability.

Like its application in oil/water separation, modified Melamine Foam (MF) has been extensively utilized as an efficient adsorbent material. In a prior study, MF served as a three-dimensional framework to limit the shrinking of alginate and provide a high surface area support for alginate coating. Alginate has been widely investigated as an adsorbent for dyes and heavy metal ions, demonstrating promising adsorption performance[83]. However, its swelling behavior and poor mechanical strength have hindered the further development of alginate as a high-performance adsorbent. When MF is employed as a support, the melamine fibers effectively prevent alginate agglomeration and promote the exposure of more active sites for ion adsorption from

solution. This alginate-coated MF exhibited good Cu(II) adsorption capacity (maximum 90.09 mg/g), and the bulk structure of MF makes it user-friendly and easy to recover.

Apart from metal ion adsorption, modified MF has also been used for adsorbing other ions such as nitrate. Goto et al. introduced quaternary nitrogen onto carbonized MF through CH_3I treatment and utilized the resulting N-doped carbon as an anion exchanger for nitrate ion adsorption, with capacities ranging from 0.1 to 0.7 mmol/g[84]. Modified MF has also been employed for dye removal. For example, graphene-coated MF was synthesized and used as a dye adsorbent, exhibiting maximum capacities of 286.5 mg/g for methylene blue (MB) and 80.5 mg/g for orange G[85].

When used as an adsorbent, MF primarily serves as a support to load active materials for dye and ion adsorption while providing a bulk structure to facilitate adsorbent recycling. The adsorption capacity of MF-supported composite materials is mainly determined by the active materials coated onto the MF. Furthermore, strong bonding between the active materials and MF is crucial to ensure no peeling off occurs during long-term operation.

MF can also serve as a sacrificial skeleton to obtain 3D materials or hollow-structured materials. For example, nitrogen-doped hollow carbon microspheres with graphitic carbon shells and graphene aerogels that retain the original shape of MF after its removal are such materials as mentioned. These materials have shown promising applications in multifunctional pressure/strain sensors and human motion detection[86].

When modified to have a hydrophobic nature, MF can be used for fire resistance purposes. Studies have shown that hydrophobic MF, when ignited, only burns for a few seconds, and maintains its original shape even after being partially burnt.

Researchers have also explored the use of MF as a support for various materials in catalytic reactions and water disinfection. Wu et al. grafted conjugated microporous polymers (CMPs) onto MF using a CMP-gel-mediated method, which allowed for in situ covering of the foam without filling its open cells. This foam-supporting CMP composite facilitates substrate diffusion through interconnected micropores and macropores, exhibiting great efficiency in acyl transfer reactions. Additionally, the CMP-covered MF demonstrated excellent mechanical properties[87].

In another study, Yu et al. loaded Au/ceria nanowires onto MF and employed the composite material for the continuous reduction of p-nitrophenol in a flow system[88]. Deng et al. utilized MF as a support for Ag nanoparticles, using their antibacterial properties for water disinfection. The bacterial inactivation efficiency for *E. coli* increased from 11.9% to 76.8%, and for *S. aureus*, it increased from 9.8% to 65.4% when MF was loaded with Ag nanoparticles. By loading both graphene oxide (GO) sheets and Ag nanoparticles onto MF, the bacterial inactivation efficiency was further enhanced to 95.9% for *E. coli* and 89.3% for *S. aureus*, as the GO sheets helped prevent the aggregation of Ag nanoparticles[89].

Melamine foam (MF) is an attractive material due to its low cost, environmental friendliness, ease of synthesis, and its 3D macroporous reticulated structure. Besides,

MF has a high nitrogen content, which allows for the production of high-content N-doped carbon foam through simple modification. These properties have led to the widespread use of MF-based materials in various applications, with the potential for further development in new areas.

1.3 Research Objectives

The methods of detection of chemicals and toxicants have been reviewed in Chapter 1, ranging from PCR to portable biosensors. Traditional detection methods, such as PCR and flow cytometry, offer high sensitivity and specificity, enabling the detection and identification of trace amounts of substances in various samples. These methods are often considered the benchmark in environmental monitoring and medical diagnostics. However, their applicability is limited by the need for costly equipment, specialized operators, and lengthy analysis times. These methods may also be affected by matrix effects, which can interfere with the accuracy of the results. Additionally, extensive sample pre-treatment is usually required, further complicating and prolonging the analysis process. On the other hand, ELISA is a relatively user-friendly analytical method that offers good sensitivity and selectivity based on the specific interaction between antigen and antibody. Nevertheless, the traditional ELISA approach struggles to produce visually distinguishable color changes when the target analyte is present at low concentrations. Moreover, conventional ELISA also relies on specialized equipment, such as plate readers, for the detection of trace amounts of targets, which constrains its suitability for on-site detection of trace amounts of

analytes. As a promising alternative, paper-based ELISA (p-ELISA) utilizes fibrous and microporous substrates that offer several benefits, such as increased surface area of fibers, lower costs, user-friendliness, and enhanced detection sensitivity. However, the non-uniform structures of papers and fibrous membranes, particularly in the vertical direction, hinder the penetration of large biomolecules through the membranes, leading to a lower-than-anticipated amount of biomolecules immobilized on the surfaces of fibers within the media. This structural characteristic can potentially decrease the sensitivity of ELISA sensors fabricated using nitrocellulose membranes, filter papers, and even nanofibrous membranes, resulting in non-uniform colorimetric signals in p-ELISA sensors[90,91]. Therefore, an optimal substrate with a three-dimensional, homogeneous, and open macroporous structure that allows large biomolecules to migrate freely in all directions is envisioned as a superior sensing material for such immunoassay biosensors.

The literature review in Chapter 1 discusses the wide-ranging applications of Melamine Foam (MF) attributed to its three-dimensional, homogeneous, macroporous, and reticulated structure. These applications include oil/water separation, water disinfection, adsorption, strain/stress sensing, and catalysis, showcasing MF's versatility as a support material. However, the MF has barely been considered as a material for biosensing, even though it has these properties suitable for serving as the immunoassay platform. Therefore, I propose the development of a novel biosensor platform system by integrating immunoassays with foam-like materials, particularly melamine foam (MF), due to its suitable properties mentioned

earlier. This new approach, which I have termed foam-based ELISA (f-ELISA), aims to overcome the drawbacks of traditional ELISA and p-ELISA, and further serves as a foundation for the development of innovative biosensors targeting a wide range of analytes. To accomplish this goal, the dissertation is structured into three main objectives:

1) Design and fabrication of rapid, sensitive, additive, and volume-responsive colorimetric f-ELISA biosensing platform using chemically modified melamine foam (MF), which can be applied to different types of ELISA biosensors.
2) Application of the f-ELISA system in the development of a novel biosensor for the detection of *E. coli* O157:H7.
3) Investigation of the versatility and stability of chemically modified MF as a general platform for the preparation of f-ELISA biosensors using different sensing agents.

The dissertation presents the research findings in five chapters. Chapter 1 provides an introduction and literature review. Chapter 2 focuses on the design and fabrication of a rapid, sensitive, additive, and volume-responsive colorimetric f-ELISA biosensing platform using chemically modified melamine foam (MF). This platform can be adapted for various types of ELISA biosensors. In this chapter, a commercially available MF was chemically modified for competitive, sandwich, and direct ELISA sensing applications in the first time. Two representative detecting targets were used:

a SARS-CoV-2 spike protein receptor binding domain (SP-RBD-His), a transmembrane protein of the SARS-CoV-2 virus attached with a histidine tag, and an antibiotic, chloramphenicol (CAP). The results demonstrated that the MF-based sensors could detect SP-RBD-His at a concentration of 0.1 mg L^{-1} with the naked eye, and achieved a limit of detection (LOD) of 0.047 mg L^{-1} when supplemented by a smartphone. For CAP, the sensors could detect concentrations as low as 1 ng mL^{-1} by naked eye and 0.096 ng mL^{-1} with smartphone assistance. The MF materials can be integrated into an additive testing system, enabling simultaneous detection of two or more targets. Chapter 2 showcases the potential of f-ELISA and further demonstrates the high sensitivity, specificity, additive nature, and volume responsiveness of this novel biosensing platform. Chapter 3 describes the application of the f-ELISA system in the development of a novel biosensor for the detection of *E. coli* O157:H7. Building upon the advantages of f-ELISA using melamine foam (MF) as a medium, which were demonstrated in the previous chapter, this chapter explores the suitability of f-ELISA for detecting *E. coli* O157:H7. Given the larger size of bacterial cells compared to chemical compounds and proteins, the application of f-ELISA in this context could fully showcase the benefits of the macroporous features offered by the chemically modified MF. In contrast to conventional ELISA (c-ELISA), which is restricted by the limited surface area of a 96-well plate and other p-ELISA methods, bacteria as antigens can move freely in every direction within this macroporous 3D matrix. This enhanced freedom of movement facilitates an amplified interaction between the immobilized antibodies and antigens, leading to substantial enrichment

and heightened sensitivity in colorimetric detection. The testing process needs less than 1.5 h to complete both preparation and detection, and the results indicated that the sensors made of the modified MF materials can detect *E. coli* O157:H7 at a level of 10 CFU/mL by the naked eye with a limit of detection (LOD) at 5 CFU/mL when supplemented by a smartphone. Following a brief enrichment period of 1 h, the sensitivity was further amplified to 2 CFU/mL, which is considered to be ultrasensitive for bacteria detection. Chapter 4 investigates the versatility of chemically modified MF as a general platform for preparing f-ELISA biosensors using different sensing agents, including antibodies, nanobodies, and peptides. Incorporating varied ligands expands the f-ELISA system's adaptability and functionality, making it a versatile and effective diagnostic tool with broader applications and improved detection processes across various fields. The successful use of nanobodies and peptides also demonstrates the biosensors' enhanced storage stability. Chapter 5 serves as the executive conclusion, summarizing the key findings and insights from the previous chapters.

1.4 Reference

1. Templeton, N. S. (1992). The polymerase chain reaction history methods, and applications. *Diagnostic Molecular Pathology*, *1*(1), 58-72.

2. Rahman, M. T., Uddin, M. S., Sultana, R., Moue, A., & Setu, M. (2013). Polymerase chain reaction (PCR): a short review. *Anwer Khan Modern Medical College Journal*, *4*(1), 30-36.

3. Schochetman, G., Ou, C. Y., & Jones, W. K. (1988). Polymerase chain

reaction. *The Journal of infectious diseases*, *158*(6), 1154-1157.

4. Bachman, J. (2013). Reverse-transcription PCR (rt-PCR). In *Methods in enzymology* (Vol. 530, pp. 67-74). Academic Press.

5. Bustin, S. A. (2002). Quantification of mRNA using real-time reverse transcription PCR (RT-PCR): trends and problems. *Journal of molecular endocrinology*, *29*(1), 23-39.

6. Dorak, M. T. (Ed.). (2007). *Real-time PCR*. Taylor & Francis.

7. Huggett, J. F., Cowen, S., & Foy, C. A. (2015). Considerations for digital PCR as an accurate molecular diagnostic tool. *Clinical chemistry*, *61*(1), 79-88.

8. Huggett, J. F., & Whale, A. (2013). Digital PCR as a novel technology and its potential implications for molecular diagnostics. *Clinical chemistry*, *59*(12), 1691-1693.

9. Innis, M. A., Gelfand, D. H., Sninsky, J. J., & White, T. J. (Eds.). (2012). *PCR protocols: a guide to methods and applications*. Academic press.

10. McDonald, C., Taylor, D., & Linacre, A. (2024). PCR in Forensic Science: A Critical Review. *Genes*, *15*(4), 438.

11. Belgrader, P., Benett, W., Hadley, D., Richards, J., Stratton, P., Mariella Jr, R., & Milanovich, F. (1999). PCR detection of bacteria in seven minutes. *Science*, *284*(5413), 449-450.

12. Shan, L., Rabi, S. A., Laird, G. M., Eisele, E. E., Zhang, H., Margolick, J. B., & Siliciano, R. F. (2013). A novel PCR assay for quantification of HIV-1 RNA. *Journal of virology*, *87*(11), 6521-6525.

13. Abe, A., Inoue, K., Tanaka, T., Kato, J., Kajiyama, N., Kawaguchi, R., Tanaka, S., Yoshiba, M., & Kohara, M. (1999). Quantitation of hepatitis B virus genomic DNA by real-time detection PCR. *Journal of Clinical Microbiology, 37*(9), 2899-

2903.

14. Tahamtan, A., & Ardebili, A. (2020). Real-time RT-PCR in COVID-19 detection: issues affecting the results. *Expert review of molecular diagnostics*, *20*(5), 453-454.

15. Liu, R., Han, H., Liu, F., Lv, Z., Wu, K., Liu, Y., Feng, Y., & Zhu, C. (2020). Positive rate of RT-PCR detection of SARS-CoV-2 infection in 4880 cases from one hospital in Wuhan, China, from Jan to Feb 2020. *Clinica Chimica Acta, 505*, 172–175.

16. Yu, L., Wu, S., Hao, X., Dong, X., Mao, L., Pelechano, V., Chen, W.-H., & Yin, X. (2020). Limits of Detection of 6 Approved RT–PCR Kits for the Novel SARS-Coronavirus-2 (SARS-CoV-2). *Clinical Chemistry*, *66*(7), 977-979.

17. McKinnon, K. M. (2018). Flow cytometry: an overview. *Current protocols in immunology*, *120*(1), 5-1.

18. Adan, A., Alizada, G., Kiraz, Y., Baran, Y., & Nalbant, A. (2017). Flow cytometry: basic principles and applications. *Critical reviews in biotechnology*, *37*(2), 163-176.

19. Barlogie, B., Raber, M. N., Schumann, J., Johnson, T. S., Drewinko, B., Swartzendruber, D. E., Göhde, W., Andreeff, M., & Freireich, E. J. (1983). Flow cytometry in clinical cancer research. *Cancer Research, 43*(9), 3982-3997.

20. Laerum, O. D., & Farsund, T. (1981). Clinical application of flow cytometry: a review. *Cytometry: The Journal of the International Society for Analytical Cytology*, *2*(1), 1-13.

21. Giorgi, J. V., Cheng, H. L., Margolick, J. B., Bauer, K. D., Ferbas, J., Waxdal, M., Schmid, I., Hultin, L. E., Jackson, A. L., Park, L., & Taylor, J. M. (1990). Quality control in the flow cytometric measurement of T-lymphocyte subsets: the multicenter

AIDS cohort study experience. *Clinical Immunology and Immunopathology, 55*(2), 173-186.

22. Horndler, L., Delgado, P., Abia, D., Balabanov, I., Martínez-Fleta, P., Cornish, G., Llamas, M. A., Serrano-Villar, S., Sánchez-Madrid, F., Fresno, M., van Santen, H. M., & Alarcón, B. (2021). Flow cytometry multiplexed method for the detection of neutralizing human antibodies to the native SARS-CoV-2 spike protein. *EMBO Molecular Medicine, 13*(3), e13549.

23. Kanegane, H., Hoshino, A., Okano, T., Yasumi, T., Wada, T., Takada, H., Okada, S., Yamashita, M., Yeh, T. W., Nishikomori, R., Takagi, M., Imai, K., Ochs, H. D., & Morio, T. (2018). Flow cytometry-based diagnosis of primary immunodeficiency diseases. *Allergology International, 67*(1), 43-54.

24. Tamai, M., Tanimura, H., Yamaue, H., Iwahashi, M., Tsunoda, T., Tani, M., ... & Arii, K. (1993). Expression of carcinoembryonic antigen in fresh human gastric cancer cells assessed by flow cytometry. *Journal of surgical oncology*, *52*(3), 176-180.

25. Lewis, J. A., & Fleming, J. T. (1995). Basic culture methods. *Methods in cell biology*, *48*, 3-29.

26. Lagier, J. C., Edouard, S., Pagnier, I., Mediannikov, O., Drancourt, M., & Raoult, D. (2015). Current and past strategies for bacterial culture in clinical microbiology. *Clinical microbiology reviews*, *28*(1), 208-236.

27. Sousa, A. M., & Pereira, M. O. (2013). A prospect of current microbial diagnosis methods.

28. Gerber, M. A. (1989). Comparison of throat cultures and rapid strep tests for diagnosis of streptococcal pharyngitis. *The Pediatric infectious disease journal*, *8*(11), 820-824.

29. Sanderson, M. W., Gay, J. M., Hancock, D. D., Gay, C. C., Fox, L. K., & Besser, T. E. (1995). Sensitivity of bacteriologic culture for detection of Escherichia coli O157: H7 in bovine feces. *Journal of Clinical Microbiology*, *33*(10), 2616-2619.

30. Hyatt, D. R., & Weese, J. S. (2004). Salmonella culture: sampling procedures and laboratory techniques. *Veterinary Clinics: Equine Practice*, *20*(3), 577-585.

31. Serrano, M. R. G., Escartín, N. L., Arriaza, M. M., & Díaz, J. C. R. (2019). Microbiological diagnosis of bacteraemia and fungaemia: Blood cultures and molecular methods. *Enfermedades infecciosas y microbiologia clinica (English ed.)*, *37*(5), 335-340.

32. Armisén, R. (1991). Agar and agarose biotechnological applications. In *International Workshop on Gelidium: Proceedings of the International Workshop on Gelidium held in Santander, Spain, September 3–8, 1990* (pp. 157-166). Springer Netherlands.

33. Jain, R., Anjaiah, V., & Babbar, S. B. (2005). Guar gum: a cheap substitute for agar in microbial culture media. *Letters in Applied Microbiology*, *41*(4), 345-349.

34. Vashist, S. K., & Luong, J. H. (2018). Immunoassays: an overview. *Handbook of Immunoassay Technologies*, 1-18.

35. Poschenrieder, A., Thaler, M., Junker, R., & Luppa, P. B. (2019). Recent advances in immunodiagnostics based on biosensor technologies—from central laboratory to the point of care. *Analytical and bioanalytical chemistry*, *411*, 7607-7621.

36. Conroy, P. J., Hearty, S., Leonard, P., & O'Kennedy, R. J. (2009, February). Antibody production, design and use for biosensor-based applications. In *Seminars in cell & developmental biology* (Vol. 20, No. 1, pp. 10-26). Academic Press.

37. Goode, J. A., Rushworth, J. V. H., & Millner, P. A. (2015). Biosensor

regeneration: a review of common techniques and outcomes. *Langmuir*, *31*(23), 6267-6276.

38. Bhardwaj, T. (2015). Review on biosensor technologies. *Int. J. Adv. Res. Eng. Technol*, *6*(2), 36-62.

39. Mohanty, S. P., & Kougianos, E. (2006). Biosensors: A tutorial review. *Ieee Potentials*, *25*(2), 35-40.

40. Shah, K., & Maghsoudlou, P. (2016). Enzyme-linked immunosorbent assay (ELISA): the basics. *British journal of hospital medicine*, *77*(7), C98-C101.

41. Tabatabaei, M. S., & Ahmed, M. (2022). Enzyme-linked immunosorbent assay (ELISA). In *Cancer cell biology: methods and protocols* (pp. 115-134). New York, NY: Springer US.

42. Hayrapetyan, H., Tran, T., Tellez-Corrales, E., & Madiraju, C. (2023). Enzyme-linked immunosorbent assay: types and applications. *ELISA: Methods and Protocols*, 1-17.

43. Lin, A.V. (2015). Direct ELISA. In: Hnasko, R. (eds) ELISA. *Methods in Molecular Biology*, vol 1318. Humana Press, New York, NY.

44. Lin, A.V. (2015). Indirect ELISA. In: Hnasko, R. (eds) ELISA. *Methods in Molecular Biology*, vol 1318. Humana Press, New York, NY.

45. Meyer, T. (2010). Competitive ELISA. In: Kontermann, R., Dübel, S. (eds) Antibody Engineering. Springer Protocols Handbooks. Springer, Berlin, Heidelberg.

46. Aydin, S. (2015). A short history, principles, and types of ELISA, and our laboratory experience with peptide/protein analyses using ELISA. *Peptides, 72*, 4-15

47. Crowther, J. R. (2008). *The ELISA guidebook* (Vol. 149). Springer Science & Business Media.

48. Plested, J. S., Coull, P. A., & Gidney, M. A. J. (2003). Elisa. *Haemophilus*

influenzae Protocols, 243-261.

49. Welch, N. G., Scoble, J. A., Muir, B. W., & Pigram, P. J. (2017). Orientation and characterization of immobilized antibodies for improved immunoassays. *Biointerphases*, *12*(2).

50. Craig, W. Y., Poulin, S. E., Nelson, C. P., & Ritchie, R. F. (1994). ELISA of IgG antibody to oxidized low-density lipoprotein: effects of blocking buffer and method of data expression. *Clinical chemistry*, *40*(6), 882-888.

51. Kueng, W., Silber, E., & Eppenberger, U. (1989). Quantification of cells cultured on 96-well plates. *Analytical biochemistry*, *182*(1), 16-19.

52. Pitt, A. M., & Lee, C. (1996). High throughput screening protein kinase assays optimized for reaction, binding, and detection totally within a 96-well plate. *Journal of Biomolecular Screening*, *1*(1), 47-51.

53. Cheng, C.-M., Martinez, Andres W., Gong, J., Mace, Charles R., Phillips, Scott T., Carrilho, E., Mirica, Katherine A., & Whitesides, George M. (2010). Paper-Based ELISA. *Angewandte Chemie International Edition, 49*(28), 4771–4774.

54. Hu, J., Wang, S., Wang, L., Li, F., Pingguan-Murphy, B., Lu, T. J., & Xu, F. (2014). Advances in paper-based point-of-care diagnostics. *Biosensors and Bioelectronics*, *54*, 585-597.

55. Ma, L., Nilghaz, A., Choi, J. R., Liu, X., & Lu, X. (2018). Rapid detection of clenbuterol in milk using microfluidic paper-based ELISA. *Food Chemistry*, *246*, 437-441.

56. Ma, Y., Yi, J., Pan, B., Nitin, N., & Sun, G. (2020). Chlorine rechargeable biocidal N-halamine nanofibrous membranes incorporated with bifunctional zwitterionic polymers for efficient water disinfection applications. *ACS Applied Materials & Interfaces*, *12*(45), 51057-51068.

57. Zhao, C., Si, Y., Pan, B., Taha, A. Y., Pan, T., & Sun, G. (2020). Design and fabrication of a highly sensitive and naked-eye distinguishable colorimetric biosensor for chloramphenicol detection by using ELISA on nanofibrous membranes. *Talanta*, *217*, 121054.

58. Yu, X., Pan, B., Zhao, C., Shorty, D., Solano, L. N., Sun, G., Liu, R., & Lam, K. S. (2023). Discovery of peptidic ligands against the SARS-CoV-2 spike protein and their use in the development of a highly sensitive personal use colorimetric COVID-19 biosensor. *ACS Sensors*, 8, 2159-2168.

59. Reverté, L., Prieto-Simón, B., & Campàs, M. (2016). New advances in electrochemical biosensors for the detection of toxins: Nanomaterials, magnetic beads and microfluidics systems. A review. *Analytica chimica acta*, *908*, 8-21.

60. Li, Y., Schluesener, H. J., & Xu, S. (2010). Gold nanoparticle-based biosensors. *Gold Bulletin*, *43*, 29-41.

61. Bae, J., Park, J., Kim, S., Cho, H., Kim, H. J., Park, S., & Shin, D. S. (2020). Tailored hydrogels for biosensor applications. *Journal of Industrial and Engineering Chemistry*, *89*, 1-12.

62. Kuila, T., Bose, S., Khanra, P., Mishra, A. K., Kim, N. H., & Lee, J. H. (2011). Recent advances in graphene-based biosensors. *Biosensors and bioelectronics*, *26*(12), 4637-4648.

63. Tîlmaciu, C. M., & Morris, M. C. (2015). Carbon nanotube biosensors. *Frontiers in chemistry*, *3*, 59.

64. Algar, W. R., Tavares, A. J., & Krull, U. J. (2010). Beyond labels: a review of the application of quantum dots as integrated components of assays, bioprobes, and biosensors utilizing optical transduction. *Analytica chimica acta*, *673*(1), 1-25.

65. Zaytseva, N. V., Goral, V. N., Montagna, R. A., & Baeumner, A. J. (2005).

Development of a microfluidic biosensor module for pathogen detection. *Lab on a Chip*, *5*(8), 805-811.

66. Lv, M., Zhou, W., Tavakoli, H., Bautista, C., Xia, J., Wang, Z., & Li, X. (2021). Aptamer-functionalized metal-organic frameworks (MOFs) for biosensing. *Biosensors and Bioelectronics*, *176*, 112947.

67. Lakard, B. (2020). Electrochemical biosensors based on conducting polymers: A review. *Applied Sciences*, *10*(18), 6614.

68. Wang, W., Singh, S., Zeng, D. L., King, K., & Nema, S. (2007). Antibody structure, instability, and formulation. *Journal of pharmaceutical sciences*, *96*(1), 1-26.

69. Haab, B. B. (2006). Applications of antibody array platforms. *Current opinion in biotechnology*, *17*(4), 415-421.

70. Li, D., Cui, Y., Morisseau, C., Wagner, K. M., Cho, Y. S., & Hammock, B. D. (2020). Development of a Highly Sensitive Enzyme-Linked Immunosorbent Assay for Mouse Soluble Epoxide Hydrolase Detection by Combining a Polyclonal Capture Antibody with a Nanobody Tracer. *Analytical chemistry*, *92*(17), 11654-11663.

71. Salvador, J. P., Vilaplana, L., & Marco, M. P. (2019). Nanobody: outstanding features for diagnostic and therapeutic applications. *Analytical and bioanalytical chemistry*, *411*, 1703-1713.

72. Blasco, H., Lalmanach, G., Godat, E., Maurel, M. C., Canepa, S., Belghazi, M., Paintaud, G., Degenne, D., Chatelut, E., Cartron, G., & Le Guellec, C. (2007). Evaluation of a peptide ELISA for the detection of rituximab in serum. *Journal of Immunological Methods*, *325*(1-2), 127-139.

73. Lam, K. S., Salmon, S. E., Hersh, E. M., Hruby, V. J., Kazmierski, W. M., & Knapp, R. J. (1991). A new type of synthetic peptide library for identifying ligand-

binding activity. *Nature*, *354*(6348), 82-84.

74. Dunn, M. R., Jimenez, R. M., & Chaput, J. C. (2017). Analysis of aptamer discovery and technology. *Nature Reviews Chemistry*, *1*(10), 0076.

75. Darmostuk, M., Rimpelova, S., Gbelcova, H., & Ruml, T. (2015). Current approaches in SELEX: An update to aptamer selection technology. *Biotechnology advances*, *33*(6), 1141-1161.

76. Kim, Y. S., Raston, N. H. A., & Gu, M. B. (2016). Aptamer-based nanobiosensors. *Biosensors and Bioelectronics*, *76*, 2-19.

77. Wang, D., Zhang, X., Luo, S., & Li, S. (2012). Preparation and property analysis of melamine formaldehyde foam. *Advances in Materials Physics and Chemistry*, *2*(04), 63-67.

78. Feng, Y., & Yao, J. (2018). Design of melamine sponge-based three-dimensional porous materials toward applications. *Industrial & Engineering Chemistry Research*, *57*(22), 7322-7330.

79. Stolz, A.; Le Floch, S.; Reinert, L.; Ramos, S. M. M.; Tuaillon-Combes, J.; Soneda, Y.; Chaudet, P.; Baillis, D.; Blanchard, N.; Duclaux, L.; San-Miguel, A. (2016). Melamine-derived carbon sponges for oil-water separation. *Carbon*, *107*, 198– 208.

80. Hou, K., Jin, Y., Chen, J., Wen, X., Xu, S., Cheng, J., & Pi, P. (2017). Fabrication of superhydrophobic melamine sponges by thiol-ene click chemistry for oil removal. *Materials Letters*, *202*, 99-102.

81. Wang, C. F., Huang, H. C., & Chen, L. T. (2015). Protonated melamine sponge for effective oil/water separation. *Scientific Reports*, *5*(1), 14294.

82. Ji, C., Zhang, K., Li, L., Chen, X., Hu, J., Yan, D., ... & He, X. (2017). High performance graphene-based foam fabricated by a facile approach for oil

absorption. *Journal of materials chemistry A*, *5*(22), 11263-11270.

83. Feng, Y., Wang, Y., Wang, Y., Zhang, X. F., & Yao, J. (2018). In-situ gelation of sodium alginate supported on melamine sponge for efficient removal of copper ions. *Journal of colloid and interface science*, *512*, 7-13.

84. Goto, T., Amano, Y., & Machida, M. (2017). Preparation of anion exchangers derived from melamine sponge and its adsorption characteristics of nitrate ion. *Journal of Chemical Engineering of Japan*, *50*(9), 692-695.

85. Du, Q., Zhou, Y., Pan, X., Zhang, J., Zhuo, Q., Chen, S., Liu, T., Xu, F., & Yan, C. (2016). A graphene–melamine-sponge for efficient and recyclable dye adsorption. *RSC advances*, *6*(59), 54589-54596.

86. Ma, F., Zhao, H., Sun, L., Li, Q., Huo, L., Xia, T., Gao, S., Pang, G., Shi, Z., & Feng, S. (2012). A facile route for nitrogen-doped hollow graphitic carbon spheres with superior performance in supercapacitors. *Journal of Materials Chemistry*, *22*(27), 13464-13468.

87. Wu, K., Guo, J., & Wang, C. (2016). An elastic monolithic catalyst: A microporous metalloporphyrin-containing framework-wrapped melamine foam for process-intensified acyl transfer. *Angewandte Chemie International Edition*, *55*(20), 6013-6017.

88. Yu, X. F., Mao, L. B., Ge, J., Yu, Z. L., Liu, J. W., & Yu, S. H. (2016). Three-dimensional melamine sponge loaded with Au/ceria nanowires for continuous reduction of p-nitrophenol in a consecutive flow system. *Science bulletin*, *61*(9), 700-705.

89. Deng, C. H., Gong, J. L., Zhang, P., Zeng, G. M., Song, B., & Liu, H. Y. (2017). Preparation of melamine sponge decorated with silver nanoparticles-modified graphene for water disinfection. *Journal of colloid and interface science*, *488*, 26-38.

90. Zhao, C., Si, Y., Zhu, S., Bradley, K., Taha, A. Y., Pan, T., & Sun, G. (2021). Diffusion of protein molecules through microporous nanofibrous polyacrylonitrile membranes. *ACS applied polymer materials*, *3*(3), 1618-1627.

91. Zhao, C., Pan, B., Wang, M., Si, Y., Taha, A. Y., Liu, G., Pan, T., & Sun, G. (2022). Improving the sensitivity of nanofibrous membrane-based ELISA for on-site antibiotics detection. *ACS sensors*, *7*(5), 1458-1466.

Chapter 2. Highly Sensitive Naked Eye Detectable Colorimetric Biosensors Made from Macroporous Framework Melamine Foams for Onsite and Simultaneous Detection of Multiple Environmental Hazards in Flowing Through Sensing Systems

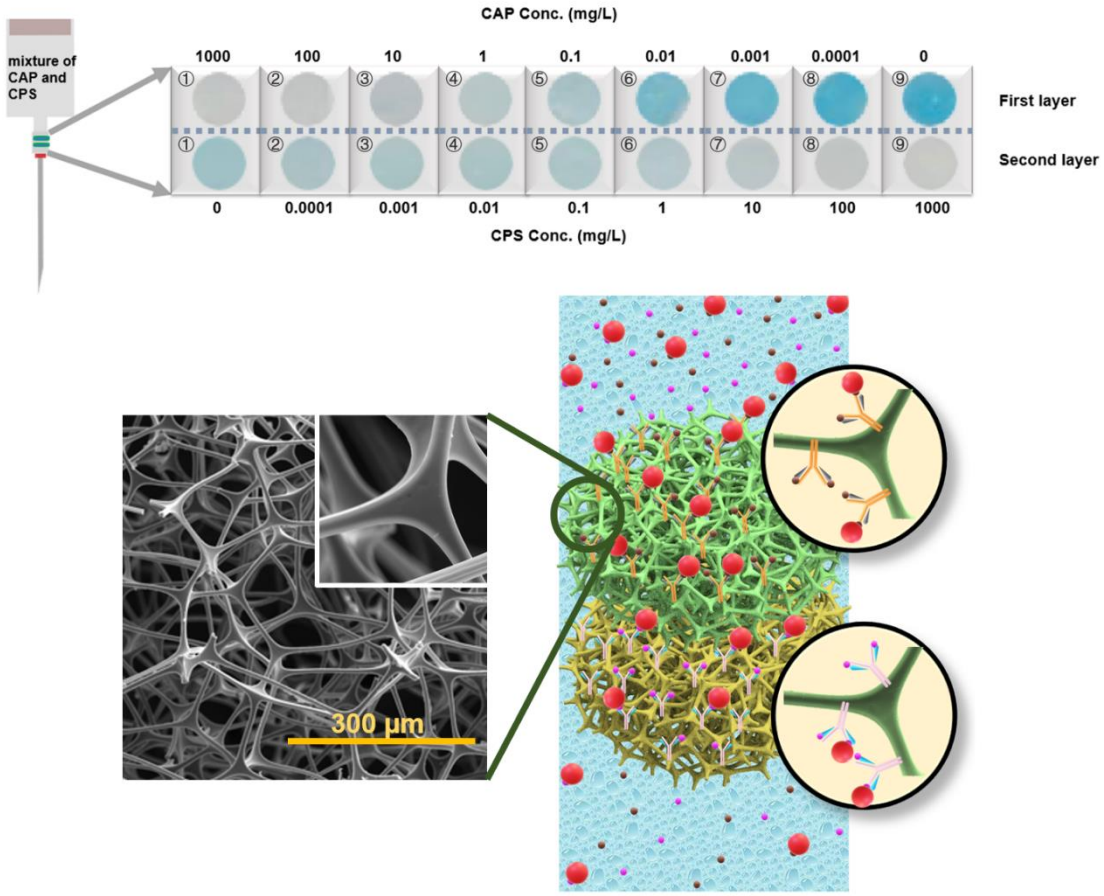

Abstract

Personal-use, naked eye readable, low-cost, highly sensitive, and selective biosensors for rapid detection of environmental toxicants are relevant for many application scenarios. Here, we report the recent developments of highly sensitive and naked eye distinguishable colorimetric sensors by using commercially available melamine foam (MF) as basic sensing materials for instant and volume-responsive simultaneous detection of multiple targets in fluid systems. The MF possesses a unique reticulated three-dimensional (3D) macroporous framework structure enabling rapid mass transfer of large biomolecules through the structures in all directions, ensuring easy access of numerous active binding sites of the chemically modified framework to the proteins and target molecules, and subsequently providing significantly increased sensitive and volume-responsive detection of target molecules in flowing through sensor systems. Promising results in direct, sandwich, and competitive ELISA tests demonstrated great application potential of the materials. Besides, an additive and simultaneous detection of two targets in one system was achieved by using different layers of the sensor materials in a flowing through filtering device. The novel biosensors are expected to significantly improve the sensitivity and broaden the applications of ELISA in rapid detections of trace amounts of toxicants in liquid and aerosol systems.

2.1 Introduction

Enzyme-linked Immunosorbent Assay (ELISA) is a common tool that can selectively and sensitively detect a variety of target analytes, such as antibodies, pesticides,

antibiotics, proteins, and pathogens[1,2,3,4]. Conventional ELISA sensors can detect hazardous chemicals in foods environment and are used in biomedical diagnosis and chemical quality controls[5,6,7]. However, certain limitations of the current ELISA sensing materials exist, including relatively high cost, lack of scalability and flexibility for personal use and simultaneous examinations of multi-target chemicals in very low concentrations, as well as dependence on specialized instrumentation[8]. As an alternative, paper-based ELISA (p-ELISA) uses fibrous and microporous platforms with advantages of increased surface areas of fibers, reduced cost, ease of use, and improved detection sensitivity[9,10,11,12,13]. However, the heterogeneous structures of papers and fibrous membranes, especially along the vertical direction, inhibit penetration of large biomolecules through the membranes, resulting in lower than the expected amount of biomolecules incorporated onto surfaces of fibers inside the media[14,15,16,17]. Such a structural feature could consequently lower the sensitivity of ELISA sensors made by nitrocellulose membranes, filter papers, and even nanofibrous membranes, resulting in inhomogeneous colorimetric signals of p-ELISA sensors[18,19,20]. Thus, an ideal media with three-dimensional homogenous and open macroporous structure that can allow large biomolecules migrate freely inside in all directions was envisioned as a better material for such ELISA biosensors. Macroporous aerogels have some 3D structural features. However, most aerogels are highly hygroscopic, causing increased non-specific adsorption of molecules and potentially high false-positive rates, together with reduced sensitivity and accuracy in applications[21]. In addition, most aerogels are not structurally macroporous in all directions, blocking large molecules from moving

freely[22,23,24].

Reticulated melamine foam (MF) is an ideal fit to the envisioned materials for biological sensors. MF has 3D uniformed pore sizes of 60~150 μm, large enough for rapid mass transfer of biomolecules within the media; proper hydrophilicity, high porosity, and high nitrogen content for various chemical modifications, enabling covalent immobilization of biomolecules for immunoassay interactions (Figure S2.1); high elasticity and excellent mechanical properties for fabricating into different filtering materials; as well as being chemically stable and nonflammable[25]. MFs have been chemically modified for a wide range of applications in water treatments, such as oil/water separation, water disinfection, adsorption, strain/stress sensing, catalysis, and so on[26,27]. However, the MF has rarely been considered as a material for biological sensors, even though it has these desired porous structures and properties suitable for serving as the immunoassay platform [28,29].

Herein, a commercially available MF was chemically modified for competitive, sandwich, and direct ELISA sensing applications. A SARS-CoV-2 spike protein, a transmembrane protein of SARS-CoV-2 virus, attached with a histidine tag, and an antibiotic, chloramphenicol (CAP), were employed as representatives of various detecting targets. The results revealed that the sensors made of the MF materials could detect SARS-CoV-2 spike protein receptor binding domain (SP-RBD-His) at 0.1 mg/L level by naked eyes, with a limit of detection (LOD) at 0.047 mg/L when supplemented by a smartphone. In the case of chloramphenicol (CAP), the sensors could detect

concentrations as low as 1 ng/mL by naked eyes and 0.096 ng/mL with smartphone assistance. The materials can be fabricated in an additive testing system to simultaneously detect two or more targets.

2.2 Experimental Section

Information on materials and chemicals, the protocol for measuring diffusion of biomolecules in the chamber through different membrane materials, and the characterization of the materials are shown in the supporting information file (2.6.1, 2.6.2, and 2.6.3).

2.2.1 Modification of melamine foam membranes

0.5 g of MF in 1 mm thick slices and 5 mm diameter circular membranes were immersed into a N, N′-disuccinimidyl carbonate (DSC) modification solution (prepared by dissolving 5 g DSC and 0.4 g triethylamine (TEA) in 100 mL of 1,4 dioxane). The mixture was stirred for two hours at 70 °C. The modified membranes (NHS@MF) were thoroughly washed with 1,4-dioxane for 15 minutes twice and with acetone for 10 minutes and vacuum dried.

2.2.2 Immobilization of proteins

The chemically modified MF membranes (NHS@MF) were immersed into His Tag monoclonal antibody with Alexa Fluor 647 (Ab-His-647) solution (200 μL) for 30min and were washed several times using a phosphate-buffered saline (PBS) buffer before the following measurements. A confocal microscope (FV 1000 system, Olympus

America) was used to observe the distribution of immobilized proteins on the membranes. Using a 60× bright field objective and 633 nm (Ar laser) excitation, 665-755 nm emission was collected for the Ab-His-647 conjugate used in this experiment[28]. The images were acquired at 640 × 640 pixels with 12.5 μs/pixel scanning speed. FTIR was employed to characterize the membrane before and after the modification and immobilization of proteins following the protocols. Fluorescent signals from Ab-His-647 conjugate were used to determine the concentration of proteins that are covalently immobilized on MF membranes according to the calibration curves (Figure S2.2).

2.2.3 NHS@MF in Direct, Sandwich, and Competitive ELISA applications

Direct and Sandwich ELISA assays were tested on the NHS@MF membranes to detect a SARS-CoV-2 spike protein receptor-binding domain with His tag (SP-RBD-His)[29]. For direct ELISA, 100 μL varied concentrations (ranging between 0 to 100 mg/L) of the SP-RBD-His were added to the NHS@MF membranes (5 mm in diameter), and an incubation lasted for 30 min under gentle agitation. Then the membrane was exposed to 3% BSA (200 μL) to block the remaining active sites on the NHS@MF. Subsequently, 100 μL of 1 mg/L His Tag monoclonal antibody HRP (Ab-His-HRP) was added to each membrane. After 20 min, the membranes were first washed with a tween-20 (0.05%) solution and then washed with the PBS buffer and dried in air. 25 μL of TMB substrate (ThermoFisher) was then applied onto the membranes, and membranes were placed in an LED lightbox (E mart). The colorimetric signal from the interaction between HRP

and TMB substrate was captured by a smartphone (iPhone 8) and analyzed using Photoshop (Adobe) software[30,31]. To take pictures of each result, the smartphone was placed over membranes at a fixed distance of 50 cm. For Sandwich ELISA, 100 μL of the 5 mg/L SARS-CoV-2 spike protein RBD recombinant human monoclonal antibody (Ab-SP) was added to the membrane platform and incubated for 30 min. Then the membrane was exposed to 200 μL of 3% skim milk to block the remaining active sites[32,33]. After the blocking step, 100 μL varied concentrations (ranging between 0 to 100 mg/L) of SP-RBD-His were added to the NHS@MF membranes, and the incubation lasted for 30 min under gentle agitation. Subsequently, 100 μL of 1 mg/L Ab-His-HRP was added to each membrane. After 20 min, the membranes were first washed with tween-20 (0.05%) and then washed with a PBS buffer and dried in air[34,35]. To obtain the outcome of colorimetric signals, the following steps were the same as in the direct ELISA.

A competitive ELISA assay was used to detect chloramphenicol (CAP) in aqueous systems, an antibiotic banned in use in the USA but is still used in other countries. First, 100 μL of 25 mg/L Anti-CAP antibody (Ab-CAP) was added to the membranes and incubated for 30 min. Then the membrane was exposed to 200 μL of 3% BSA to block the remaining active sites. After 30 min, 50 μL varied concentrations (ranging between 0 to 100 mg/L) of CAP were mixed with 50 μL of 2 mg/L CAP-labelled horseradish peroxidase (CAP-HRP) conjugate, and 100 μL of the mixed solution was then added to each membrane. After 20 min, the membranes were first washed with a tween-20 (0.05%) solution and then washed with the PBS buffer, and lastly dried in air. The

subsequent experimental steps were the same as the first two experiments. The red channel values (R value) were read by using the Photoshop color histogram. The R values were correlated to the concentrations of analytes[36]. To further investigate the dependence of the sample volumes of the materials in different types of immunoassays, the varied volumes of samples (100 μL, 500 μL, 1 mL, 2 mL) were applied to each experiment. In this study, except for the addition of varied volumes of analytes, the rest steps followed the same protocols as we mentioned above. The sample size of all experiments was 3.

2.2.4 Simultaneous detection of multiple targets

A competitive ELISA assay was used to achieve simultaneous and on-site detection of multiple targets in samples. First, 100 μL 25 mg/L Ab-CAP and anti-chlorpyrifos monoclonal antibody (Ab-CPS) were added into two different groups of NHS@MF membranes separately. Then both groups of the membranes were exposed to 3% BSA to block the remaining active sites. Afterward, one membrane from the Ab-CAP immobilized group and one membrane from the Ab-CPS immobilized group were selected and placed together into a 20 mL syringe needle as a filtration column, as shown in Figure 2.6b. The order of different layers should be remembered. Then 2 mL of a mixture of CAP and chlorpyrifos (CPS) in specific concentrations, and 40 μL of a mixture solution of CAP-HRP and chlorpyrifos HRP (CPS-HRP) in a concentration of 100 mg/L each were filled into the syringe. The filtration flow rate was controlled by a SyringeONE programmable syringe pump (NewEra Instruments, USA) with a flow rate

of 6 mL/h. Then the column was successively washed with 20 mL tween-20 (0.05%) and the PBS buffer. The membranes mounted in the syringe needles were collected separately, and 25 μL of TMB substrate (ThermoFisher) was then applied to the membranes. By analyzing the colorimetric signals obtained from the picture of a smartphone (iPhone 8), simultaneous detection of multiple targets can be achieved on-site.

2.2.5 Colorimetric data processing

When TMB was added to the membranes, the membranes were placed in an LED lightbox (E mart), and images were captured through the smartphone camera. The R channel value of the area of interest was obtained by using Photoshop software.

The red channel (R) values from RGB values represent the color intensity[19,37]. Here, the red channel intensity change could be represented by ΔRGB value, which was obtained by the RGB value difference between the white background and each membrane, as the equation of

$$\Delta RGB = RGB_{background} - RGB_{membranes} \quad (1)$$

2.2.6 Statistical analysis

All experiments were repeated three times. Data are expressed as mean ± standard deviations (SD). Intergroup comparison was analyzed by Student's t-test (two-tailed). The level of significance was defined as $*P < 0.05$, $**P < 0.01$, $***P < 0.001$.

The limit of detection (LOD) was calculated based on the standard deviation of the response and the slope using 3.3σ/S, where σ is the standard deviation of the response and S is the slope of the calibration curve.

The correlation coefficient (R) was used to measure the linear correlation between observed and predicted values. A value of $P<0.05$ was considered statistically significant. All statistical analyses were performed using GraphPad Prism 8.0.2.

2.3 Results and Discussion

2.3.1 Molecule Diffusion in Melamine Foam Membranes

Diffusion of large biomolecules in electro-spun microporous and nanofibrous membranes was proven heterogeneous and very slow in vertical directions due to the fact of layered nanofibrous mats and significantly reduced effective pore sizes[18]. The framework MF materials possess a unique 3D macroporous fibrous structure and could allow large biomolecules to penetrate through them without much resistance. A side-by-side diffusion chamber was employed to measure the transport behavior of biomolecules through different membranes (Figure 2.1a). Fluorescein isothiocyanate linked dextran (FITC-Dextran, 40 kDa) and Human IgG (HIgG) were employed as sample biomolecules to study their diffusion patterns through the MF membranes because the FITC-dextran and HIgG have similar molecular sizes as horseradish peroxidase (HRP) (~40 kDa) and immunoglobulin (~150 kDa), respectively, which are widely used in immunoassays. The concentration changes of HIgG and FITC dextran in the receiver chamber versus diffusion times of the biomolecule through MF

membranes in varied thicknesses of 1 mm to 3 mm, nanofibrous membrane (NF), and nitrocellulose paper (NP) are plotted and shown in Figure 2.1b and Figure 2.1c, respectively. With the thickness increase of the membranes from 1 mm to 3 mm, the diffusion times of HIgG to reach the steady-state diffusion slightly rose from 8 min to 10 min, while the FITC-dextran needed shorter times (6 min, 7 min, and 8 min) to reach the steady state diffusion pattern, respectively (Figure 2.1c). The large HIgG molecules showed a slower diffusion rate through the membranes. However, compared to the diffusion performances of the large biomolecules in nanofibrous membranes (PVA-co-PE) and nitrocellulose papers[18,36], which required hours to reach the steady state of diffusion, the thicknesses of membranes and sizes of biomolecules did not show any significant impact and can be ignored if the time of interaction between the MF and substrate is longer than 10 min. Thus, the open framework structure, high porosity, and large pore size of the MF allow large biomolecules to penetrate through the membranes without significant mass transfer resistance.

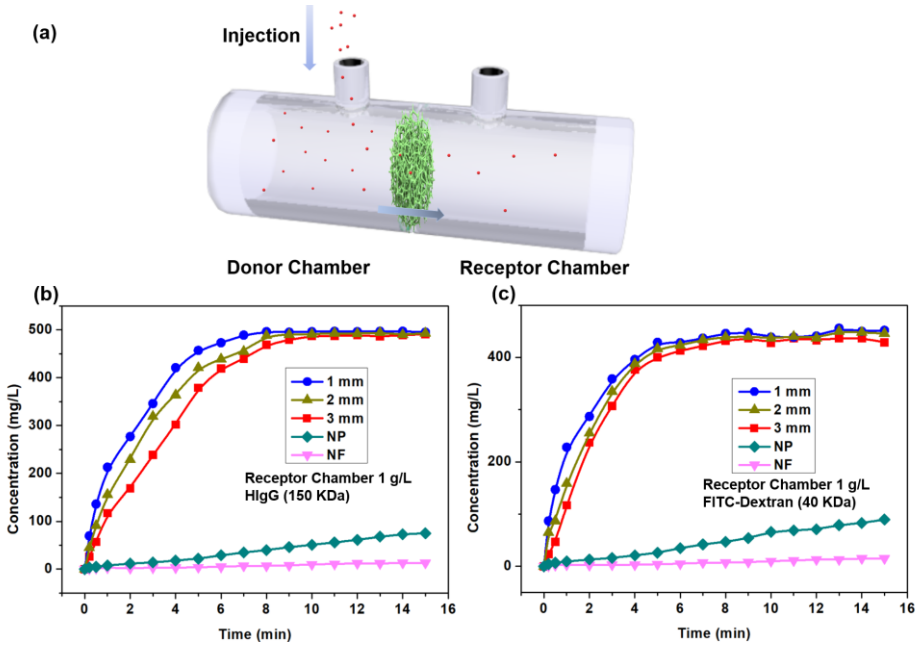

Figure 2.1. (a) Scheme of a side-by-side chamber used in this research; the correlation between time and concentration of (b) HIgG (150 kDa) and (c) FITC-Dextran (40 kDa) inside receptor chamber with NF, NP, and different thicknesses of MF membranes (1 mm, 2 mm, and 3 mm). (NF =nanofibrous membrane, thickness =0.21 mm; NP =nitrocellulose paper, thickness =0.18 mm)

2.3.2 Modification and protein immobilization on MF

The melamine foam (MF) is a framework structured material consisting of active secondary amine groups as shown in Figure S2.1. To covalently immobilize proteins on the MF, chemical modification of the secondary amino groups on the material is necessary (Figure 2.2a), which is achieved by using DSC to introduce the N-hydroxysuccinimide (NHS) functional groups on the material (NHS@MF) that can readily react with amino groups in proteins[38]. The reactions of chemical modification and protein immobilization on the MF are shown in Figure 2.2b. Fourier-transform infrared spectroscopy (FTIR) proved successful incorporations of the reactive groups (NHS) and immobilization of the protein onto the MF, based on the carbonate peak of NHS@MF at 1730 cm^{-1} and amide I peak at 1625 cm^{-1} (Figure 2.2c)[39,40,]. DSC reagent could increase the hydrophobicity of surfaces of materials such as hydrophilic PVA-co-PE NF membranes[36]. As shown in Figure 2.2d, the NHS@MF indeed showed slightly reduced hydrophilicity of the MF with the water contact angle increased to 81.3° from 0°. Despite the decrease of hydrophilicity, the liquid drop could still completely spread out on the NHS@MF membranes after around 40 seconds, and the membrane still

retains the desired hydrophilicity, which can reduce non-specific protein adsorption, promote protein diffusion through the membrane, and ease the complete removal of any unbonded substances in each step, subsequently improving sensitivity in detection of target molecules. After the immobilization of antibodies onto the NHS@MF, there was an increase in hydrophilicity, which is attributed to the inherent hydrophilic domains of the antibodies and the interactions between the protein's hydrophilic regions and water. The SEM images shown in Figure 2.2a indicate that before and after the modification and protein immobilization, the morphologies of the MF framework structures stay intact, with a pore size of around 150 μm and a fiber diameter of around 5 μm in the framework.

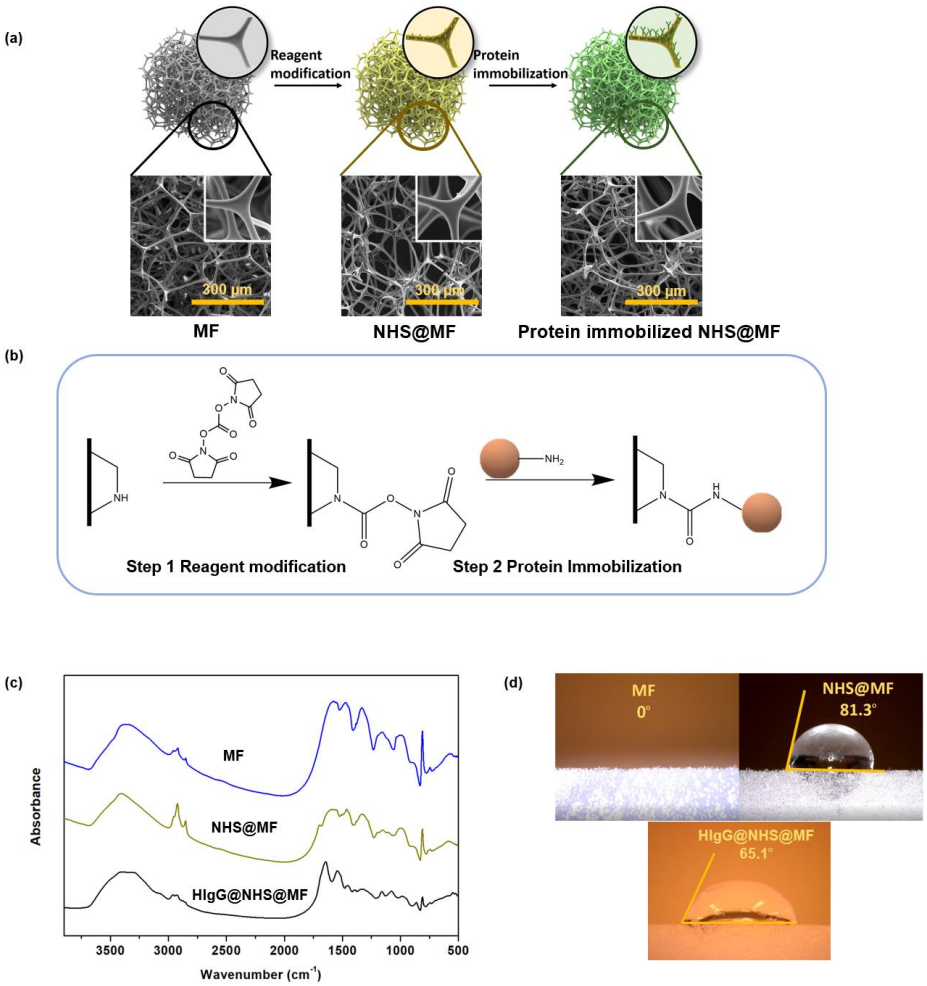

Figure 2.2. (a) Schematic illustration of the protein immobilization on NHS@MF and SEM images of MF, NHS@MF, and protein immobilized NHS@MF. (b) Reaction of MF with DSC and proteins. (c) FTIR results of MF at different steps: pristine MF, NHS@MF, and protein immobilized NHS@MF. (d) Water contact angles of MF, NHS@MF, and protein immobilized NHS@MF.

The diffusion and penetration of proteins through the framework membrane and the binding between the chemically modified surfaces of the MF and the substrate during the diffusion process could be visualized by confocal imaging. As shown in Figure 2.3a, Ab-His-647 could completely penetrate inside the NHS@MF membrane and homogeneously distribute and become immobilized on the skeleton of the entire NHS@MF membrane.

The amount of NHS immobilized on the NHS@MF was measured and compared to a nanofibrous membrane with the same area and treatment conditions (5% DSC in 100 mL 1,4-dioxane at 70 °C)[41], as nanofibers have smaller diameters and higher surface areas than nitrocellulose paper. Per a unit square meter, the NHS@MF showed a higher content of immobilized NHS groups than the nanofibrous membrane (NHS@NF) (Figure 2.3b), which was exactly as we have speculated based on structural analysis. Structurally speaking, the average diameter of the fibrous frames in MF is significantly coarse in micrometers, and the surface areas per mass should be several scales smaller than that of NF and even NP materials. However, even though the nanofibrous membranes have a higher specific surface area than that of the MF, the overlaid

nanofiber webs could be further reduced observed and measured pore sizes when the NF membranes are formed in varied thicknesses. The effective pore sizes, which are corresponding to the diffusion of molecules through the NF membranes, could be reduced to one hundredth or thousandth of the measured pore sizes in the vertical direction[18]. Such a structure is perfect for serving as filters, however, not ideal for the use as biological sensor materials, since diffusion of large biomolecules through NF, such as HIgG could be significantly reduced, leading to reduced amounts of proteins loaded onto the inside surfaces of NF membranes[19].

Different from the NF membrane materials, the MF framework structure allows diffusion and penetration of large molecules through the membranes in high speed and freedom. As demonstrated in Figure 2.1, there is no size exclusion effect in the MF. When the NHS@MF membranes were employed in the immobilization of Ab-His-647 at varied concentrations (5 mg/L, 1 mg/L, 0.5 mg/L), the amounts of the antibody used and immobilized on MF were correlating well (Figure 2.3c), indicating that the large biomolecules are homogeneously distributed in the MF membrane. Such a structural feature is quite unique for development of the biological sensors involving the use of large biomolecules and even cells. Furthermore, as shown in Figure S2.3, the loading capacity of Ab-His-647 on NHS@MF was higher than both NHS@NF and nitrocellulose paper per mass, generating more reactive sites for target molecules than the regular materials used in the p-ELISA sensors.

A direct visualization comparison test was conducted for both MF and NHS@MF in

the immobilization of antibodies[42]. 100 μL of 0.5 mg/L Ab-His-HRP solution was added onto these two membranes in the same size and thickness, respectively. Subsequent additions of TMB substrate resulted in blue color in varied intensities. Figure 2.3d shows that after thoroughly washing, the NHS@MF membranes revealed color signals with much higher intensity than that of the pristine (MF) membranes, proving the importance of the DSC modification on the MF structures for immobilization of proteins.

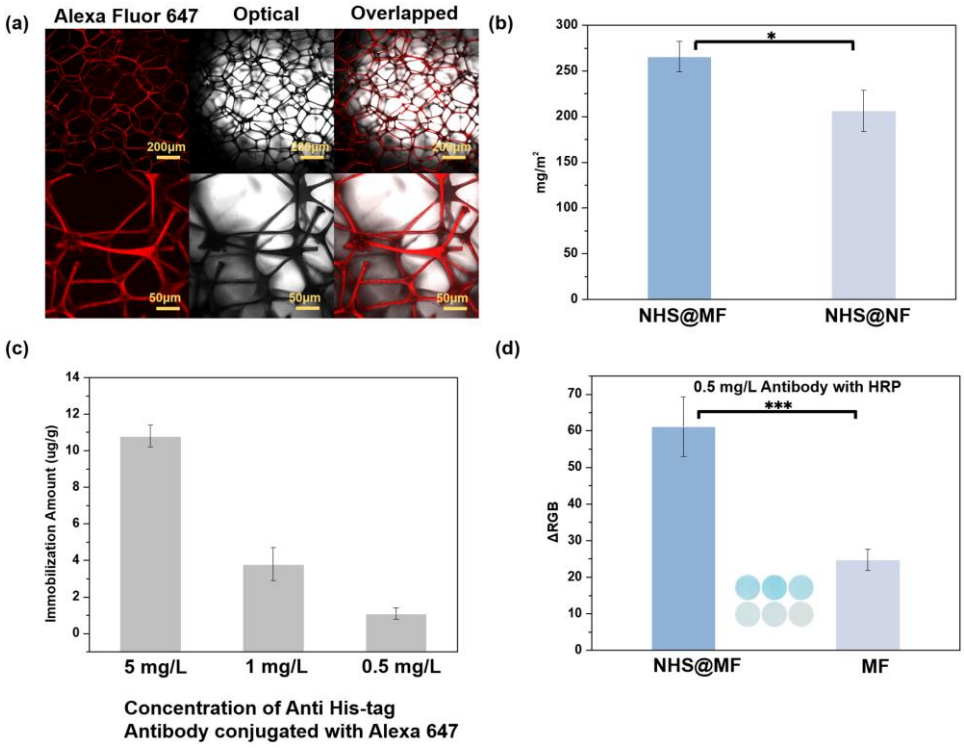

Figure 2.3. (a) Protein Immobilization distribution visualized by a laser scanning confocal microscope (lower ones are in higher magnification ratio). (b) Loaded NHS amount on NHS@MF and NHS@NF after the modification of DSC (5%). Data are presented as mean ± SD, with n = 3 independent experiments. *P < 0.05 (two-tailed

Student's t-test). (c) Immobilized antibody amounts on NHS@MF from 5 mg/L, 1 mg/L, and 0.5 mg/L of 100 μL of antibody solutions. Data are presented as mean ± SD, with n = 3 independent experiments. (d) Optical images and colorimetric signals generated from the interaction between immobilized HRP and TMB substrate on NHS@MF and pristine MF. Data are presented as mean ± SD, with n = 3 independent experiments. ***P < 0.001 (two-tailed Student's t-test).

2.3.3 Direct ELISA on the melamine foam membranes

To demonstrate the applicability of the MF as biological sensor material, direct ELISA was employed on the NHS@MF membranes. A SARS-CoV-2 spike protein receptor-binding domain with C-His tag (SP-RBD-His) in different concentrations from 0 to 100 mg/L was employed in the immobilization reaction on the NHS@MF membranes, and Ab-His-HRP was introduced to specifically bind with the immobilized protein and generate colorimetric signals from the reaction between the HRP and TMB substrate (Scheme 2.1a). To find a proper concentration of HRP and enzyme-substate reaction time, optimization experiments were conducted as shown in Table S2.1. The concentration of the Ab-His-HRP at 1 mg/L was identified as the optimal concentration and a reaction time of 5 min between the TMB substrate and HRP was chosen accordingly[43]. Besides, to demonstrate the specificity of the assay, different control assays were conducted, and the results were collected and are shown in Figure S2.4. In addition to the negative control experiments without the use of the HRP, there was no color or very low response in terms of color change in the absence of SP-RBD-His

(Figure S2.4).

To explore the sensitivity of the material in detecting target agents, a detection assay with the use of varied SP-RBD-His concentrations (0 to 100 mg/L) was conducted, and the naked-eye readable blue color signals corresponding to different concentrations of the SP-RBD-His are shown in Figure 2.4a. By examining the color intensities via the Photoshop software following the equation (1)[19], where $RGB_{background}$ is the R value of the white background (no HRP), and $RGB_{membranes}$ is R value of the NHS@MF membranes, the linear equation for the colorimetric assay was fitted as y=13.67x+2.48 (R^2=0.97) between the protein concentrations of 0.1 mg/L to 1.5 mg/L. Naked eye recognizable SP-RBD-His reached 1 mg/L level with a limit of detection (LOD) at 0.52 mg/L with the help of a smartphone and further analysis from software for the direct ELISA sensor (Figure 2.4a).

2.3.4 Sandwich and competitive ELISA on the melamine foam membranes

With these promising results in direct ELISA tests, the NHS@MF membranes were also employed in sandwich and competitive ELISAs. Again, SP-RBD-His was also used as the detecting target with a testing protocol shown in Scheme 2.1b. In the presence of the Ab-SP immobilized on the NHS@MF, the His-tag in SP-RBD-His could be recognized by the antibody[44]. Then the introduction of the Ab-His-HRP would generate colorimetric signals from the reaction between the HRP and TMB substrate as shown in Scheme 2.1b. To minimize any background signal of control groups (without primary antibodies), the type and concentration of the blocking buffers were optimized.

As shown in Figure S2.5, the colorimetric signals of the sample groups blocked with skim milk were lower than that of the groups blocked with BSA under the same treatment, while 3% skim milk presented the lowest colorimetric signal among other concentrations. Therefore, we chose skim milk (3%) as the blocking and dilution buffer in the following experiments.

To explore the sensitivity of the MF as a sandwich ELISA material, different SP-RBD-His concentrations (0 to 100 mg/L) were employed, and the naked-eye readable color signals corresponding to the concentrations of the target are shown in Figure 2.4b. By examining the intensity of colorimetric signals following the same procedure as in the direct ELISA, the linear equation for the colorimetric assay was fitted as $y=101.65x+18.03$ ($R^2=0.99$) between 0.01 mg/L to 0.20 mg/L of the protein. Naked eye recognizable SP-RBD-His concentrations reached 0.1 mg/L level with a limit of detection (LOD) at 0.047 mg/L with the help of a smartphone and further analysis from software for a sandwich ELISA sensor, which is consistent with the fact that the sandwich ELISA tests normally produce more sensitive results than that of the direct ELISA[45].

The MF was employed in competitive ELISA for quantitative detection of chloramphenicol (CAP) as well, an antibiotic used in aquacultural farming but banned in the US currently. An antibody (Ab-CAP) was immobilized on NHS@MF, and the detection procedure is schematically described in Scheme 2.1c. Different from the other two assays, an unlabeled antigen (CAP) in samples and a labeled antigen (CAP-HRP)

compete for binding to the immobilized antibody on the MF. A decrease in color signal from the MF membranes indicates the presence of the antigen in samples when compared to control groups with the labeled antigen. To explore the sensitivity of the MF in the competitive ELISA, a detection assay using different CAP concentrations (0 to 10000 ng/mL) and measuring corresponding naked-eye readable color intensities are shown in Figure 2.4c. By examining the intensity of colorimetric signals following the same procedure employed in both direct and sandwich ELISA assays, a linear equation for the colorimetric assay was fitted as $y = -122.88x + 226.13$ ($R^2 = 0.96$) between 0.01 ng/mL to 0.20 ng/mL of CAP. Naked eye recognizable CAP concentrations reached 1 ng/mL level with a limit of detection (LOD) at 0.096 ng/mL with the help of a smartphone and further analysis from the software for a competitive ELISA sensor.

Compared to literature results of other developed ELISA biosensing materials that can perform onsite detection of both Spike protein and CAP without using any specialized instruments, the NHS@MF based sensor has the advantage of high sensitivity in short testing time (Table 2.1). With the use of commercially available material, the commercial scalability and low cost make the MF more competitive and advantageous to be a new material for the development of biological sensors.

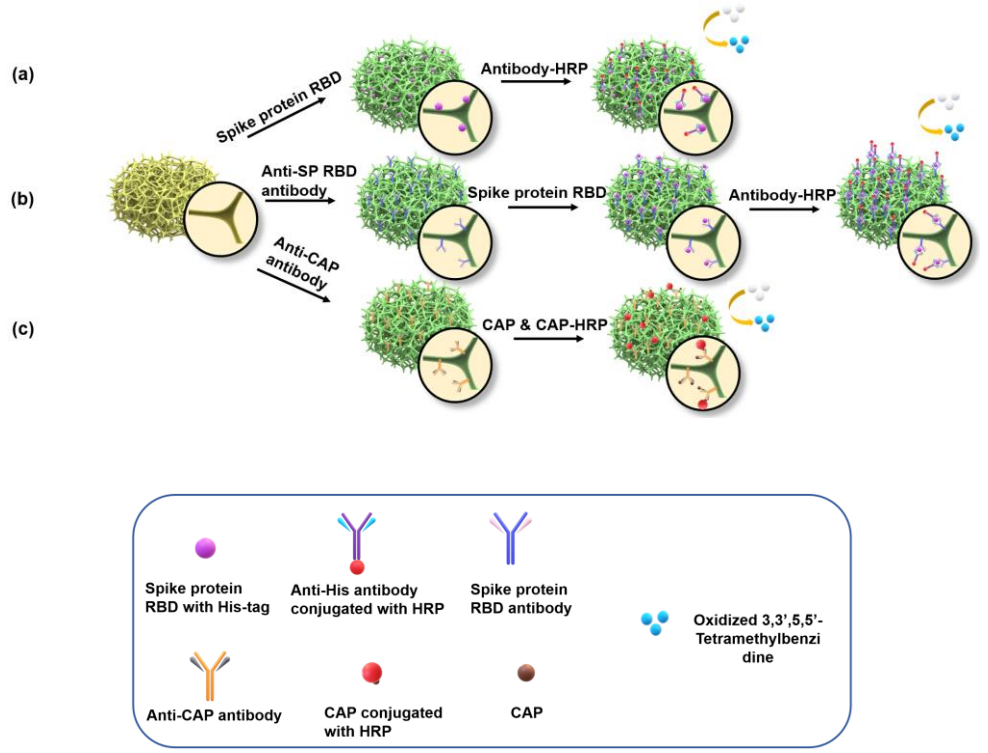

Scheme 2.1. Mechanism of NHS@MF based (a) direct ELISA, (b) sandwich ELISA, and (c) competitive ELISA.

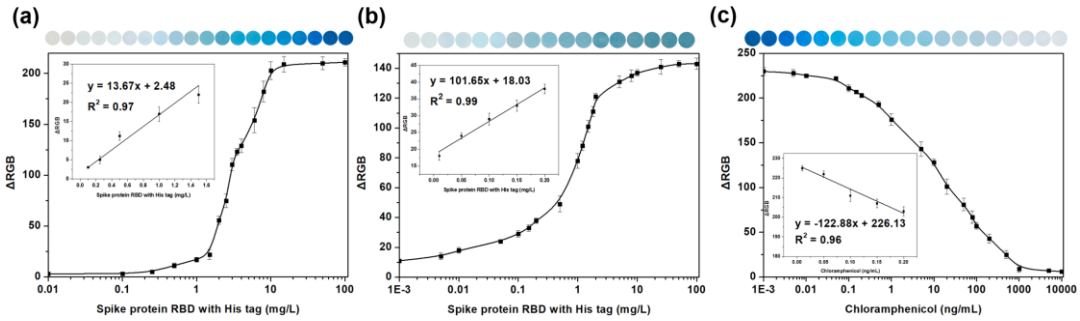

Figure 2.4. Optical images and the calibration curve of membranes in the detection of SARS-CoV-2 spike protein RBD using (a) direct ELISA approach and (b) Sandwich ELISA. (c) optical image and the calibration curve of membranes treated by varied concentrations of CAP using a competitive ELISA approach. All data are presented as mean ± SD, with n = 3 independent experiments.

2.3.5 Impact of sample volumes in immunoassays

Traditional ELISA assays use a very narrow range of sample volumes. Recently, p-ELISA managed to further scale down the volume through the miniaturization of sample sizes[46]. However, different from point-of-care clinical analysis, pollutants could be in very low concentrations in various scenarios, such as ground and surface water, treated industrial wastes, and food samples[47,48], but in abundant volumes of samples. The framework structure of the NHS@MF retains a high content of active sites (Figure 2.3b), and the MF membranes in varied thicknesses did not result in a significant increase in resistance to fluids (Figure 2.1). While increasing test sample volume could increase amounts of targets bound on the MF structure and magnify the intensity of signals, detection of trace amounts of targets could be achieved by flowing varied volumes of testing solutions through a filtering setup of the MF sensing materials. The volume responsive performances of the MF materials in three immunoassays were further investigated with target sample volumes varied in 100 μL, 500 μL, 1 mL, and 2 mL, respectively. Here, except for the added volumes of the analytes, the testing steps were the same as the protocols used in the earlier discussions. As shown in Figure 2.5a, in a direct ELISA sensing test, by changing the sample volume from 100 μL to 2 mL, the color intensities of the MF sensing material changed dramatically under varied target concentrations of 0.1 mg/L, 0.5 mg/L, and 1 mg/L of SP-RBD-His, respectively. The colorimetric sensing signal intensities of a direct ELISA sensor made of the NHS@MF showed consistent increases as the volumes of the samples in three different concentrations were raised. Higher target concentration resulted in much stronger signal

intensity, while for the very low concentration (0.1 mg/L) of SP-RBD-His, the intensity was increased coordinately with the increase of the sample volume (Figure 2.5a). Similar results were observed on the sandwich assay tests of the SP-RBD-His on the NHS@MF (Figure 2.5b) as well. In competitive ELISA tests, the signal intensity inversely changed corresponding to increased concentrations of CAP from 50 ng/mL to 200 ng/mL, respectively (Figure 2.5c). In all three types of ELISA sensing tests, increasing sample volumes led to profoundly stronger colorimetric signal differences for target concentrations respectively, demonstrating the potential in improving the sensitivity and broadening the ranges of detection limits. Compared to other sensing materials, such a unique feature of the NHS@MF allows sensors to handle varied sample volumes (Table 2.1) and potentially as a flowing through filtering sensor system for large volume target solutions.

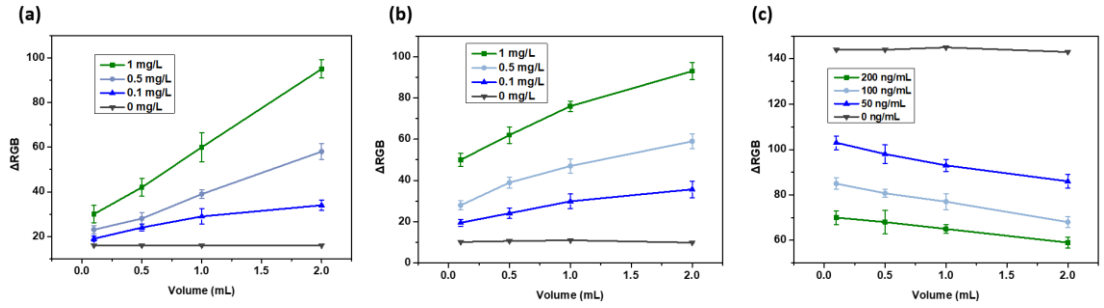

Figure 2.5. Effect of the sample volume in color signal intensities of (a) direct ELISA, (b) Sandwich ELISA, and (c) Competitive ELISA. All data are presented as mean ± SD, with n = 3 independent experiments.

Table 2.1 Comparison of colorimetric sensors for detection of SARS-CoV-2 spike protein (SP-RBD) and chloramphenicol (CAP) without employing any instrument.

Target	Sensing Materials	Capture reagent	Assay/Signal	Sample volume	Time (min)	LOD*	Ref.
SP RBD	Nitrocellulose paper	N-acetyl neuraminic acid	LFIA/Color/ naked eye	50 µL	30	5 mg/L	51
	Nitrocellulose membrane	Glycopolymers	LFIA/Color/ naked eye	25 µL	25	3.1 mg/L	52
	Nitrocellulose membrane	Cellular receptor (ACE2)	LFIA/Color/ phone	100 µL	30	0.5 mg/L	53
	NHS@MF	NA	ELISA/Color/ phone	100 µL-2 mL	90	0.52 mg/L	This work
	NHS@MF	Anti-spike protein antibody	ELISA/Color/ phone	100 µL-2 mL	60	0.047 mg/L	This work
CAP	Nitrocellulose membranes	Anti-CAP antibody	ELISA/Color/ Scanner	2 mL	10	0.3 ng/mL	54
	Cellulose Paper discs	LacZ DNA	ELISA/Color/ Scanner	2 µL	120	100 ng/mL	55
	96 well plates	Anti-CAP antibody	ELISA/color/ phone	100 µL	2.5 h	10 ng/mL	36
	Nitrocellulose membranes	Anti-CAP antibody	ELISA/Color/ phone	100 µL	45	1 ng/mL	36
	Nanofibrous membranes	Anti-CAP antibody	ELISA/Color/ phone	100 µL	45	0.1 ng/mL	36
	NHS@MF	Anti-CAP antibody	ELISA/Color/ phone	100µL-2 mL	40	0.096 ng/mL	This work

*LOD =Limit of detection *LFIA =Lateral flow immunochromatographic assays

2.3.6 Simultaneous detection of multiple targets

The structural features of the MF membranes also provide potential in additive sensing of multiple targets simultaneously in a flowing through filtering sensor system. As illustrated in Figure 2.6a, antibodies (Ab-CAP and Ab-CPS) of CAP and CPS were immobilized on two different NHS@MF membranes, respectively. After blocking with

the BSA buffer, these two membranes (5 mm in diameter) were mounted into a syringe needle pocket as a filtering sensing device, and 2 mL of a mixture of CAP and CPS in varied concentrations, together with CAP-HRP and CPS-HRP in a concentration of 1 mg/L each, was filled into a 20 mL syringe and flow through the filtering needle with a flow rate of 6 mL/h, controlled by a SyringeONE programmable syringe pump (NewEra Instruments, USA) (Figure 2.6b). As shown in Figure 2.6c, nine groups of the sample mixtures were tested and collected through the sensing device following the varied concentrations of CAP and CPS in Figure 2.6c. The intensity of the colorimetric signals of the first-layer membranes showed an increasing trend, and that of the second-layer membranes showed a decreasing trend, indicating that simultaneous detection of CAP and CPS could be achieved without any interference of the two targets in the same system, an advantage of potential additive detection of multiple targets in one system. The total testing time was less than 40 min from running the sample liquid through the sensor to the completion of tests.

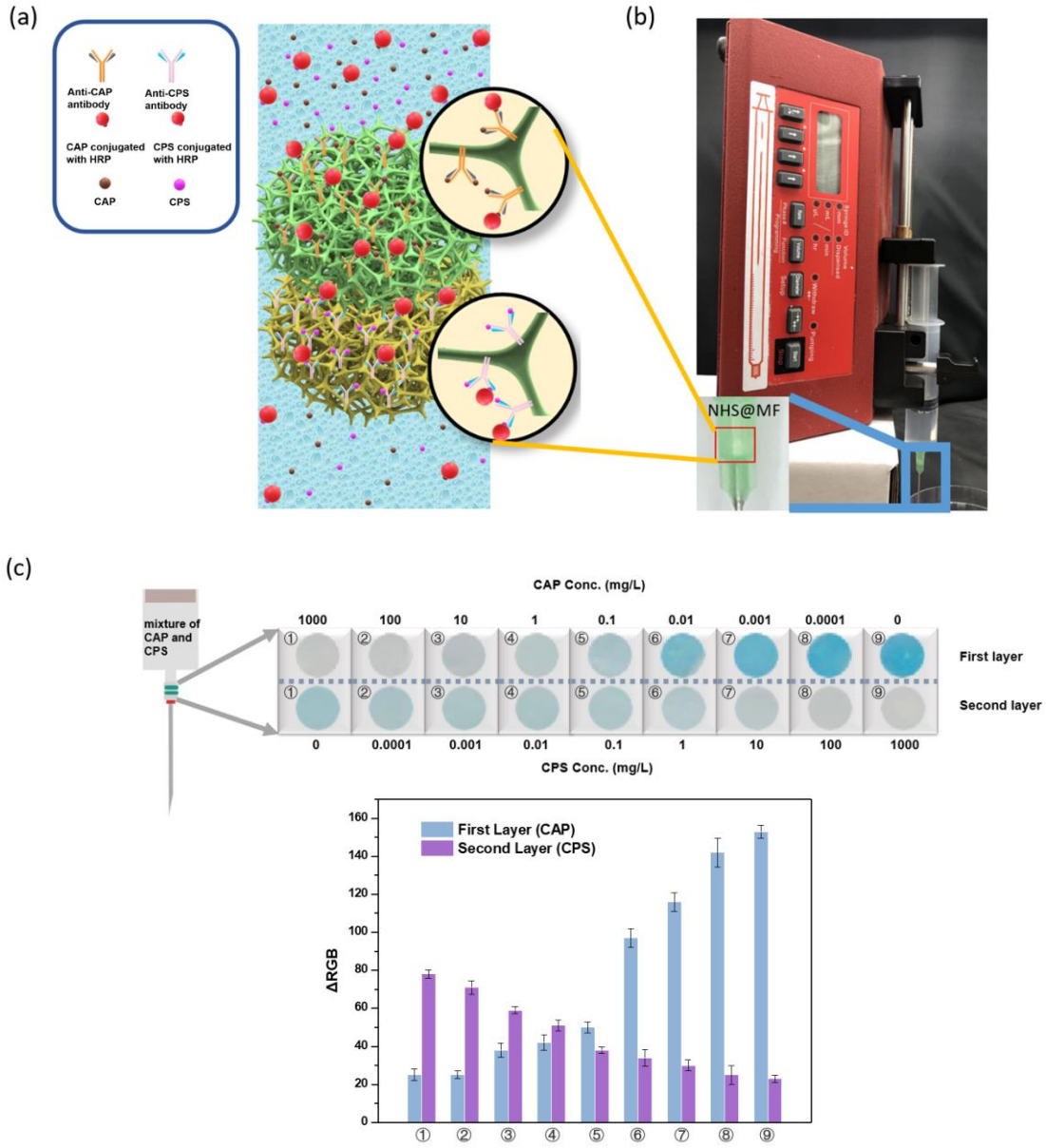

Figure 2.6. (a) Schematic illustration of the mechanism of simultaneous multiple on-site targets detection. (b) Photograph demonstrated the fast-flow device driven by a syringe pump. (c) Optical image and ΔRGB values of membranes treated by the mixture of varied concentrations of CAP and CPS using a competitive ELISA approach. All data are presented as mean ± SD, with n = 3 independent experiments.

2.4 Conclusions

Unique rapid, sensitive, additive, and volume responsive colorimetric sensor materials were fabricated from using chemically modified framework melamine foam (MF), which can be applied in competitive, direct, and sandwich ELISA biosensors. The MF sensor materials demonstrated promising detection sensitivity to a SARS-CoV-2 spike protein with histidine tag (SP-RBD-His), a transmembrane protein of the SARS-CoV-2 virus, and chloramphenicol (CAP), often used as an antibiotic. Naked eye recognizable SP-RBD-His reached a 1 mg/L level with a limit of detection (LOD) at 0.52 mg/L when supplemented by a smartphone for the direct ELISA sensor. In the case of the sandwich ELISA sensor, it's capable of detecting SP-RBD-His at a concentration of 0.1 mg/L by the naked eye and can reduce the LOD to as low as 0.047 mg/L with the help of a smartphone. In addition, using a competitive ELISA, chloramphenicol (CAP) can be detected at 1 ng/mL level with the naked eye and at 0.096 ng/mL with the help of a smartphone. Moreover, due to the excellent mechanical properties and framework structure of the MF, diffusion of the analyte through the different membrane layers is fast and homogeneous in all directions, making the MF suitable for the simultaneous detection of trace amounts of two or more targets in samples with large volumes in one integrated system. The successful fabrication of such sensor materials is expected to improve the sensitivity and broaden the applications of ELISA sensors for onsite and personal uses.

2.5 Reference

1. Reen, D. J. (1994). Enzyme-linked immunosorbent assay (ELISA). Basic Protein and Peptide Protocols, 461-466.

2. Mungroo, N. A., & Neethirajan, S. (2014). Biosensors for the detection of antibiotics in poultry industry—a review. *Biosensors*, *4*(4), 472-493.

3. Salimi-Bejestani, M. R., McGarry, J. W., Felstead, S., Ortiz, P., Akca, A., & Williams, D. J. (2005). Development of an antibody-detection ELISA for Fasciola hepatica and its evaluation against a commercially available test. *Research in veterinary science*, *78*(2), 177-181.

4. Gascon, J., Oubiña, A., & Barceló, D. (1997). Detection of endocrine-disrupting pesticides by enzyme-linked immunosorbent assay (ELISA): application to atrazine. *TrAC Trends in Analytical Chemistry*, *16*(10), 554-562.

5. Conti, G. O., Copat, C., Wang, Z., D'Agati, P., Cristaldi, A., & Ferrante, M. (2015). Determination of illegal antimicrobials in aquaculture feed and fish: an ELISA study. *Food Control*, *50*, 937-941.

6. Iha, K., Inada, M., Kawada, N., Nakaishi, K., Watabe, S., Tan, Y. H., Shen, C., Ke, L.-Y., Yoshimura, T., & Ito, E. (2019). Ultrasensitive ELISA developed for diagnosis. *Diagnostics*, *9*(3), 78.

7. Lee, J. K., Ahn, K. C., Park, O. S., Kang, S. Y., & Hammock, B. D. (2001). Development of an ELISA for the detection of the residues of the insecticide imidacloprid in agricultural and environmental samples. *Journal of Agricultural and Food Chemistry*, *49*(5), 2159-2167.

8. Hay Burgess, D. C., Wasserman, J., & Dahl, C. A. (2006). Global health diagnostics. *Nature*, *444*(1), 1-2.

9. Cheng, C.-M., Martinez, A. W., Gong, J., Mace, C. R., Phillips, S. T., Carrilho, E., Mirica, K. A., & Whitesides, G. M. (2010). Paper-based ELISA. *Angewandte Chemie International Edition*, *49*(28), 4771-4774.

10. Mabey, D., Peeling, R. W., Ustianowski, A., & Perkins, M. D. (2004). Diagnostics for the developing world. *Nature Reviews Microbiology*, *2*(3), 231-240.

11. Liu, X. Y., Cheng, C. M., Martinez, A. W., Mirica, K. A., Li, X. J., Phillips, S. T., Mascareñas, M., & Whitesides, G. M. (2011). A portable microfluidic paper-based device for ELISA. In *2011 IEEE 24th international conference on micro electro mechanical systems*, pp. 75-78. IEEE, 2011.

12. Yager, P., Edwards, T., Fu, E., Helton, K., Nelson, K., Tam, M. R., & Weigl, B. H. (2006). Microfluidic diagnostic technologies for global public health. *Nature*, *442*(7101), 412-418.

13. Yager, P., Domingo, G. J., & Gerdes, J. (2008). Point-of-care diagnostics for global health. *Annu. Rev. Biomed. Eng.*, *10*, 107-144.

14. Hahn, R., Bauerhansl, P., Shimahara, K., Wizniewski, C., Tscheliessnig, A., & Jungbauer, A. (2005). Comparison of protein A affinity sorbents: II. Mass transfer properties. *Journal of Chromatography A*, *1093*(1-2), 98-110.

15. Garcia-Galan, C., Berenguer-Murcia, Á., Fernandez-Lafuente, R., & Rodrigues, R. C. (2011). Potential of different enzyme immobilization strategies to improve enzyme performance. *Advanced Synthesis & Catalysis*, *353*(16), 2885-2904.

16. Cannell, D. S., & Rondelez, F. (1980). Diffusion of polystyrenes through microporous membranes. *Macromolecules*, *13*(6), 1599-1602.

17. Davidson, M. G., & Deen, W. M. (1988). Hindered diffusion of water-soluble macromolecules in membranes. *Macromolecules*, *21*(12), 3474-3481.

18. Zhao, C., Si, Y., Zhu, S., Bradley, K., Taha, A. Y., Pan, T., & Sun, G. (2021).

Diffusion of protein molecules through microporous nanofibrous polyacrylonitrile membranes. *ACS applied polymer materials*, *3*(3), 1618-1627.

19. Zhao, C., Pan, B., Wang, M., Si, Y., Taha, A. Y., Liu, G., Pan, T., & Sun, G. (2022). Improving the sensitivity of nanofibrous membrane-based ELISA for on-site antibiotics detection. *ACS Sensors, 7*(5), 1458-1466.

20. Yao, Y., & Lenhoff, A. M. (2006). Pore size distributions of ion exchangers and relation to protein binding capacity. *Journal of Chromatography A*, *1126*(1-2), 107-119.

21. Jung, I. Y., Kim, J. S., Choi, B. R., Lee, K., & Lee, H. (2017). Hydrogel based biosensors for in vitro diagnostics of biochemicals, proteins, and genes. *Advanced healthcare materials*, *6*(12), 1601475.

22. Power, M., Hosticka, B., Black, E., Daitch, C., & Norris, P. (2001). Aerogels as biosensors: viral particle detection by bacteria immobilized on large pore aerogel. *Journal of Non-Crystalline Solids*, *285*(1-3), 303-308.

23. Fang, L. X., Huang, K. J., & Liu, Y. (2015). Novel electrochemical dual-aptamer-based sandwich biosensor using molybdenum disulfide/carbon aerogel composites and Au nanoparticles for signal amplification. *Biosensors and Bioelectronics*, *71*, 171-178.

24. Gao, K., Guo, Y., Niu, Q., Fang, H., Zhang, L., Zhang, Y., Wang, L., & Zhou, L. (2018). Effects of chitin nanofibers on the microstructure and properties of cellulose nanofibers/chitin nanofibers composite aerogels. *Cellulose, 25*(12), 4591-4602.

25. Feng, Y., & Yao, J. (2018). Design of melamine sponge-based three-dimensional porous materials toward applications. *Industrial & Engineering Chemistry Research*, *57*(22), 7322-7330.

26. Oribayo, O., Feng, X., Rempel, G. L., & Pan, Q. (2017). Modification of

formaldehyde-melamine-sodium bisulfite copolymer foam and its application as effective sorbents for clean up of oil spills. *Chemical Engineering Science*, *160*, 384-395.

27. Stolz, A., Le Floch, S., Reinert, L., Ramos, S. M. M., Tuaillon-Combes, J., Soneda, Y., Chaudet, P., Baillis, D., Blanchard, N., Duclaux, L., & San-Miguel, A. (2016). Melamine-derived carbon sponges for oil-water separation. *Carbon, 107*, 198-208.

28. Smith, C. L. (2011). Basic confocal microscopy. *Current protocols in neuroscience*, *56*(1), 2-2.

29. Lan, J., Ge, J., Yu, J., Shan, S., Zhou, H., Fan, S., Zhang, Q., Shi, X., Wang, Q., Zhang, L., & Wang, X. (2020). Structure of the SARS-CoV-2 spike receptor-binding domain bound to the ACE2 receptor. *Nature, 581*(7807), 215-220.

30. Alkasir, R. S., Rossner, A., & Andreescu, S. (2015). Portable colorimetric paper-based biosensing device for the assessment of bisphenol A in indoor dust. *Environmental Science & Technology*, *49*(16), 9889-9897.

31. Jia, M. Y., Wu, Q. S., Li, H., Zhang, Y., Guan, Y. F., & Feng, L. (2015). The calibration of cellphone camera-based colorimetric sensor array and its application in the determination of glucose in urine. *Biosensors and Bioelectronics*, *74*, 1029-1037.

32. Plested, J. S., Coull, P. A., & Gidney, M. A. J. (2003). Elisa. *Haemophilus influenzae Protocols*, 243-261.

33. Kim, W. S., Nishizawa, T., & Yoshimizu, M. (2007). Non-specific adsorption of fish immunoglobulin M (IgM) to blocking reagents on ELISA plate wells. *Diseases of aquatic organisms*, *78*(1), 55-59.

34. Steinitz, M. (2000). Quantitation of the blocking effect of tween 20 and bovine serum albumin in ELISA microwells. *Analytical biochemistry*, *282*(2), 232-238.

35. Julián, E., Cama, M., Martínez, P., & Luquin, M. (2001). An ELISA for five glycolipids from the cell wall of Mycobacterium tuberculosis: Tween 20 interference in the assay. *Journal of immunological methods*, *251*(1-2), 21-30.

36. Zhao, C., Si, Y., Pan, B., Taha, A. Y., Pan, T., & Sun, G. (2020). Design and fabrication of a highly sensitive and naked-eye distinguishable colorimetric biosensor for chloramphenicol detection by using ELISA on nanofibrous membranes. *Talanta*, *217*, 121054.

37. Murdock, R. C., Shen, L., Griffin, D. K., Kelley-Loughnane, N., Papautsky, I., & Hagen, J. A. (2013). Optimization of a paper-based ELISA for a human performance biomarker. *Analytical chemistry*, *85*(23), 11634-11642.

38. Hermanson, G. T. (2013). *Bioconjugate techniques*. Academic press.

39. Rehman, I., & Bonfield, W. J. J. (1997). Characterization of hydroxyapatite and carbonated apatite by photo acoustic FTIR spectroscopy. *Journal of materials science: Materials in medicine*, *8*(1), 1-4.

40. Kong, J., & Yu, S. (2007). Fourier transform infrared spectroscopic analysis of protein secondary structures. *Acta biochimica et biophysica Sinica*, *39*(8), 549-559.

41. Zhu, J., & Sun, G. (2015). Bio-functionalized nanofibrous membranes as a hybrid platform for selective antibody recognition and capturing. *RSC Advances*, *5*(36), 28115-28123.

42. Ahluwalia, A., De Rossi, D., Ristori, C., Schirone, A., & Serra, G. (1992). A comparative study of protein immobilization techniques for optical immunosensors. *Biosensors and Bioelectronics*, *7*(3), 207-214.

43. Chen, C. A., Yeh, W. S., Tsai, T. T., & Chen, C. F. (2019). Three-dimensional origami paper-based device for portable immunoassay applications. *Lab on a Chip*, *19*(4), 598-607.

44. Pogge von Strandmann, E., Zoidl, C., Nakhei, H., Holewa, B., Pogge von Strandmann, R., Lorenz, P., Klein-Hitpaß, L., & Ryffel, G. U. (1995). A highly specific and sensitive monoclonal antibody detecting histidine-tagged recombinant proteins. *Protein Engineering, 8*(7), 733-735.

45. Hnasko, R. (Ed.). (2015). *Elisa* (pp. 43-50). New York, NY, USA: Humana Press.

46. Huang, L., Xiao, W., Xu, T., Chen, H., Jin, Z., Zhang, Z., Song, Q., & Tang, Y. (2021). Miniaturized paper-based smartphone biosensor for differential diagnosis of wild-type pseudorabies virus infection versus vaccination immunization. *Sensors and Actuators B: Chemical*, *327*, 128893.

47. Zhang, P., Chen, Y. P., Wang, W., Shen, Y., & Guo, J. S. (2016). Surface plasmon resonance for water pollutant detection and water process analysis. *TrAC Trends in Analytical Chemistry*, *85*, 153-165.

48. El-Moghazy, A. Y., Zhao, C., Istamboulie, G., Amaly, N., Si, Y., Noguer, T., & Sun, G. (2018). Ultrasensitive label-free electrochemical immunosensor based on PVA-co-PE nanofibrous membrane for the detection of chloramphenicol residues in milk. *Biosensors and Bioelectronics*, *117*, 838-844.

51. Baker, A. N., Richards, S.-J., Guy, C. S., Congdon, T. R., Hasan, M., Zwetsloot, A. J., Gallo, A., Lewandowski, J. R., Stansfeld, P. J., Straube, A., Walker, M., Chessa, S., Pergolizzi, G., Dedola, S., Field, R. A., & Gibson, M. I. (2020). The SARS-CoV-2 spike protein binds sialic acids and enables rapid detection in a lateral flow point of care diagnostic device. *ACS Central Science, 6*(11), 2046-2052.

52. Kim, S. H., Kearns, F. L., Rosenfeld, M. A., Casalino, L., Papanikolas, M. J., Simmerling, C., E.Amaro, R., & Freeman, R. (2021). GlycoGrip: Cell surface-inspired universal sensor for betacoronaviruses. *ACS Central Science*, 8(1), 22-42.

53. Lee, J. H., Choi, M., Jung, Y., Lee, S. K., Lee, C. S., Kim, J., Kim, N. H., Kim, B., & Kim, H. G. (2021). A novel rapid detection for SARS-CoV-2 spike 1 antigens using human angiotensin converting enzyme 2 (ACE2). *Biosensors and Bioelectronics*, *171*, 112715.

54. Byzova, N. A., Zvereva, E. A., Zherdev, A. V., Eremin, S. A., & Dzantiev, B. B. (2010). Rapid pretreatment-free immunochromatographic assay of chloramphenicol in milk. *Talanta*, *81*(3), 843-848.

55. Duyen, T. T. M., Matsuura, H., Ujiie, K., Muraoka, M., Harada, K., & Hirata, K. (2017). based colorimetric biosensor for antibiotics inhibiting bacterial protein synthesis. *Journal of bioscience and bioengineering*, *123*(1), 96-100.

2.6 Supporting Information

2.6.1 Chemicals and materials

N, N'-disuccinimidyl carbonate (DSC), triethylamine (TEA), 1,4-dioxane, acetone, phosphate-buffered saline (PBS), chlorpyrifos polyclonal antibody, pierce BCA protein assay kit, nitrocellulose paper, and 96-well plates were purchased from ThermoFisher Scientific. A SARS-CoV-2 spike protein receptor-binding domain with C-His tag (SP-RBD-His) was purchased from Sino Biological. Chloramphenicol (CAP), Chlorpyrifos (CPS) solution, human immunoglobulin G (HIgG), and fluorescein isothiocyanate (FITC) linked dextran (FITC-Dextran, 40 kDa) were purchased from Sigma-Aldrich. Anti-CAP antibody (Ab-CAP) and CAP-labelled horseradish peroxidase (CAP-HRP) were purchased from Abcam (Cambridge, MA, USA). Anti-chlorpyrifos monoclonal antibody (Ab-CPS) and chlorpyrifos (HRP) (CPS-HRP) were purchased from CD Creative Diagnostics. 6x-His Tag Monoclonal Antibody (HIS.H8) Alexa Fluor 647 (Ab-His-647), 6x-His Tag Monoclonal Antibody (HIS.H8) HRP (Ab-His-HRP) and SARS-CoV-2 Spike Protein (RBD) Recombinant Human Monoclonal Antibody (Ab-SP) were purchased from Thermo Fisher. Melamine foams were purchased from Swisstek (Swisstek Manufacturer).

2.6.2 Measurement of diffusion of biomolecules in MF

Diffusions of the dextran (FITC-Dextran, 40 kDa) and Human IgG (HIgG, 150 kDa) in the melamine foam (MF) of different thicknesses were measured by using a side-by-side diffusion chamber (PermeGear Co.), consisting of two 3.4 mL chambers (donator

chamber and receptor chamber) with a 9 mm orifice. Nanofibrous membrane (NF) , nitrocellulose paper (NP), and MF membranes with different thicknesses (1mm, 2mm, 3mm) were placed between the two chambers separately, and the chambers were tightly sealed and placed in a water bath to maintain a temperature at 25 °C. To prewet the membranes, 3 mL of a PBS solution was added to each chamber individually for 15 min. Then, 0.3 mL of a solution (10 g/L of Dextran-FITC or HIgG in PBS buffer) was injected into the donor chamber. Throughout the tests, stirring bars were placed in both chambers at a speed of 750 rpm. At regular time intervals, 50 μL of the sample solution was taken from each chamber and replaced with the same amount of PBS buffer solution for 15 min. The concentrations of the FITC-Dextran and HIgG can be obtained with a microplate reader (SpectraMax iD3 multi-Mode) according to calibration curves shown in the supporting information (Figure S2.2). Then, the protein concentration in the receptor chamber at increasing time periods can be utilized to determine the diffusion properties of the biomolecules through the MF membranes.

2.6.3 Characterizations

The morphologies of the MF before and after the modification were observed by a scanning electron microscope (Quattro ESEM, Thermo Scientific). The thickness of the MF membranes was measured through an electronic micrometer thickness gauge (Neoteck). The amount of NHS on the DSC modified MF (NHS@MF) membrane was measured by following a BCA protocol. After drying in a vacuum oven for 10 min, the membrane was placed in 1 mL of a working solution prepared by mixing 50-parts

bicinchoninic acid (BCA) reagent A with 1-part Cu_2SO_4 reagent B.

The NHS amount can be obtained with a micro-plate reader by calibration curves, as shown in Figure S2.2.

2.6.4. Chemical structure of melamine foam and SEM-EDS results

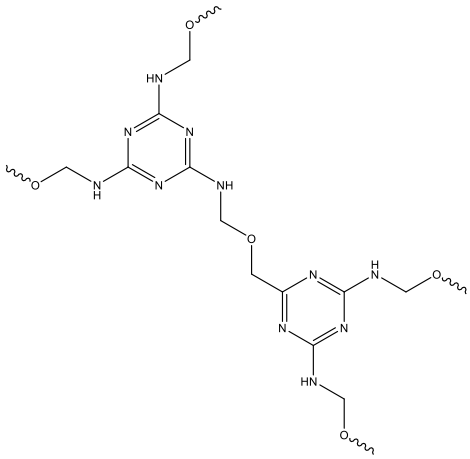

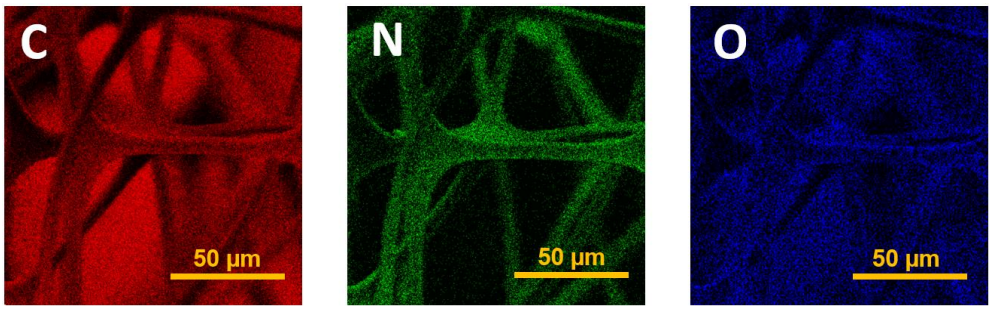

Figure S2.1. Chemical structure of melamine foam and SEM-EDS results

2.6.5. Calibration curves of FITC-dextran, HIgG, NHS group, and an antibody conjugated with fluor Alexa 647

(a)

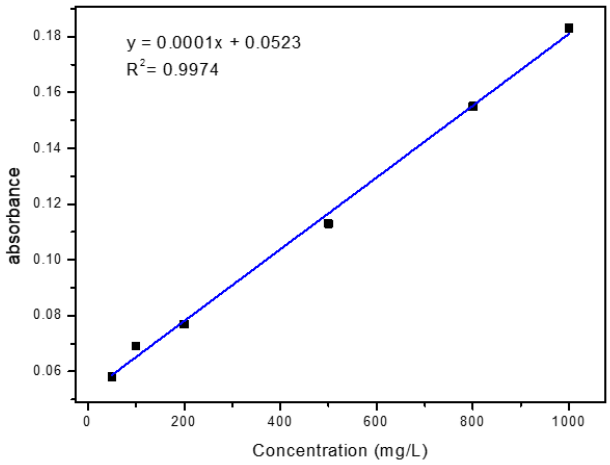

(b)

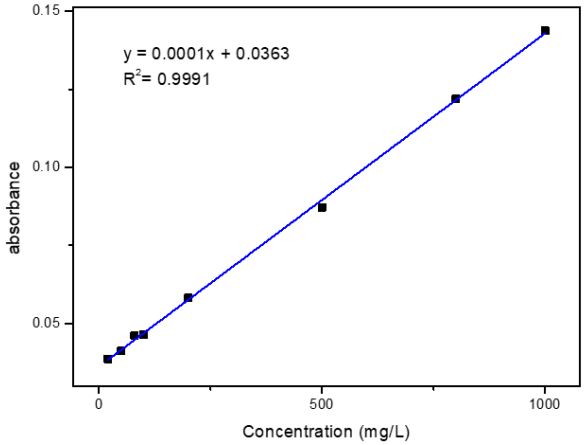

(c)

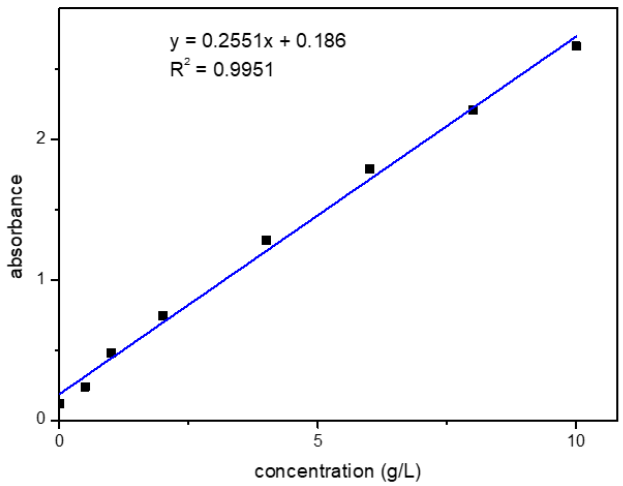

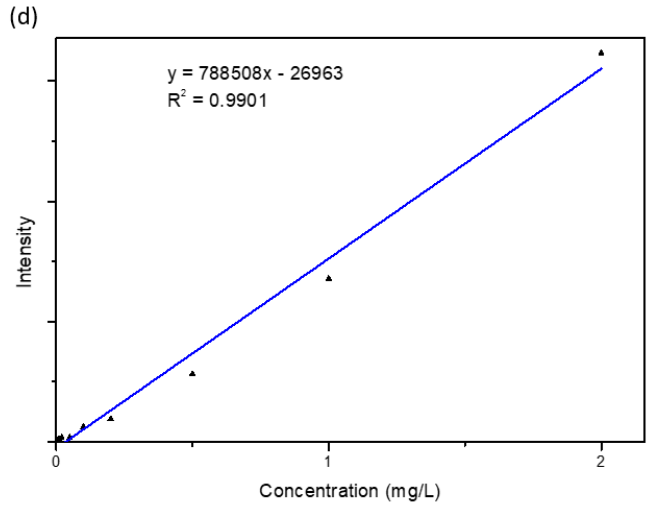

Figure S2.2. Calibration curves for (a) HIgG, (b) FITC-dextran, (c) NHS, and (d) an antibody conjugated with Alexa 647

2.6.6 Comparison of immobilized antibodies on MF, NF, and NP

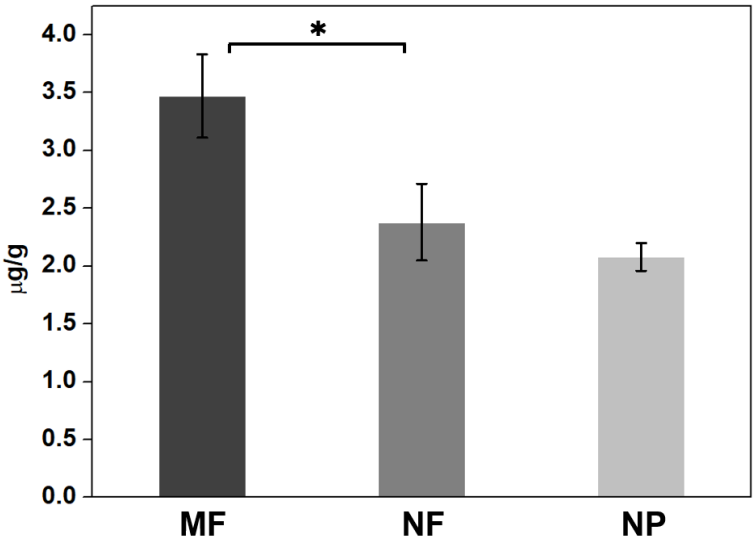

Figure S2.3. Immobilized antibody amounts on NHS@MF, NHS@NF, and nitrocellulose paper (NP) from 1 mg/L of 100 µL of antibody solution. Data are presented as mean ± SD, with n = 3 independent experiments. *P < 0.05 (two-tailed Student's t-test).

2.6.7 Optimization experiments for direct ELISA sensor

100 μL of the SP-RBD-His in a concentration of 5 mg/L were added to the NHS@MF membranes and incubated for 30 min under gentle agitation; the membranes of the control groups were immersed in PBS during the incubation. Then the membranes were exposed to 3% BSA (200 μL) to block the remaining active sites. Subsequently, 100 μL of Ab-HIS-HRP with different concentrations ranging from 0.1 mg/L to 2 mg/L were added to the membranes, respectively. After 20 min, the membranes were first washed with tween-20 (0.05%) and then washed with PBS buffer and dried in air. 25 μL of TMB substrate (ThermoFisher) was then applied onto the membranes, and membranes were placed in an LED lightbox (E mart). The colorimetric signal from the interaction between HRP and TMB substrate was captured by a smartphone (iPhone 8) and analyzed using Photoshop (Adobe) software. The difference of ΔRGB values between the sample (2 mg/L SP-RBD-His) and control (no SP-RBD-His) groups with the treatment of varied concentrations of Ab-HIS-HRP were recorded in Table S2.1 along with different reaction times between the TMB substrate and HRP.

Table S2.1. Data from the optimization tests for HRP concentrations and reaction times between HRP and TMB substrate.

Concentration / Time (min)	2 mg/L	1 mg/L	0.75 mg/L	0.5 mg/L	0.25 mg/L	0.1 mg/L
1	152.04	141.36	93.49	92.61	60.97	28.12
5	122.94	161.13	158.99	154.24	142.09	119.11
10	109.14	132.33	142.11	144.65	150.67	150.65
15	78.94	99.69	129.48	136.86	145.66	149.88
20	69.01	88.44	119.46	130.35	147.13	154.04

2.6.8 Specificity of the assay

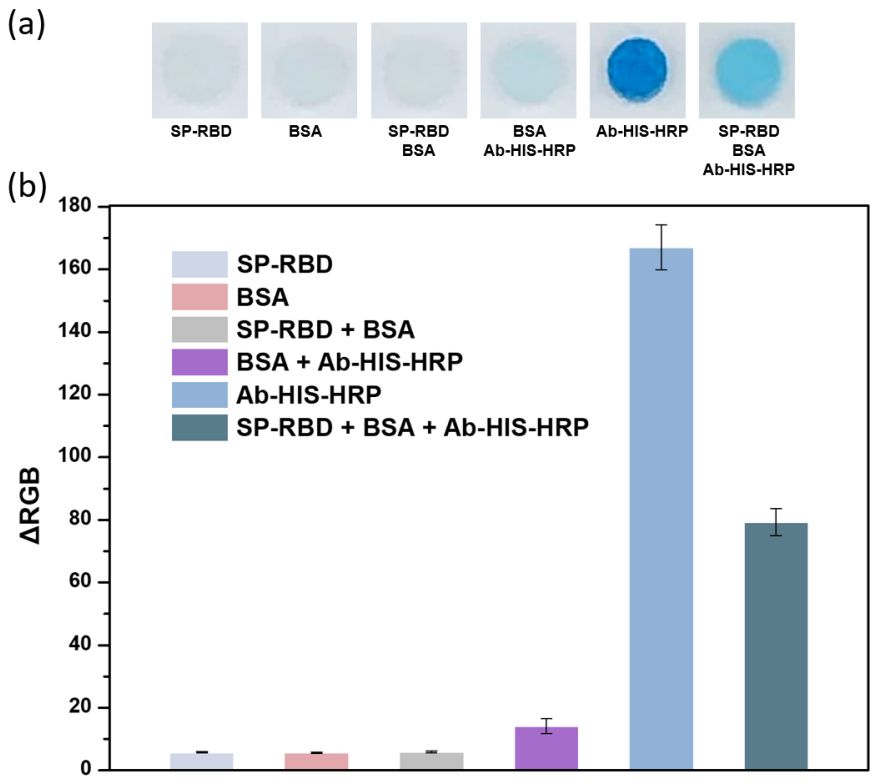

Figure S2.4. Specificity of the assay. (a) Images of the NHS@MF membranes with different treatments after the addition of TMB substrate: 100 µL SP-RBD-His (2 mg/L); 200 µL BSA (3%); 100 µL SP-RBD-His (2 mg/L), and then 200 µL BSA (3%); 200 µL BSA (3%) and then 100 µL Ab-HIS-HRP (1 mg/L); 100 µL Ab-HIS-HRP (1 mg/L); 100 µL SP-RBD-His (2 mg/L), 200 µL BSA (3%), and then 100 µL Ab-HIS-HRP (1 mg/L). (b) The bar diagram for the ΔRGB observed from the images. Data are presented as mean ± SD, with n = 3 independent experiments.

2.6.9 Optimization of the type and concentration of the blocking buffer

The NHS@MF membranes were exposed to 1%, 3%, and 5% BSA solution and 1%, 3%, and 5% skim milk solution, respectively. The membranes were then immersed into 10 mg/L SP-RBD-His for 20 min and then exposed to 1 mg/L Ab-HIS-HRP under

gentle agitation for 20 min subsequently. The results were then collected after several times washing with the PBS buffer.

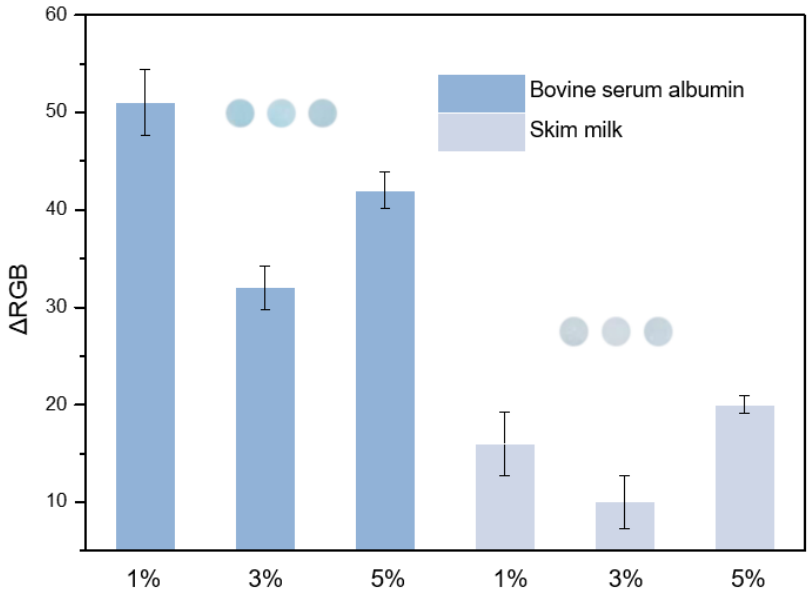

Figure S2.5. Blocking optimization. Optical images and the intensity of colorimetric signals of 1%, 3%, 5% BSA treated membranes and 1%, 3%, 5% skim milk treated membranes. Data are presented as mean ± SD, with n = 3 independent experiments.

2.6.10 Optical image without cropping

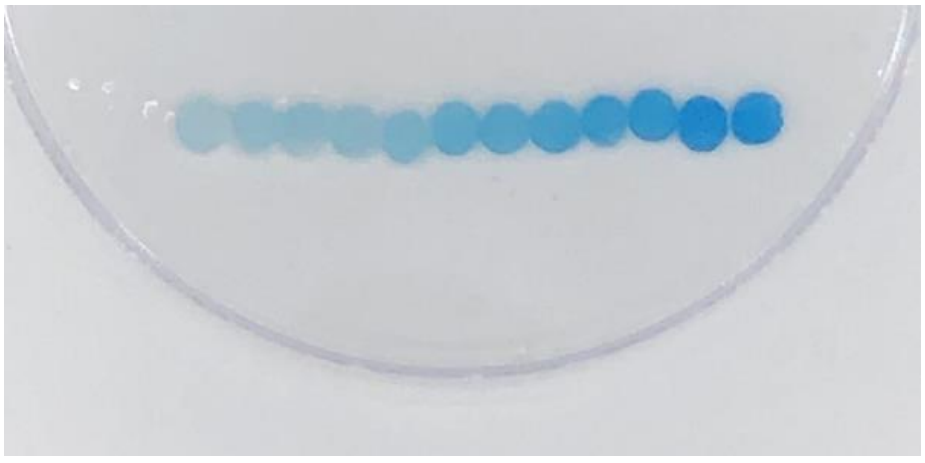

Figure S2.6. Optical image of sensing test of NHS@MF after the material was exposed to different concentrations of CAP. (without image crop)

Chapter 3. Rapid and Ultrasensitive Colorimetric Biosensors for Onsite Detection of *Escherichia coli* O157:H7 in Fluids

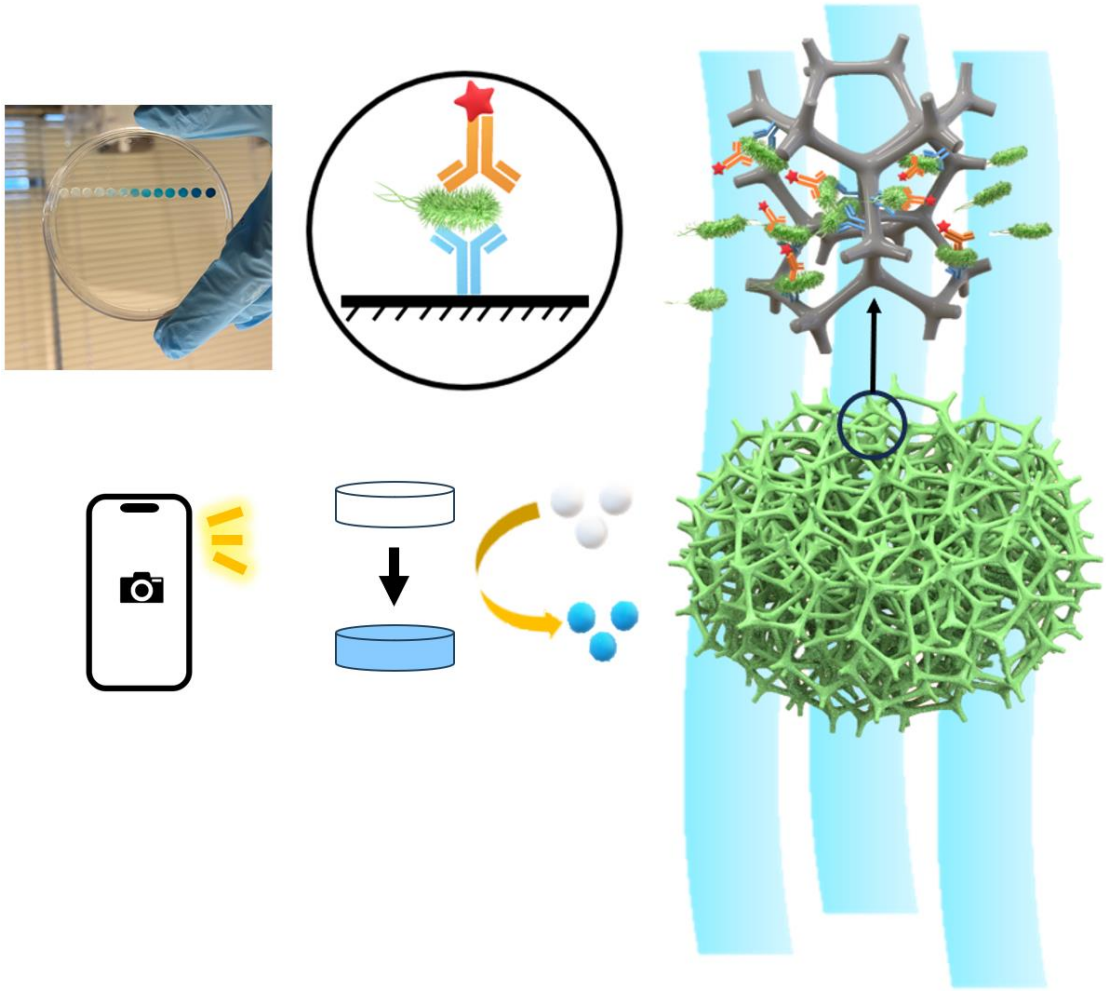

Abstract

This study presents a breakthrough in the field of onsite bacterial detection, offering an innovative, rapid, and ultra-sensitive colorimetric biosensor for detection of *Escherichia coli* (*E. coli*) O157:H7, using chemically modified melamine foam (MF). Different from conventional platforms, like 96-well plates and fiber-based membranes, the modified MF features a macroporous reticulated three-dimensional(3D) framework structure, allowing fast and free movement of large biomolecules and bacteria cells through the MF structure in every direction and ensuring good accessibility of entire active binding sites of the framework structure with the target bacteria, which significantly increased sensitive and volume-responsive detection of whole-cell bacteria. The biosensing platform requires less than 1.5 h to complete the quantitative detection with a sensitivity of 10 CFU/mL, discernible by the naked eye, and an enhanced sensitivity of 5 CFU/mL with the help of a smartphone. Following a short enrichment period of 1 hour, the sensitivity was further amplified to 2 CFU/mL. The biosensor material is volume responsive making the biosensing platform sensitivity increase as the volume of the sample increases and highly suitable for testing large-volume fluid samples. This novel material paves the way for volume-flexible biosensing platforms for the record-fast, onsite, selective, and ultra-sensitive detection of various pathogenic bacteria in real-world applications.

3.1 Introduction

Foodborne illnesses represent significant public health challenges worldwide[1]. Among

these, *E. coli* O157:H7 is a particularly concerning pathogen because of its low infectious dose and severe health consequences[2,3]. This specific serotype of *E. coli* can cause diseases varying from diarrheal illness to hemorrhagic colitis and hemolytic uremic syndrome, which can lead to kidney failure or death in extreme cases. *E. coli* O157:H7 was reported of causing an estimated 63,000 hemorrhagic colitis illnesses annually in the United State[4,5]. Its low infectious dose, high pathogenicity, and a potential risk of contamination in water and food sources make it a significant threat to food safety and public health[6,7]. Currently, the detection of existence of *E. coli* O157:H7 in food and water samples has relied heavily on conventional methods including culture-based assays, polymerase chain reaction (PCR), and isothermal amplification[8,9,10,11]. While these methods have proven effective over time, they possess several limitations. The culture-based assay, with its high reliability and sensitivity, is considered the gold standard in the field of bacterial detection[12]. However, it is time-intensive (2-3 days) and requires highly trained personnel, making it unsuitable for rapid onsite detection[13]. PCR's exceptional sensitivity is counterbalanced by its need for expensive equipment and complex preparation procedures[14,15]. Isothermal amplification methods amplify DNA at a consistent temperature, contrasting the temperature cycling of PCR. While adept at detecting pathogens in trace amounts, this method can be hindered by complex primer design and contamination risks, potentially leading to a high false-positive rate[16]. Other methods, including flow cytometry, gas chromatography (GC), Fourier transform infrared spectroscopy (FTIR), and Raman spectroscopy, etc., also require professional tools, being both costly and time-

consuming[17,18]. The existing diagnostic methods prove challenging to implement in low-income countries, where high mortality rates prevail due to a lack of adequate diagnostic tools[19,20]. Therefore, there has been a pressing need for a more efficient, affordable, and rapid detection method to combat this public health threat.

Currently, paper-based colorimetric biosensors were reported capable of detecting pathogenic bacteria in food and water with naked eyes[21,22]. The straightforward design and operation of the paper-based ELISA (p-ELISA) colorimetric sensing systems make them an appealing choice for on-site detection systems, which are disposable and potentially operatable by untrained personnel[23,24,25,26,27]. However, a variety of technical challenges restrict their use in assessing food safety in terms of microbial contamination. Detecting a small number of pathogenic bacteria within a large volume of a food or water sample proves difficult by using these conventional systems because of their relatively low detection sensitivity. Additionally, the complexity of food matrices—including existence of fats, proteins, saccharides, fibers, and various salts—can significantly affect the separation of target bacteria from the other contents in food or water sample and the subsequent color development reaction. A key factor contributing to the limitations of p-ELISA is the layered fiber mat structures of the papers and fibrous membranes formed during the manufacturing processes, making the sensor media heterogenous in their vertical direction from other directions. The inconsistency in the direction significantly impedes the penetration of large biomolecules through the p-ELISA media, leading to less incorporation of biomolecules on fiber surfaces inside the media in comparison to the outside surfaces[28]. Even though the media is often described

as having a three-dimensional structure, the inner part of the materials is seldom fully utilized. Particularly when whole cells of microorganisms are used as antigens, their micrometer sizes restrict them from diffusing and penetrating, and even if they manage to traverse the layered narrow porous structure, they often become trapped and are difficult to wash off through the system[29]. This structural characteristic may cause inhomogeneous colorimetric signals, strong sample matrix effects, and high false-positive rates of the sensors, additionally reducing the sensitivity of p-ELISA sensors fabricated from use of filter papers and nitrocellulose or nanofibrous membranes[30]. Hence, an ideal medium for ELISA bacteria biosensors is conceptualized as a homogenous, three-dimensional, and macroporous structure, enabling unrestricted bacterial cell migration in every direction.

In our previous studies, we demonstrated that the foam-based ELISA (f-ELISA) using melamine foam (MF) as a medium offers unique advantages[31]. It was proven to be rapid, sensitive, additive, and volume-responsive across different types of approaches, including direct, competitive, and sandwich ELISA by detecting SARS-CoV-2 spike protein and chloramphenicol (CAP). In this context, we believe that f-ELISA is even better suited for *E. coli* O157:H7 detection, given the larger size of bacteria compared to chemical compounds and proteins. The application of the f-ELISA in the detection of bacteria cells could fully demonstrate the advantages of the macroporous features offered by the chemically modified melamine foam. In contrast to conventional ELISA (c-ELISA), which is restricted by the limited surface area of a 96-well plate, and other p-ELISA methods, bacteria as antigens can move freely in every direction within this

macroporous 3D matrix. This enhanced freedom of movement facilitates an amplified interaction between the immobilized antibodies and antigens, leading to substantial enrichment and heightened sensitivity in colorimetric detection. The testing process needs less than 1.5 h to complete both preparation and detection, and the results indicated that the sensors made of the modified MF materials can detect *E. coli* O157:H7 at a level of 10 CFU/mL by naked-eye with a limit of detection (LOD) at 5 CFU/mL when supplemented by a smartphone. Following a brief enrichment period of 1 hour, the sensitivity was further amplified to 2 CFU/mL. Interestingly, the sensitivity increases as the volume of the sample increases, making this sensing material highly suitable for testing large-volume fluid samples, such as milk, drinking fluids, agricultural water, etc. In essence, this study paves the way for a rapid, sensitive, and volume-flexible biosensing platform, using *E. coli* O157:H7 as a proof of concept, which holds promise for the rapid and ultra-sensitive detection of various pathogenic bacteria in real-world applications.

3.2 Experimental Section

3.2.1 Materials

N, N'-disuccinimidyl carbonate (DSC), triethylamine (TEA), 1,4-dioxane, acetone, phosphate-buffered saline (PBS), 3,3′,5,5′-Tetramethylbenzidine (TMB), and 96-well plates were purchased from ThermoFisher Scientific. *Escherichia coli* O157 mouse anti-*E. coli* monoclonal antibody (Ab-*E. coli*) and *E. coli* rabbit anti-*E. coli* polyclonal (HRP) antibody (Ab-*E. coli*-HRP) were purchased from Lifespan Biosciences (Shirley,

MA, USA). Melamine foams were purchased from Swisstek (Brewster, NY, USA). Maximum recovery diluent (MRD) was purchased from Sigma-Aldrich (Louis, MO, USA). Phosphate buffer solution (PBS), tryptic soy broth (TSB), and tryptic soy agar (TSA) were purchased from Fisher Scientific (Fair Lawn, NJ, USA). All other chemicals were of analytical grade and were supplied by Merck (Darmstadt, Germany). Rifampin-resistant *E. coli* O157:H7 (ATCC700728), *E. coli* BL21 (ATCC BAA-1025), and *Listeria innocua* (ATCC 33,090) were obtained from ATCC (Manassas, VA, USA). MacConkey agar was supplied from Difco (Sparks, MD, USA). SYBR Green I nucleic acid stain (10 × concentrate) was purchased from Invitrogen (Carlsbad, CA, USA). Programmable syringe pump was purchased from NewEra Instruments (Suffolk County, NY, USA).

Morphologies of all MF based samples were analyzed using a scanning electron microscope (Quattro ESEM, Thermo Scientific). Electronic micrometer thickness gauge (Neoteck) was used to measure the thickness of the MF membranes. Ultraviolet–Visible spectrophotometer (UV-Vis, Evolution 600, Thermo Fisher) was used to measure the absorbance of bacteria solution. Laser scanning confocal microscope (Olympus FV1000) was used to obtain fluorescence microscopy Images. A light panel (5"×4", LP-100N) was employed to provide consistent lighting for capturing images of the sample results.

3.2.2 Bacterial culture and sample preparation

An overnight *E. coli* O157:H7 culture was developed and transferred by using a loop

from stored bacteria TSA plates, which were prepared following a reported method[32], into 10 mL of sterile TSB, followed by incubation at 37°C with constant shaking at 200 rpm. After incubation of 16-hours, the *E. coli* culture reached a concentration of 10^9 CFU/mL. This overnight culture was centrifuged at 13,000 rpm for 1 minute to harvest the bacterial cells, which were washed twice and resuspended in sterile PBS. The *E. coli* suspension (10^9 CFU/mL) was then diluted in PBS to achieve varying bacterial concentrations.

3.2.3 Measurement of diffusion of biomolecules and bacteria

The diffusions of *E. coli* O157:H7 through the melamine foams (MF) in three different thicknesses, nitrocellulose paper (NP), and nanofibrous membrane (NF) were measured using a side-by-side diffusion chamber (PermeGear Co.)[29]. MF membranes at different thicknesses (1-3mm), as well as NP and NF, were separately placed between the two chambers, which were tightly sealed in a water bath with a temperature of 25 °C. To pre-wet the membranes, each chamber was filled with 3 mL of a PBS solution for 15 minutes. Following this, 3 mL of *E. coli* O157:H7 suspension (10^7 CFU/mL) was injected into the donor chamber. Stirring bars were set in both chambers, operating at a speed of 750 rpm throughout the tests. At regular time intervals, 1 mL of the sample solution was extracted from each chamber and added back to the chambers after the measurement via UV-Vis at the wavelength of 600 nm[33]. The concentration of *E. coli* O157:H7 was determined with the UV-Vis, based on calibration curves provided in the supporting information (Figure S3.1). The subsequent analysis of bacteria

concentration in the receptor chamber over increasing time intervals allowed for an assessment of the diffusion properties of the biomolecules through the MF membranes.

3.2.4 Vertical flow test through materials

The vertical flow test was carried out by separately placing MF membranes at different thicknesses (1-3 mm), NP and NF in the bottom of a 20 mL syringe creating a filtration column (Figure S3.2). A 1 mL of *E. coli* O157:H7 suspension at a concentration of 10^3 CFU/mL was passed through the columns containing the different testing matrices. The collected filtrates were serially diluted and plated for bacterial counting using TSA containing 0.05 g/L rifampicin, which allows the growth of the inoculated rifampicin-resistant *E. coli* O157:H7 with prevention contamination from the tested matrices. After passing 10 mL sterile PBS to replace any remaining bacterial solutions, the different membranes were transferred into a sterile centrifugal tube (15 mL size) containing 1 mL of a releasing buffer (MRD with 0.01% lecithin), which were incubated for 2 min then vortexed vigorously for 1 min to recover any captured bacterial cells[32]. The quantification of the recovered bacterial cells was performed by the same serial dilution and plate counting method using the TSA (containing 0.05 g/L rifampicin).

3.2.5 Foam-based ELISA platform preparation

A typical chemical structure of melamine foams is shown in Figure S3.3. The chemical modification processes of MF were same as reported in a previous publication (Figure S3.4a)[31]. The MF samples were all in the circular form of 1.0 mm thickness and 5.0 mm diameter. The structures of MF and DSC modified MF membranes (NHS@MF)

samples were characterized by FTIR with spectra same as the ones reported in literature (Figure S3.4b)[31]. Then, a 100 µL of Ab-*E. coli* solution (10 mg/L) was added to the NHS@MF membranes and incubated for 30 min at room temperature. After the antibodies immobilization, the remaining active sites were blocked using 200 µL of 3% skim milk (SKM), we defined the material as Ab@NHS@MF.

3.2.6 Foam-based ELISA in *E. coli* O157:H7 detection

The analytical performance of the biosensing platform-based MF (f-ELISA) was evaluated by adding 200 µL of *E. coli* O157:H7 at varied concentrations (ranging between 0 to 10^7 CFU/mL) to the f-ELISA membranes. The incubation process continued for 30 min with mild shaking. After incubation, any unbound bacteria were removed by washing with PBS buffer. Subsequently, 100 µL of Ab-*E. coli*-HRP (1 mg/L) was applied to each membrane. After incubation of 20 minutes, the membranes were washed with a PBST solution (PBS plus 0.05% v/v tween-20), followed by a rinse with PBS buffer and subsequent air drying. Next, 35 µL of TMB substrate was added onto the membranes, and color images of the membranes were obtained following the method in the literature[31].

In order to further investigate the impact of the sample volume on *E. coli* O157:H7 detection, varied volumes of the bacterial samples (from 100 µL to 10 mL) were employed in experiments following the above protocol.

To ensure the long-term efficacy and repeatability of the f-ELISA system, we examined

the stability and activity of stored antibodies on the modified MF. The Ab@NHS@MF membranes were treated using 10% sucrose as a stabilizer followed by freeze-drying[34,35]. They were stored at a consistent temperature of 4°C and assessed over a duration of 90 days. At predetermined time intervals, aliquots were retrieved and utilized in the f-ELISA assay to detect *E. coli* O157:H7 following the same protocols.

3.2.7 Fluorescence images of *E. coli* O157:H7 cells captured by Ab@NHS@MF

E. coli O157:H7 cells harvested from centrifuging 1 mL of its overnight culture at 13,000 rpm for 1 min were washed twice and resuspended with sterile PBS. A 100 µL of 10x SYBR green I was added and incubated in the dark for 5 min. Afterward, the labeled bacterial cells were recovered, washed with sterile PBS three times to remove the excess SYBR green I dye, and resuspended with sterile PBS. The labeled *E. coli* suspension was diluted in PBS to obtain a cell concentration of 10^5 CFU/mL. Then, 100 µL of *E. coli* O157:H7 (10^5 CFU/mL) were added to the Ab@NHS@MF membranes and allowed for incubation for 30 min under mild shaking. Afterward, the membranes were washed with PBST and then with PBS buffer and followed by air-drying. A laser scanning confocal microscope (Olympus FV1000) with a tetramethylrhodamine-isothiocyanate (TRITC ex 541 nm/ em 572 nm) filter was employed to acquire fluorescence Images of the SYBR green I labeled *E. coli*, with the assistance of image processing software ImageJ to convert the acquired fluorescence image files from TIFF into JPG[36].

3.2.8 Detection of *E. coli* O157:H7 in real samples

The irrigation water sample was collected from the Campbell tract at the University of California, Davis, the Solano County District agricultural irrigation water system(Agwater). The Agwater sample was autoclaved to remove any background noise created by the Agwater. Then, the autoclaved Agwater sample was spiked with *E. coli* O157:H7 in a concentration range of 10 -10^4 CFU/mL. Non-spiked autoclaved Agwater sample was employed as a control. For analysis of the samples using f-ELISA, the Ab@NHS@MF membrane was mounted into a syringe needle pocket, 5 mL of the prepared sample solution was loaded into a 20 mL syringe and flowed through the filtering media in the needle at a controlled flow rate of 10 mL/h using a syringe pump (NewEra Instruments, USA). Moreover, a non-autoclaved Agwater sample was tested without spiking using the f-ELISA and the achieved results were compared with the plate counting assay approach using a selective medium (MacConkey agar plates). The presence of red colonies on the MacConkey agar plates indicates the presence of *E. coli* O157:H7 in the Agwater sample.

3.2.9 Colorimetric data processing

Upon the addition of TMB substrate to the Ab@NHS@MF membranes, they were positioned inside an LED lightbox and on a light panel (5”x4”, LP-100N) with an illuminance of 12000 lux. Images were taken using a smartphone camera (iPhone 14pro max) fixed at 50 cm above the membranes. The intensity of the color was represented by the red channel (R) from the RGB values obtained from Adobe Photoshop (2022)

following Equation 1[37].

$$\Delta RGB = RGB_{background} - RGB_{membranes} \quad (1)$$

where $RGB_{background}$ represents the R value of the white background (without HRP), and $RGB_{membranes}$ is R value of the Ab@NHS@MF membranes.

3.2.10 Statistical analysis

All assays for the study were performed in triplicate. The data are presented as mean ± standard deviations (SD). Intergroup comparisons were analyzed using Student's t-test (two-tailed). The level of significance was defined as $*P < 0.05$, $**P < 0.01$, $***P < 0.001$.

The linear relationship between observed and predicted values was assessed using the correlation coefficient (R). A P-value of less than 0.05 was considered statistically significant. All statistical analyses were conducted using GraphPad Prism version 8.0.2.

3.3 Results and Discussion

3.3.1 Filtering and Diffusion Test of Bacteria in MF Membranes

Diffusion of large molecules and particles in chartaceous materials is heterogeneous and notably slow in vertical directions of the materials because of the layered fiber mat structure and substantially decreased effective pore sizes[28]. However, the homogeneous 3D macroporous framework structure of the MF materials in all directions enable the penetration of large biomolecules or particles moving around with minimal resistance.

Based on our previous studies[31], we found that compared to the diffusion performances of the biomolecules in various sizes (40 kDa to 150 kDa) in nanofibrous membranes and nitrocellulose papers, which need several hours to achieve a steady state of diffusion, the thicknesses of the MF materials and sizes of protein molecules did not exhibit noticeable effect and could be considered negligible if the duration of interaction between MF and the substrates extends beyond 10 minutes. However, the diffusion properties of bacteria in the macroporous MF materials could be different, as bacteria cells are in significantly larger dimensions than proteins and other biomolecules—with lengths ranging from 1 to 10 microns and widths between 0.2 to 1 micron[38]. Thus, as depicted in Figure 3.1a, a side-by-side diffusion chamber was utilized to investigate the diffusion behaviors of *E. coli* O157:H7, aligning with our focus on this bacterial strain in subsequent experiments using the innovative f-ELISA system. The concentration changes of *E. coli* O157:H7 in the receiver chamber represent the bacterial cells that have diffused through the MF materials with thicknesses of 1.0 mm, 2.0 mm, and 3.0 mm, or through nanofibrous membrane (NF) and nitrocellulose paper (NP), respectively, for a duration of 18 min, and the results are plotted in Figure 3.1b. In both nanofibrous membranes [poly(vinyl alcohol-co-ethylene), PVA-co-PE] and nitrocellulose papers, the diffusion of *E. coli* O157:H7 required several hours to attain a steady state. Conversely, in all MF membranes, regardless of their thickness, the steady state of diffusion was achieved in less than 11 min. The variation in concentrations observed in the MF membranes with different thicknesses could be attributed to the fact that the increased thickness in MF corresponds to a greater material

volume. This increased volume can potentially retain more of the bacterial solution, resulting in a slightly reduced concentration in the Receptor Chamber upon reaching steady state. The diffusion test simulates the process of the MF membranes encountering with bacteria solution samples under a specific stirring rate. As evidenced by the results, the highly porous and homogeneous framework structure and macropore size of the MF materials allow easy penetration of whole bacterial cells through the media with minimum resistance. This facilitates the thorough exposure of the MF's 3D framework to pathogens in liquid form, substantially augmenting the likelihood of interactions between the immobilized antibody and *E. coli* O157:H7, increasing the sensitivity in pathogen detection of the f-ELISA media. A liquid filtering test was also conducted to evaluate the potential application of the MF media in additive filtering sensing devices (Figure S3.2). As shown in Figure 3.1c, minimal amount of *E. coli* O157:H7 was trapped when the solution flew through a 1 mm thick MF membrane, and only slight increases in trapped bacteria cells were observed for the 2 mm and 3 mm thick MF membranes. Both NF and NP could trap or block more bacterial cells with significantly reduced concentrations of the bacteria shown in the filtered solutions. The non-specific adsorption results of each medium after buffer wash were consistent with the vertical flow test (Figure 3.1d). Besides, the non-specific binding of *E. coli* O157:H7 on the MF membranes of varying thicknesses (1 mm to 3 mm) was investigated, and the results revealed that while the 1 mm thick MF membrane showed no measurable non-specific bacterial binding, the 2 mm and 3 mm membranes, due to their increased volumes, retained relatively more bacteria solutions, as evidenced in

Figure 3.1d, which highlights the use of 1mm MF in the sensors. In contrast, NP and NF samples exhibited significant retention of the bacteria. This retention could elevate the background in biosensors using these two materials as detection platforms, potentially increasing the false-positive rate, and reducing the sensitivity of the assay. Therefore, the 1mm thick MF was selected for subsequent tests to optimize the accuracy and sensitivity of the f-ELISA for *E. coli* O157:H7 detection.

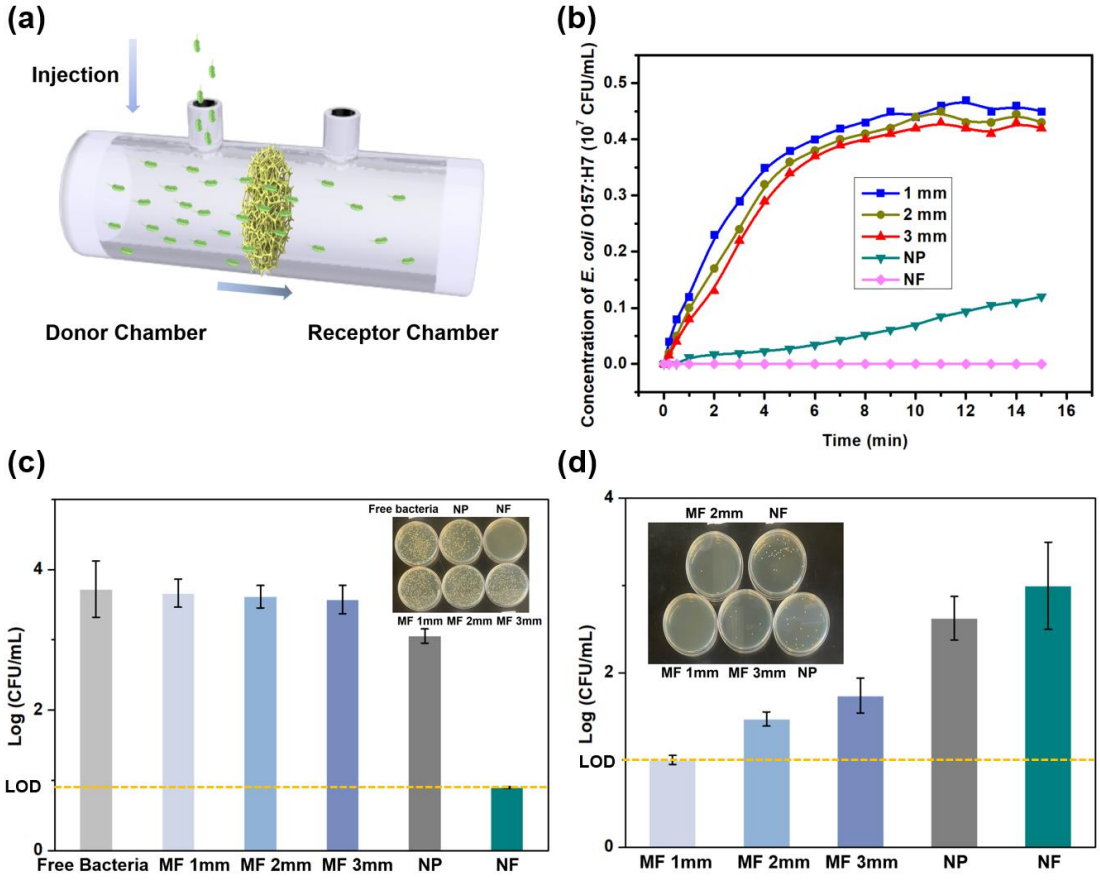

Figure 3.1. (a) Scheme of the used side-by-side chamber; (b) the correlation between diffusion time and concentration of *E. coli* O157:H7 diffused through NF, NP, and MF in different thicknesses. (c) Vertical flow test of *E. coli* O157:H7 solution (at 10^4 CFU/mL concentration) through various materials: NF, NP, and MF with different thicknesses, with each material positioned at the base of a syringe. (d) The unspecific

adsorption of *E. coli* onto the tested materials after buffer wash. (NF thickness =0.21mm; NP thickness =0.18mm). Data are shown as mean ± SD, based on n = 3 independent experiments. *LOD =Limit of detection.

3.3.2 Capture of *E. coli* O157:H7 based on Ab@NHS@MF

As our previous results indicated, the covalent immobilization of proteins onto the MF was achieved by chemically modifying the secondary amino groups of the melamine polymer following the reported method (Figure S3.3)[31]. The chemical modification and protein immobilization reactions on the MF are depicted in Figure S3.4. The successful incorporations of the reactive N-hydroxysuccinimide (NHS) groups to the MF and formation of NHS@MF were confirmed with the band of 1730 cm^{-1} in Fourier-transform infrared spectroscopy (FTIR)[39]. The antibody loading capacity on the NHS@MF exceeded the capacities on both NHS@NF and nitrocellulose paper, when compared by mass, resulting in considerably high number of interactive sites for target bacterial cells than those on the materials used in p-ELISA sensors[31]. After the immobilization of anti-*E. coli* O157:H7 antibodies, the Ab@NHS@MF should be able to capture the target bacteria specifically from the liquid samples as illustrated in Figure 3.2a. From SEM characterization results, it is evident that the morphology of the MF framework structures remains unchanged after the chemical modification, protein immobilization, and bacteria capture (Figure 3.3a-c). As demonstrated in Figure 3.3b, in the absence of immobilized antibodies on the material, no unspecific binding was observed. This suggests a low background in subsequent f-ELISA tests, corroborating

the results from the diffusion and vertical flow tests mentioned earlier. Furthermore, as shown in Figure 3.3c,3.3d, it is very clear that when the Ab@NHS@MF membranes were used in the capture of *E. coli* O157:H7 in varied concentrations (10^3 and 10^5 CFU/mL), the amounts of the bacteria used and captured on the MF media were related. From the results of the fluorescent microscope, after being modified with anti-*E. coli* O157:H7 antibodies, blocked with SKM, and incubated with *E. coli* O157:H7 solution at a concentration of 10^7 CFU/mL, the difference in signal intensities of NHS@MF and Ab@NHS@MF is statistically significant, and the green dots, representing the bacterial cells, homogeneously distribute through the framework of the entire membrane (Figure 3.3e-g). Given these attributes, f-ELISA could be a highly promising platform for detecting whole-cell antigens.

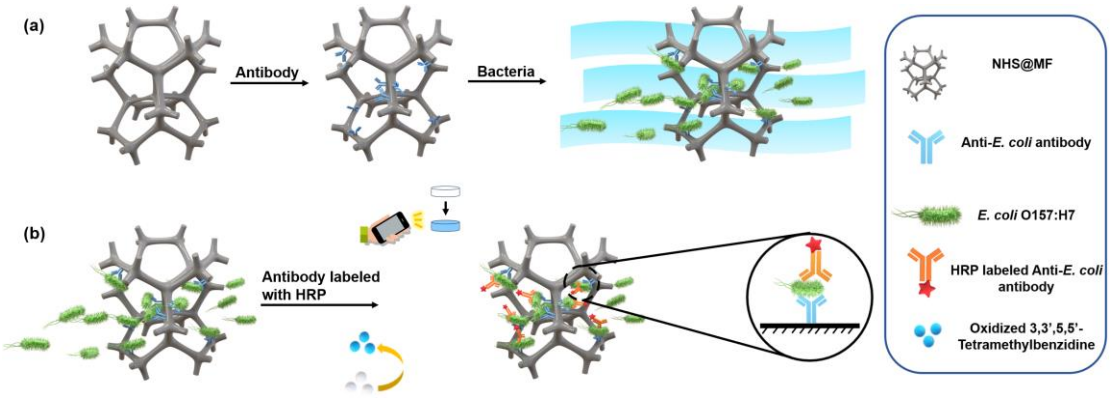

Figure 3.2. Schematic illustration of preparation and use of foam-based sandwich ELISA (f-ELISA). (a) Immobilizing antibodies and capturing bacteria; (b) Adding HRP-labeled secondary antibody and enzymatic substrate TMB to generate color signals, and obtaining images using a smartphone.

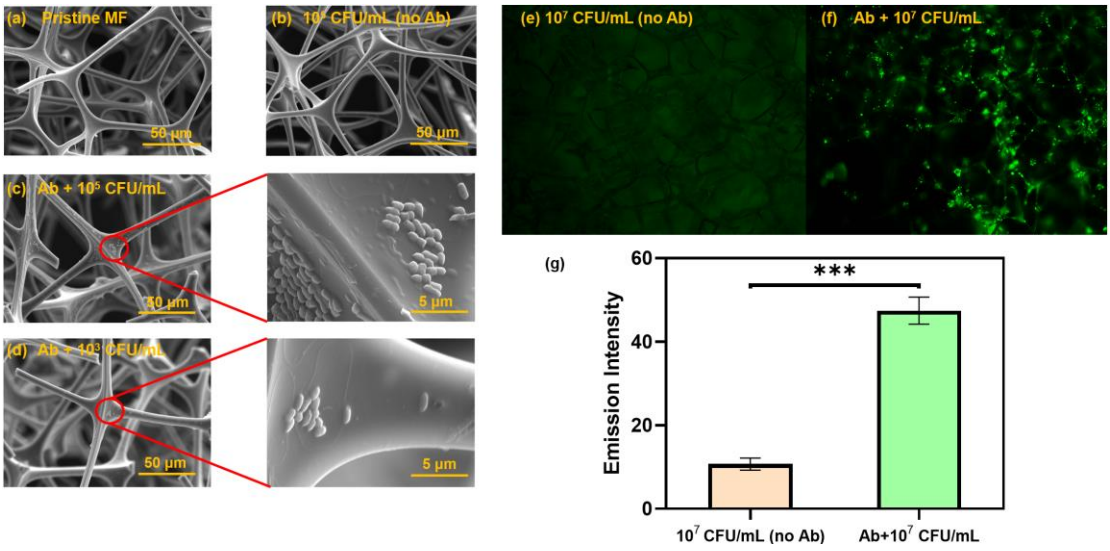

Figure 3.3. SEM images of (a) Pristine MF, (b) NHS@MF after incubation with *E. coli* O157:H7 solution (10^5 CFU/mL); (c) Ab@NHS@MF incubated with *E. coli* O157:H7 solution (10^5 CFU/mL); (d) Ab@NHS@MF after incubation with *E. coli* O157:H7 solution (10^3 CFU/mL). Fluorescent microscopic images of (e) NHS@MF and (f) Ab@NHS@MF, after incubation with *E. coli* O157:H7 solution at a concentration of 10^7 CFU/mL. Data are shown as mean ± SD, based on n = 3 independent experiments. ***P < 0.001 (two-tailed Student's t-test).

3.3.3 Analytical performance of f-ELISA

The f-ELISA sensing system, rooted in its novel approach for detecting whole-cell antigens, showed great potential in the initial experiments. In the following section, we will detail the performance metrics of this innovative system, focusing on its specificity and sensitivity. The general f-ELISA procedure of detecting *E. coli* O157:H7 is shown in Figure 3.2. In the presence of the anti-*E. coli* O157:H7 antibodies immobilized on the NHS@MF, the *E. coli* O157:H7 is recognized and then captured by the MF based

sensor media. Then the addition of Ab-*E. coli*-HRP to the system and its reaction with TMB leads to the generation of colorimetric signals. By analyzing the colorimetric signals of the f-ELISA obtained from the pictures taken by a smartphone (Figure 3.2b), the detection of bacteria can be achieved on-site.

First, the optimization of experimental conditions, including the concentrations of antibody and HRP, and reaction time of HRP with TMB substrate, were conducted, with results shown in Figure S3.5. The optimal concentrations of Ab-*E. coli* and Ab-*E. coli*-HRP were identified as 5 mg/L and 2 mg/L, respectively, and a reaction time of 6 min was selected for the interaction between TMB substrate and HRP. To attest the specificity of the assay, we carried out an array of control experiments, including the tests without Ab-*E. coli*-HRP, Ab-*E. coli*, SKM, or target, respectively. The data from these controls, shown in Figure S3.6, further confirmed the robustness of the f-ELISA sensor.

Besides the negative control experiments that did not utilize HRP, there was either no color development or a minimal color response in scenarios where Ab-*E. coli* was absent, as illustrated in Figure S3.6, aligning perfectly with the results of SEM and fluorescent microscope (Figure 3.3).

To assess the sensitivity of the f-ELISA for detecting target agents, a detection assay was carried out using 200 μL samples with concentrations of *E. coli* O157:H7 ranging from 0 to 10^7 CFU/mL. The visually discernible blue color signals in varied intensities correspond to different *E. coli* O157:H7 concentrations, as shown in Figure 3.4a.

Through analysis of the color intensities using Photoshop software and applying equation (1), a linear equation for the colorimetric assay was determined as y=0.0749x + 26.499 (R^2=0.989) between the bacteria concentrations of 50 CFU/mL to 10^3 CFU/mL (Figure 3.4b). Based on Figure 3.4a, the color signal for *E. coli* O157:H7 at 50 CFU/mL level was naked-eye readable, while a limit of detection (LOD) of 10 CFU/mL was achieved using a smartphone acquired image and further analysis of the image from Photoshop for the f-ELISA sensor.

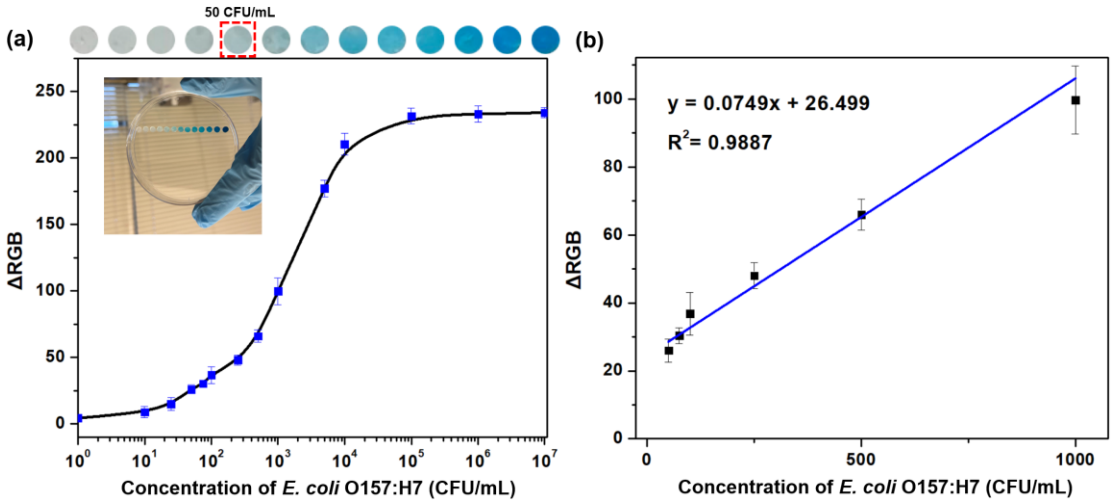

Figure 3.4. (a) Optical images and the calibration curve of the MF media in the detection of *E. coli* O157:H7. (b) Linear equation for the colorimetric assay was fitted to be y= 0.0749x+ 26.499 (R^2= 0.989) between 50 and 10^3 CFU/mL. Data are shown as mean ± SD, based on n = 3 independent experiments.

3.3.4 Impact of sample volumes in immunoassays

Traditional ELISA assays are typically operated within a limited range of sample volumes. Recent innovations, particularly with p-ELISA, have pivoted towards

miniaturization, leading to even smaller sample volumes, which are suitable for most biological samples. However, unlike point-of-care clinical analysis, pathogens might exist at very low concentrations in different sources such as various ground and surface water, food samples, and treated industrial wastes. Large volumes of those samples are available and meaningful for the detection of low concentrations of pathogens. Due to the fact that the MF materials in different thicknesses did not lead to a significant increase in fluid resistance (Figure 3.1) and no non-specific retention of the targeted microorganism, amplifying the test sample volume allows for a larger number of pathogen binding on the MF structure, thereby increasing the signal intensities. Consequently, even trace amounts of pathogens become detectable when large volumes of test solutions are passed through the foam sensing material. The volume-responsive performances of the f-ELISA were extensively investigated with *E. coli* O157:H7 solution at different volumes: 100 µL, 200 µL, 500 µL, 1 mL, 2 mL, 5 mL, and 10 mL. Apart from the alterations in analyte volumes, all other testing steps were the same as the protocols used in the previous discussions. As shown in Figure 3.5a, it is clear that different volume sizes produced varying calibration curves. Importantly, when the sample volume was increased from 100 µL to 2 mL, the sensitivity of the f-ELISA in detecting *E. coli* O157:H7 improved significantly, reducing the LOD to 5 CFU/mL (Figure 3.5b). Due to the unique macroporous structure of the MF facilitates large volume liquid samples can flow without any hindrance, maximizing contact, reactivity, and effective use of the available surface area. Thus, the increase in f-ELISA sensitivity with larger sample volumes can lead to the enhanced probability of antigen-antibody

interactions in increased volume of fluids, creating a stronger signal from accumulated targets. This distinctive structural feature of the f-ELISA sensors makes it suitable in detecting fluid samples in varied volumes and also functioning as a flow-through filtering sensor system for large-volume target solutions with low fluid resistance.

Compared to other sensing materials listed in Table 3.1, conventional ELISAs using 96-well plates exhibit a limit of detection (LOD) of 10^4 CFU/mL, requiring at least two hours to complete the tests[44]. Paper-based ELISAs on Whatman paper reached a LOD of 10^4 CFU/mL within 3 hours[41]. The foam-based ELISA (f-ELISA) significantly advanced the field with a LOD of 5 CFU/mL achieved in just 56 minutes when 2 mL of aqueous sample was tested, making it more sensitive and less time-consuming than most other optical biosensors, as shown in Table 3.1. These capabilities highlight the suitability of the f-ELISA for applications where rapid and highly sensitive on-site detection of bacteria is essential.

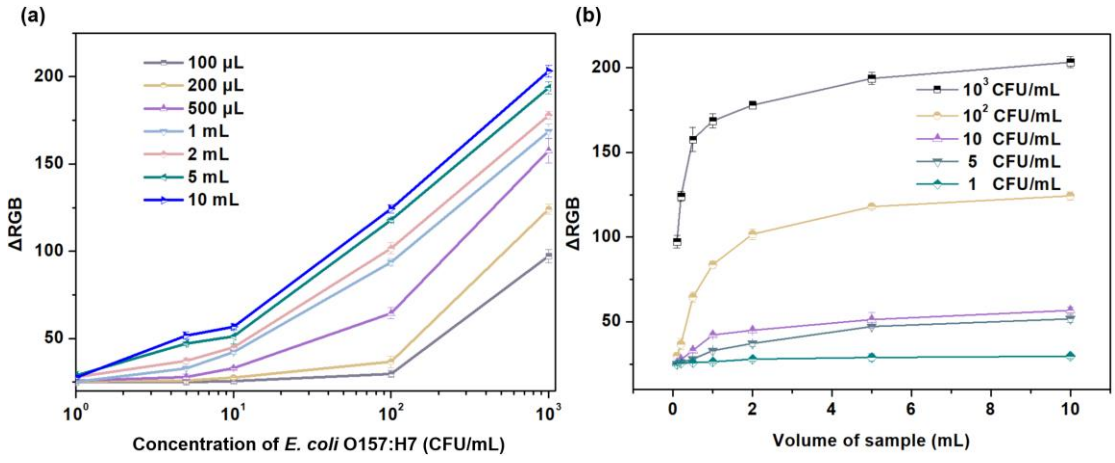

Figure 3.5. (a) Calibration curves generated using varying sample volumes for the detection of *E. coli* O157:H7. (b) Influence of sample volume on the colorimetric signal

intensities in the f-ELISA method. Data are shown as mean ± SD, based on n = 3 independent experiments.

3.3.5 Enhanced sensitivity through pre-enrichment

To further enhance the biosensor's sensitivity, we incubated the target specimen in the TSB medium for an hour under 37°C prior to the f-ELISA detection. Consequently, the colorimetric signal of 2 mL *E. coli* O157:H7 at a concentration of 2 CFU/mL became discernible through analysis of images taken by a smartphone (Figure 3.6). Even though an extra hour is needed, the overall time taken by the f-ELISA-based biosensor, including incubation, remains under 2 hours, a duration that is relatively rapid for detecting bacteria concentrations.

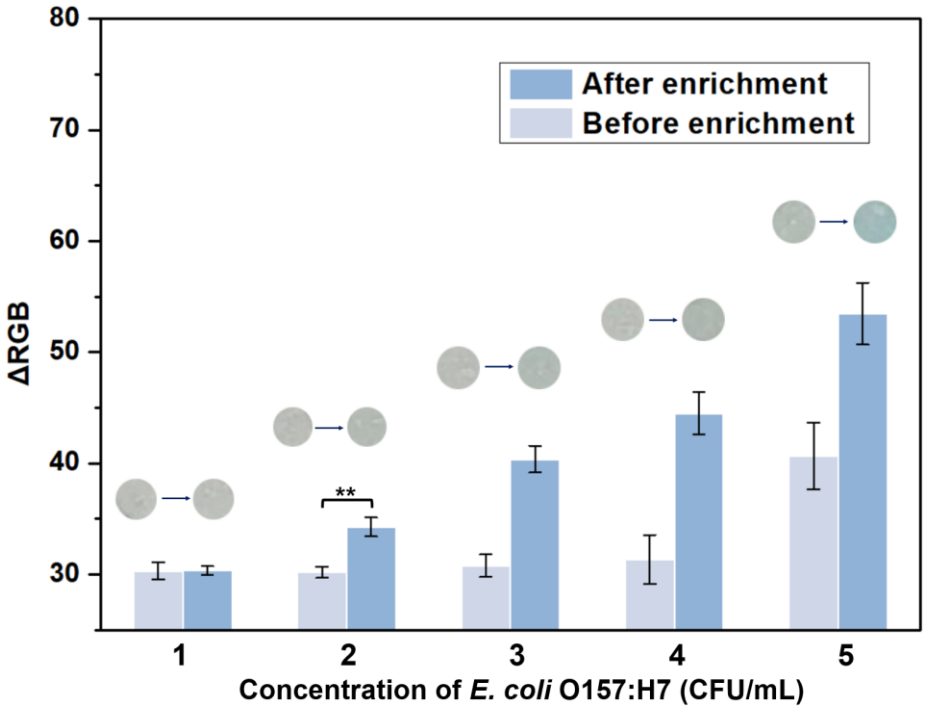

Figure 3.6. Optical images and the colorimetric signals before and after 1h enrichment of *E. coli* O157:H7 at various concentrations. Data are shown as mean ± SD, based on n = 3 independent experiments. **P < 0.01 (two-tailed Student's t-test).

Table 3.1. Comparison of optical biosensors for detection of *E. coli* O157:H7

Sensor platform	Capture reagent	LOD (CFU/mL)	Time	Application	Reference
Whatman paper	Antibody	10^5	<5 hours	urine	[40]
Whatman filter paper	Antibody	10^4	<3 hours	lixivium samples	[41]
Wax-printed paper	Antibody	10^4	2.5 hours	Beef samples	[42]
PDA vesicle	Antibody	10^4	2 hours	Fecal samples and water	[43]
96-well plate	Antibody	10^4	2 hours	Green tea sample	[44]
GO-Fe_3O_4	Aptamer	467	30 min	Complex biological samples	[45]
Iron quantum cluster	amino acids	$8.3x10^3$	30 min	Urine, tap water	[46]
T-bacteriophage	PP0 1ccp phage	1	15 hours	Apple juice	[47]
Functionalized Gold NPs	Reduce exogenous	10^2	1 hour	complex artificial sepsis blood	[48]
Chemically modified MF	Antibody	5	56 min	Agricultural water and milk	This work
Chemically modified MF	Antibody	2	2 hours	Agricultural water and milk	This work

*LOD =Limit of detection *PDA = Polydiacetylene *GO = Graphene oxide

3.3.6 Selectivity of f-ELISA

The selectivity of the developed f-ELISA biosensing platform was evaluated using various bacterial strains: *Pseudomonas fluorescens*, *Listeria innocua*, *Listeria monocytogenes*, *Salmonella enterica*, and *E. coli* BL21. In our tests, only *E. coli* O157:H7 produced a discernible colorimetric signal, as illustrated in Figure 3.7. Intriguingly, even a different strain of *E. coli* (BL21) failed to yield a significant signal, underscoring the good selectivity of the immobilized antibody on this biosensor. This specific reaction with only *E. coli* O157:H7 and the non-reactivity with other bacterial strains provides confidence in the applications of the f-ELISA-based biosensor. It offers the potential for accurate pathogen detection in real-world scenarios without being

affected by the presence of other bacterial strains.

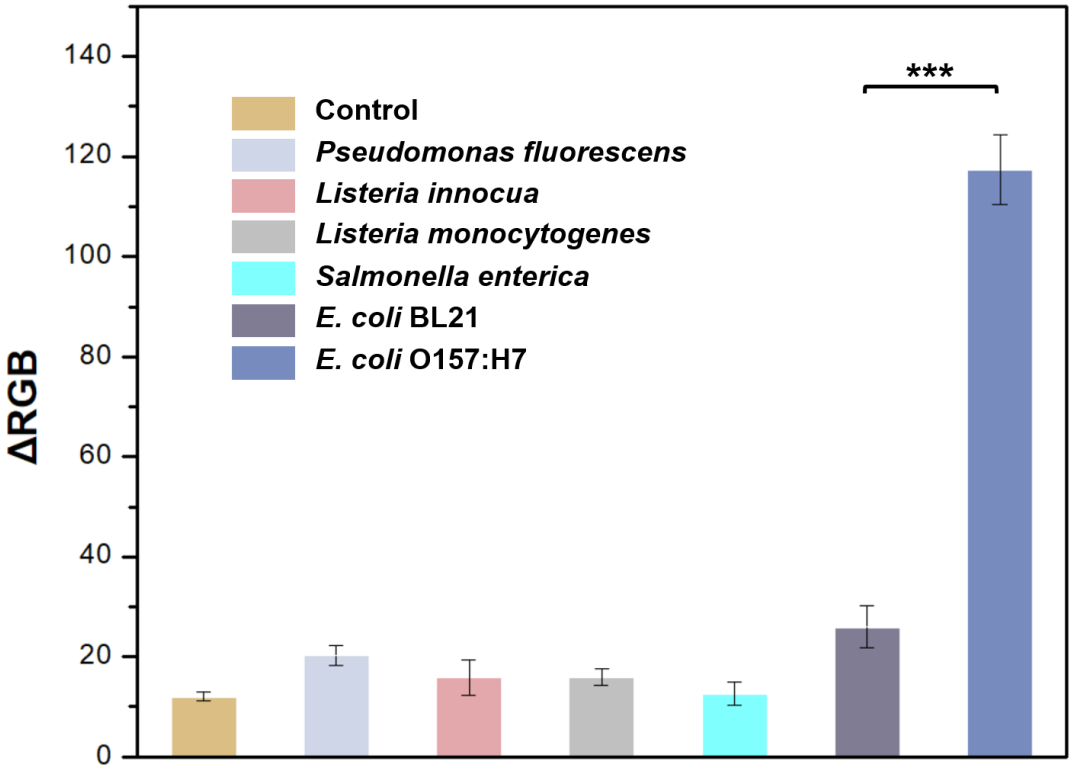

Figure 3.7. Selectivity of f-ELISA toward *E. coli* O157:H7 detection in comparison with other bacteria strains, including *Pseudomonas fluorescens, Listeria innocua, Listeria monocytogenes, Salmonella enterica* and *E. coli* BL21. The concentration of each bacteria strain used in this experiment is 10^5 CFU/mL. Data are shown as mean ± SD, based on n = 3 independent experiments. ***P < 0.001 (two-tailed Student's t-test).

3.3.7 Real Sample Analysis

To investigate the efficiency of the f-ELISA in real-world scenarios of *E. coli* O157:H7 detection, we designed artificially contaminated milk samples bought from a local grocery market and agricultural water (Agwater) collected from the irrigation facility at UC Davis, California. The MF membrane was mounted into a syringe needle pocket,

5 mL of a sample solution was loaded into a 20 mL syringe and flowed through the MF in the needle with a controlled flow rate of 10 mL/h (Figure 3.8a). For each test, *E. coli* O157:H7 was detectable at a concentration of 10 CFU/mL with a sample volume of 5 mL in a flowing-through filtering sensor system demonstrated in Figure 3.8b and Figure S3.7. Interestingly, for the non-sterilized agricultural water, the f-ELISA's colorimetric intensity was just above that of a 10 CFU/mL spiked sample. Subsequent culture plate assays confirmed the presence of *E. coli* O157:H7 at 12 CFU/mL in the agricultural water sample by using SMAC as a selective and differential medium for the detection of *E. coli* O157:H7, which aligns with the biosensor results (Figure 3.8c). The bacteria colonies grown in the TSA medium indicated that there were some other strains of bacteria that existed in the Agwater (Figure 3.8c). This instance effectively confirms the biosensing platform’s specificity and precision. Overall, the results suggest that the developed f-ELISA biosensor is reliable and accurate in detecting *E. coli* O157:H7 in complex matrices.

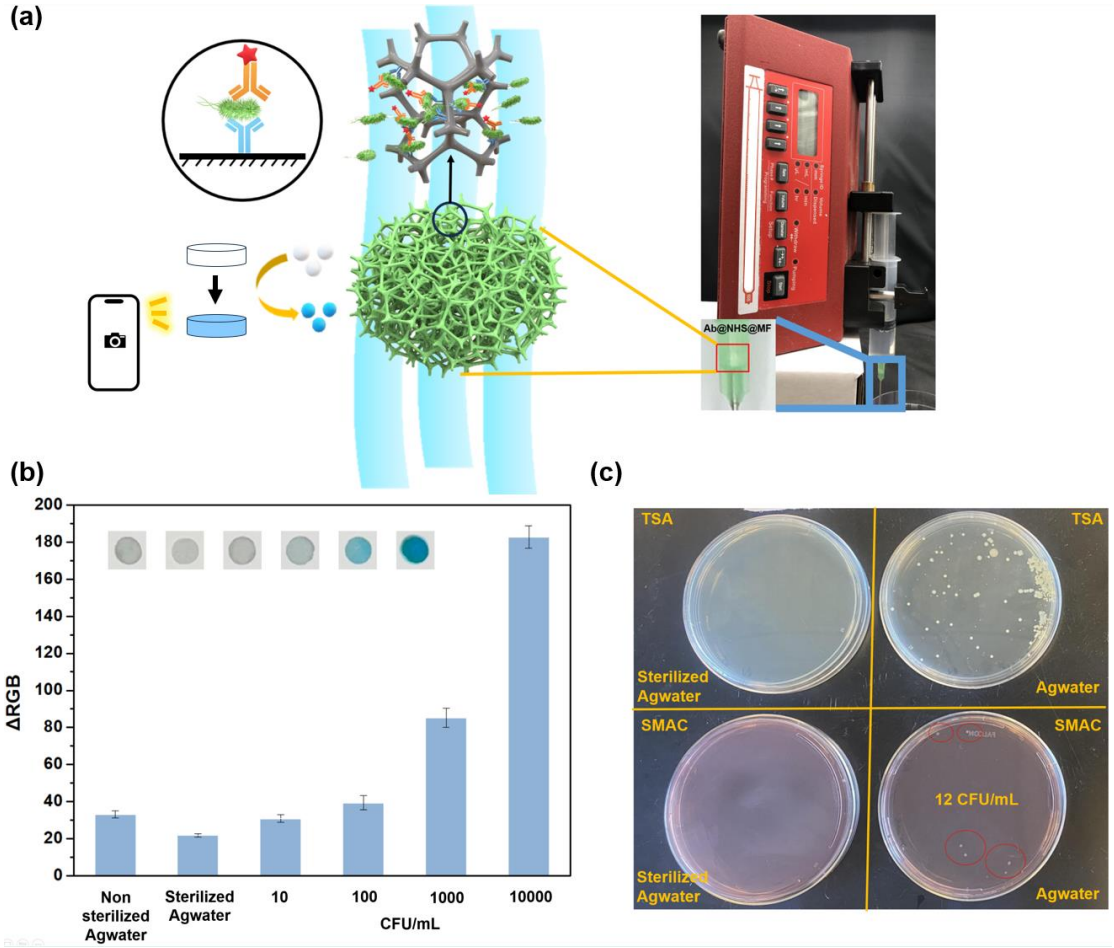

Figure 3.8. (a) The scheme illustrated the sensing of *E. coli* O157:H7 in agricultural water and the photograph showcased a rapid-flow device operated by a syringe pump. (b) Optical images and ΔRGB values of membranes treated by different concentrations of *E. coli* O157:H7 in spiked samples, sterilized Agwater, and non-sterilized Agwater. (c) Whole plate images of bacterial cultures upon exposure to non-sterilized agricultural water. Data are shown as mean ± SD, based on n = 3 independent experiments.

3.3.8 Storage Stability Evaluation for f-ELISA

Oxidation, isomerization, and hydrolysis prevent the antibody from existing long-term in the liquid state, diminishing the efficiency of the antibody-antigen interaction[49]. In contrast, when antibodies are immobilized on a solid phase, they can retain their activity

for an extended period[50]. To ensure the long-term efficacy and repeatability of the f-ELISA system, we examined the stability and activity of the stored f-ELISA biosensing platform. The Ab@NHS@MF membranes were prepared using 10% sucrose as a stabilizer followed by freeze-drying[51]. They were stored at a consistent temperature of 4°C and assessed over a period of 90 days. At predetermined time intervals, sample membranes were retrieved and utilized in the f-ELISA assay to detect *E. coli* O157:H7 following the same protocols. The results indicate that the antibodies stored at 4°C maintained their activity for up to 80 days, showing minimal variation from the results obtained with fresh Ab@NHS@MF membranes (Figure S3.8). Therefore, with the employment of sucrose as a stabilizer for antibodies, prolonged storage without compromising the efficiency of the f-ELISA system can be achieved.

3.4 Conclusion

The development and evaluation of a novel f-ELISA biosensor for the detection of *E. coli* O157:H7 are presented here. This sensor, constructed with NHS@MF, possessing a macroporous reticulated three-dimensional (3D) framework structure, demonstrated high sensitivity, specificity, and selectivity, outperforming other conventional methods presented in the literatures. The method required less than 56 min to complete the detection and demonstrated a sensitivity of 10 CFU/mL, with color signals discernible by the naked eye, and an enhanced sensitivity of 5 CFU/mL with the help of a smartphone. Following a brief bacteria enrichment period of 1 hour, the sensitivity was further amplified to 2 CFU/mL. Interestingly, the sensitivity increases as the volume of

the sample increases, making this method highly suitable for testing large-volume samples, such as milk, agricultural water, etc. In essence, using *E. coli* O157:H7 as a proof of concept, this work not only paves the way for improved bacterial detection in environmental and food samples but also introduces f-ELISA as a new model that could be adapted for other pathogens and contaminants.

3.5 Reference

1. Nguyen, Y., & Sperandio, V. (2012). Enterohemorrhagic *E. coli* (EHEC) pathogenesis. *Frontiers in cellular and infection microbiology*, *2*, 90.
2. Riley, L. W., Remis, R. S., Helgerson, S. D., McGee, H. B., Wells, J. G., Davis, B. R., ... & Cohen, M. L. (1983). Hemorrhagic colitis associated with a rare Escherichia coli serotype. *New England journal of medicine*, *308*(12), 681-685.
3. Griffin, P. M., Ostroff, S. M., Tauxe, R. V., Greene, K. D., Wells, J. G., Lewis, J. H., & Blake, P. A. (1988). Illnesses associated with *Escherichia coli* 0157: H7 infections: a broad clinical spectrum. *Annals of Internal Medicine*, *109*(9), 705-712.
4. Tapia, D., Ross, B. N., Kalita, A., Kalita, M., Hatcher, C. L., Muruato, L. A., & Torres, A. G. (2016). From in silico protein epitope density prediction to testing Escherichia coli O157: H7 vaccine candidates in a murine model of colonization. *Frontiers in Cellular and Infection Microbiology*, 6, 94.
5. Ameer MA, Wasey A, Salen P. *Escherichia coli* (*E. Coli* 0157 H7) [Updated 2023 Aug 8]. In: StatPearls [Internet]. Treasure Island (FL): StatPearls Publishing; 2023 Jan-. Available from: https://www.ncbi.nlm.nih.gov/books/NBK507845/
6. Doyle, M. P. (1991). *Escherichia coli* O157: H7 and its significance in foods. *International journal of food microbiology*, *12*(4), 289-301.

7. Bavaro, M. F. (2012). *E. coli* O157: H7 and other toxigenic strains: the curse of global food distribution. *Current gastroenterology reports*, *14*, 317-323.

8. Saxena, T., Kaushik, P., & Mohan, M. K. (2015). Prevalence of *E. coli* O157: H7 in water sources: an overview on associated diseases, outbreaks and detection methods. *Diagnostic microbiology and infectious disease*, *82*(3), 249-264.

9. Deisingh, A. K., & Thompson, M. (2004). Strategies for the detection of *Escherichia coli* O157: H7 in foods. *Journal of applied microbiology*, *96*(3), 419-429.

10. Notomi, T., Okayama, H., Masubuchi, H., Yonekawa, T., Watanabe, K., Amino, N., & Hase, T. (2000). Loop-mediated isothermal amplification of DNA. *Nucleic acids research*, *28*(12), e63-e63.

11. Tomita, N., Mori, Y., Kanda, H., & Notomi, T. (2008). Loop-mediated isothermal amplification (LAMP) of gene sequences and simple visual detection of products. *Nature protocols*, *3*(5), 877-882.

12. Zadik, P. M., Chapman, P. A., & Siddons, C. A. (1993). Use of tellurite for the selection of verocytotoxigenic Escherichia coli O157. *Journal of Medical Microbiology*, *39*(2), 155-158.

13. Sanderson, M. W., Gay, J. M., Hancock, D. D., Gay, C. C., Fox, L. K., & Besser, T. E. (1995). Sensitivity of bacteriologic culture for detection of Escherichia coli O157: H7 in bovine feces. *Journal of Clinical Microbiology*, *33*(10), 2616-2619.

14. Bayardelle, P., & Zafarullah, M. (2002). Development of oligonucleotide primers for the specific PCR-based detection of the most frequent Enterobacteriaceae species DNA using wec gene templates. *Canadian journal of microbiology*, *48*(2), 113-122.

15. Campbell, G. R., Prosser, J., Glover, A., & Killham, K. (2001). Detection of *Escherichia coli* O157: H7 in soil and water using multiplex PCR. *Journal of Applied*

Microbiology, *91*(6), 1004-1010.

16. Li, Y., Fan, P., Zhou, S., & Zhang, L. (2017). Loop-mediated isothermal amplification (LAMP): A novel rapid detection platform for pathogens. *Microbial pathogenesis*, *107*, 54-61.

17. Karo, O., Wahl, A., Nicol, S. B., Brachert, J., Lambrecht, B., Spengler, H. P., ... & Montag, T. (2008). Bacteria detection by flow cytometry. *Clinical chemistry and laboratory medicine*, *46*(7), 947-953.

18. Davis, R., Irudayaraj, J., Reuhs, B. L., & Mauer, L. J. (2010). Detection of *E. coli* O157: H7 from ground beef using fourier transform infrared (FT-IR) spectroscopy and chemometrics. *Journal of Food Science*, *75*(6), M340-M346.

19. Gous, N., Boeras, D. I., Cheng, B., Takle, J., Cunningham, B., & Peeling, R. W. (2018). The impact of digital technologies on point-of-care diagnostics in resource-limited settings. *Expert review of molecular diagnostics*, *18*(4), 385-397.

20. Rubach, M. P., Halliday, J. E., Cleaveland, S., & Crump, J. A. (2013). Brucellosis in low-income and middle-income countries. *Current opinion in infectious diseases*, *26*(5), 404.

21. Nguyen, Q. H., & Kim, M. I. (2020). Nanomaterial-mediated paper-based biosensors for colorimetric pathogen detection. *TrAC Trends in Analytical Chemistry*, *132*, 116038.

22. Xing, G., Zhang, W., Li, N., Pu, Q., & Lin, J. M. (2022). Recent progress on microfluidic biosensors for rapid detection of pathogenic bacteria. *Chinese Chemical Letters*, *33*(4), 1743-1751.

23. Hu, J., Wang, S., Wang, L., Li, F., Pingguan-Murphy, B., Lu, T. J., & Xu, F. (2014). Advances in paper-based point-of-care diagnostics. *Biosensors and Bioelectronics*, *54*, 585-597.

24. Zhao, C., Si, Y., Pan, B., Taha, A. Y., Pan, T., & Sun, G. (2020). Design and fabrication of a highly sensitive and naked-eye distinguishable colorimetric biosensor for chloramphenicol detection by using ELISA on nanofibrous membranes. *Talanta*, *217*, 121054.

25. Yu, X., Pan, B., Zhao, C., Shorty, D., Solano, L. N., Sun, G., Liu, R., & Lam, K. S. (2023). Discovery of Peptidic Ligands against the SARS-CoV-2 Spike Protein and Their Use in the Development of a Highly Sensitive Personal Use Colorimetric COVID-19 Biosensor. *ACS sensors*, *8*, 2159−2168.

26. Shang, Y., Xing, G., Lin, H., Chen, S., Xie, T., & Lin, J. M. (2023). Portable Biosensor with Bimetallic Metal–Organic Frameworks for Visual Detection and Elimination of Bacteria. *Analytical Chemistry*, *95*(35), 13368-13375.

27. Shang, Y., Xing, G., Liu, X., Lin, H., & Lin, J. M. (2022). Fully integrated microfluidic biosensor with finger actuation for the ultrasensitive detection of *Escherichia coli* O157: H7. *Analytical Chemistry*, *94*(48), 16787-16795.

28. Zhao, C., Pan, B., Wang, M., Si, Y., Taha, A. Y., Liu, G., Pan, T., & Sun, G. (2022). Improving the sensitivity of nanofibrous membrane-based ELISA for on-site antibiotics detection. *ACS sensors*, *7*(5), 1458-1466.

29. Zhao, C., Si, Y., Zhu, S., Bradley, K., Taha, A. Y., Pan, T., & Sun, G. (2021). Diffusion of protein molecules through microporous nanofibrous polyacrylonitrile membranes. *ACS applied polymer materials*, *3*(3), 1618-1627.

30. Tang, R., Xie, M. Y., Li, M., Cao, L., Feng, S., Li, Z., & Xu, F. (2022). Nitrocellulose membrane for paper-based biosensor. *Applied Materials Today*, *26*, 101305.

31. Pan, B., Zhao, C., Norwood, M., Wang, M., Liu, G., & Sun, G. (2023). Highly Sensitive Naked Eye Detectable Colorimetric Biosensors Made from Macroporous

Framework Melamine Foams for Onsite and Simultaneous Detection of Multiple Environmental Hazards in Flowing Through Sensing Systems. *Advanced Sensor Research*, *3*(1), 2300080.

32. El-Moghazy, A. Y., Wisuthiphaet, N., Amaly, N., & Nitin, N. (2022). Enhanced sampling of bacteria and their biofilms from food contact surfaces with robust cationic modified swabs. *Cellulose*, *29*(8), 4509-4524.

33. Koch, A. L. (1970). Turbidity measurements of bacterial cultures in some available commercial instruments. *Analytical biochemistry*, *38*(1), 252-259.

34. Cleland, J. L., Lam, X., Kendrick, B., Yang, J., Yang, T. H., Overcashier, D., Brooks, D., Hsu, C., & Carpenter, J. F. (2001). A specific molar ratio of stabilizer to protein is required for storage stability of a lyophilized monoclonal antibody. *Journal of Pharmaceutical Sciences*, *90*(3), 310-321.

35. Chen, C. A., Yeh, W. S., Tsai, T. T., & Chen, C. F. (2019). Three-dimensional origami paper-based device for portable immunoassay applications. *Lab on a Chip*, *19*(4), 598-607.

36. Schneider, C. A., Rasband, W. S., & Eliceiri, K. W. (2012). NIH Image to ImageJ: 25 years of image analysis. *Nature Methods*, *9*(7), 671-675.

37. Murdock, R. C., Shen, L., Griffin, D. K., Kelley-Loughnane, N., Papautsky, I., & Hagen, J. A. (2013). Optimization of a paper-based ELISA for a human performance biomarker. *Analytical chemistry*, *85*(23), 11634-11642.

38. Levin, P. A., & Angert, E. R. (2015). Small but mighty: cell size and bacteria. *Cold Spring Harbor perspectives in biology*, *7*(7), a019216.

39. Rehman, I., & Bonfield, W. J. J. (1997). Characterization of hydroxyapatite and carbonated apatite by photo acoustic FTIR spectroscopy. *Journal of materials science: Materials in medicine*, *8*(1), 1-4.

40. Shih, C. M., Chang, C. L., Hsu, M. Y., Lin, J. Y., Kuan, C. M., Wang, H. K., Huang, C. T., Chung, M. C., Huang, K. C., Hsu, C. E., Wang, C. Y., Shen, Y. C., & Cheng, C. M. (2015). Paper-based ELISA to rapidly detect Escherichia coli. *Talanta*, *145*, 2-5.

41. Pang, B., Zhao, C., Li, L., Song, X., Xu, K., Wang, J., ... & Li, J. (2018). Development of a low-cost paper-based ELISA method for rapid *Escherichia coli* O157: H7 detection. *Analytical Biochemistry*, *542*, 58-62.

42. Zhao, Y., Zeng, D., Yan, C., Chen, W., Ren, J., Jiang, Y., Xue, F., Ji, D., Tang, F., Zhou, M., & Dai, J. (2020). Rapid and accurate detection of *Escherichia coli* O157: H7 in beef using microfluidic wax-printed paper-based ELISA. *Analyst*, *145*(8), 3106-3115.

43. Wu, W., Zhang, J., Zheng, M., Zhong, Y., Yang, J., Zhao, Y., Wu, W., Ye, W., Wen, J., Wang, Q., & Lu, J. (2012). An aptamer-based biosensor for colorimetric detection of *Escherichia coli* O157: H7. *PloS one*, *7*(11), e48999.

44. Feng, M., Yong, Q., Wang, W., Kuang, H., Wang, L., & Xu, C. (2013). Development of a monoclonal antibody-based ELISA to detect *Escherichia coli* O157: H7. *Food and agricultural immunology*, *24*(4), 481-487.

45. Yao, Y., Xie, G., Zhang, X., Yuan, J., Hou, Y., & Chen, H. (2021). Fast detection of *E. coli* with a novel fluorescent biosensor based on a FRET system between UCNPs and GO@ Fe 3 O 4 in urine specimens. *Analytical Methods*, *13*(19), 2209-2214.

46. Vaezi, Z., Azizi, M., Mohammadi, S. S., Hashemi, N., & Naderi-Manesh, H. (2020). A novel iron quantum cluster confined in hemoglobin as fluorescent sensor for rapid detection of *Escherichia coli*. *Talanta*, *218*, 121137.

47. Hoang, H. A., & Dien, L. T. (2015). Rapid and simple colorimetric detection of

Escherichia coli O157: H7 in apple juice using a novel recombinant bacteriophage-based method. *Biocontrol science*, *20*(2), 99-103.

48. Mou, X. Z., Chen, X. Y., Wang, J., Zhang, Z., Yang, Y., Shou, Z. X., Tu, Y. X., Du, X., Wu, C., Zhao, Y., Qiu, L., Jiang, P., Chen, C., Huang, D. S., & Li, Y. Q. (2019). Bacteria-instructed click chemistry between functionalized gold nanoparticles for point-of-care microbial detection. *ACS applied materials & interfaces*, *11*(26), 23093-23101.

49. Allison, S. D., Manning, M. C., Randolph, T. W., Middleton, K., Davis, A., & Carpenter, J. F. (2000). Optimization of storage stability of lyophilized actin using combinations of disaccharides and dextran. *Journal of pharmaceutical sciences*, *89*(2), 199-214.

50. Wang, J., Yiu, B., Obermeyer, J., Filipe, C. D., Brennan, J. D., & Pelton, R. (2012). Effects of temperature and relative humidity on the stability of paper-immobilized antibodies. *Biomacromolecules*, *13*(2), 559-564.

51. Chen, C. A., Yeh, W. S., Tsai, T. T., & Chen, C. F. (2019). Three-dimensional origami paper-based device for portable immunoassay applications. *Lab on a Chip*, *19*(4), 598-607.

3.6 Supporting Information

3.6.1 Measurement of diffusion of bacteria in MF

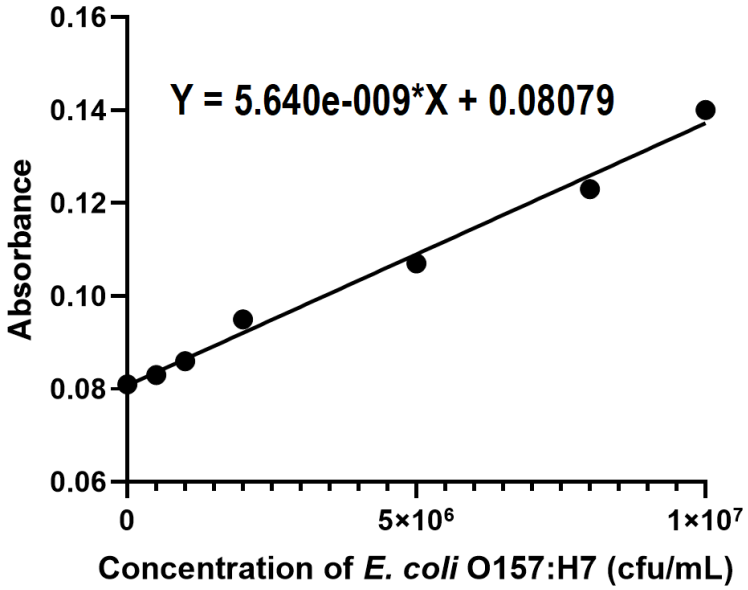

Figure S3.1. Calibration curve for *E. coli* O157:H7 at the wavelength of 600 nm.

3.6.2 Vertical flow test through materials

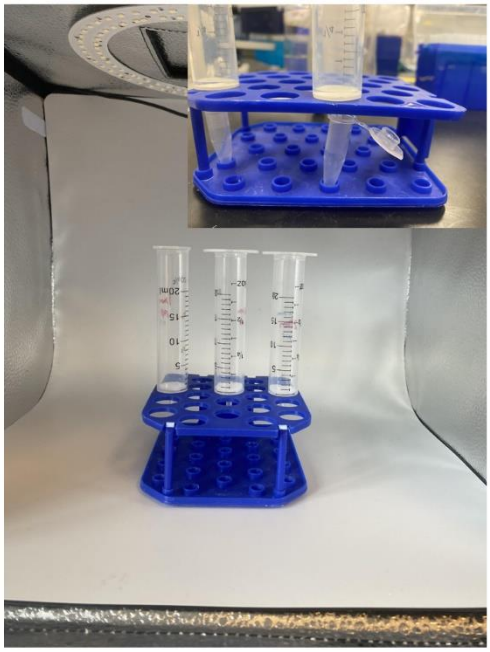

Figure S3.2. Photograph demonstrating the liquid filtering test using syringes and vials.

3.6.3 Reagent modification and protein immobilization

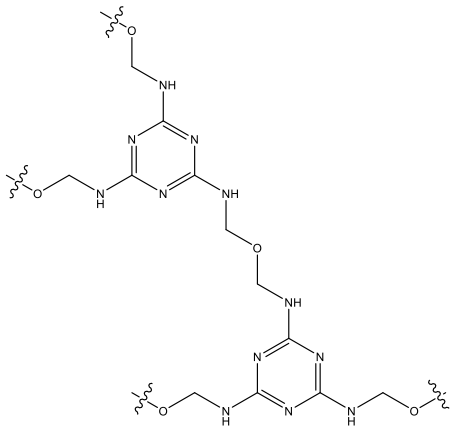

Figure S3.3. Chemical structure of melamine foam

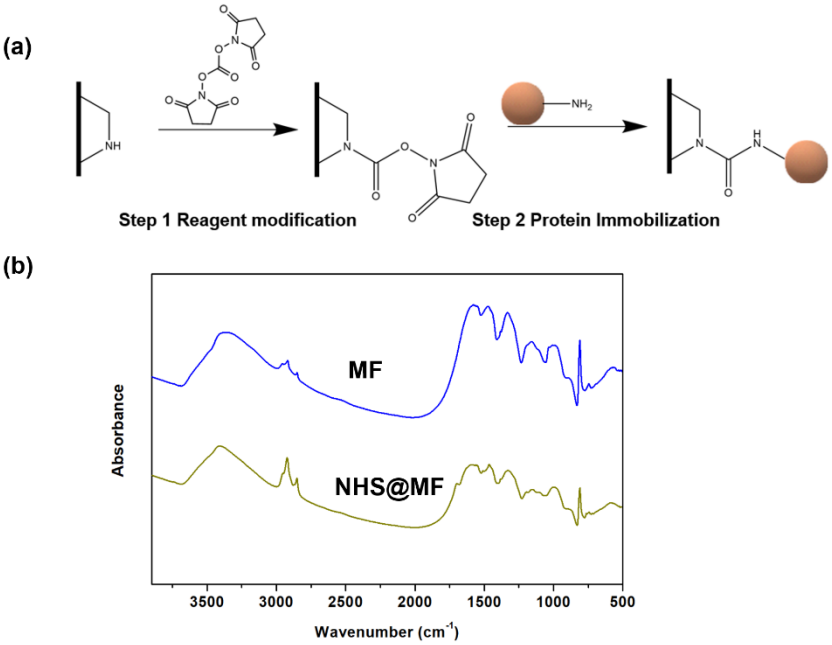

Figure S3.4. (a) Reaction of MF with DSC and proteins and (b) FTIR results of MF and NHS@MF.

3.6.4 Optimization experiments for the detection of *E. coli* O157:H7

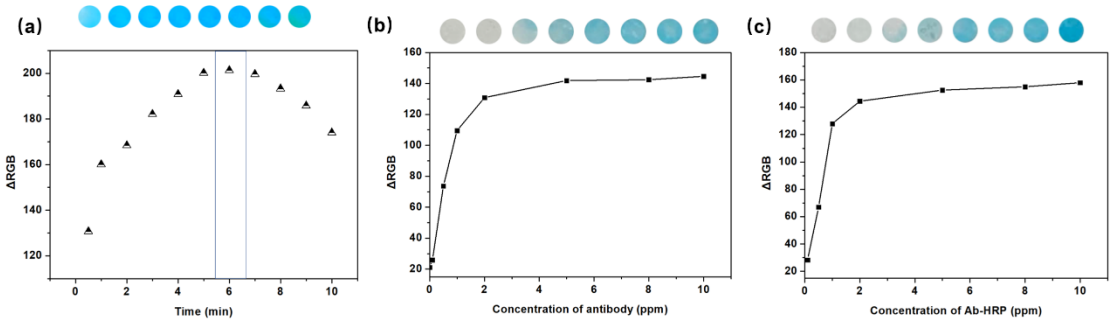

Figure S3.5. Optimization of (a) the reaction time between HRP and TMB substrate; (b) the concentration anti-*E. coli* O157:H7 antibodies used for immobilization; (c) the concentration of Anti-*E. coli* O157:H7 antibodies conjugated with HRP used as the secondary antibody in f-ELISA.

3.6.5 Specificity of the assay

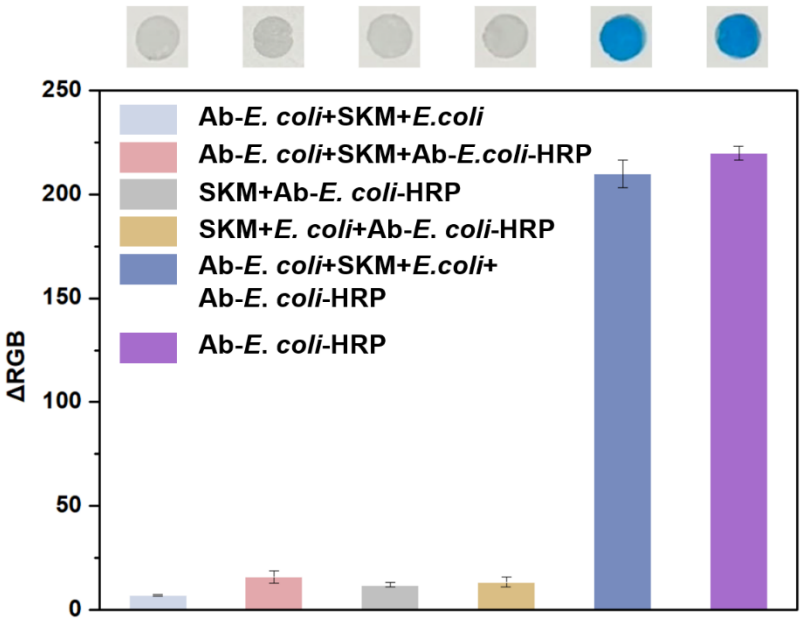

Figure S3.6. Specificity of the assay. Images of the NHS@MF membranes with different treatments after the addition of TMB substrate: 100 µL Ab-*E. coli* (5 mg/L), 200 µL skimmed milk (SKM) (3%), 200 µL *E. coli* O157:H7 (10^7 CFU/mL), and 100 µL Ab-*E. coli*-HRP (2 mg/L) were used accordingly. The bar diagram for the ΔRGB

was observed from the images. Data are presented as mean ± SD, with n = 3 independent experiments.

3.6.6 Onsite detection of *E. coli* O157:H7 in spiked mike samples

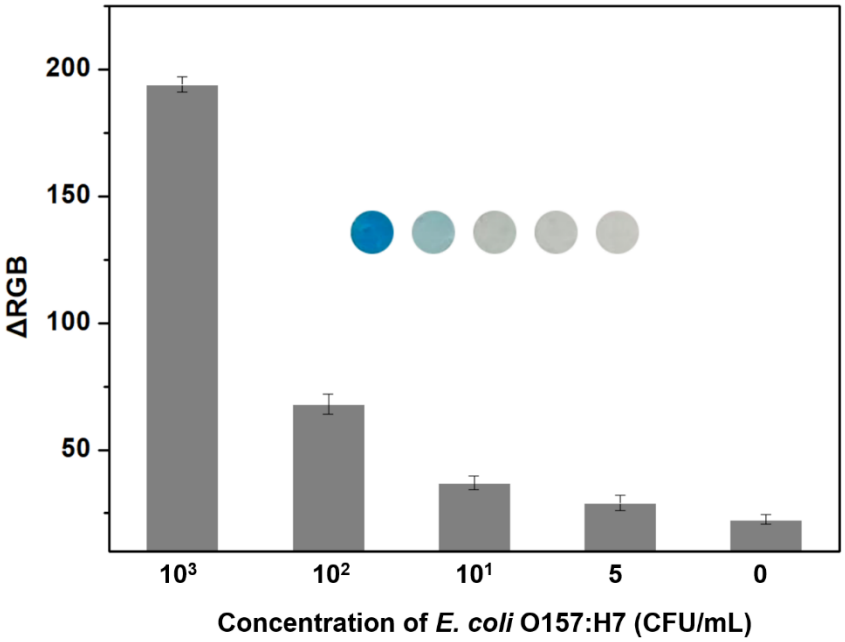

Figure S3.7. Optical image and ΔRGB values of membranes treated by different concentrations of *E. coli* O157:H7 in spiked milk samples. Data are presented as mean ± SD, with n = 3 independent experiments.

3.6.7 Antibody Storage Evaluation for f-ELISA

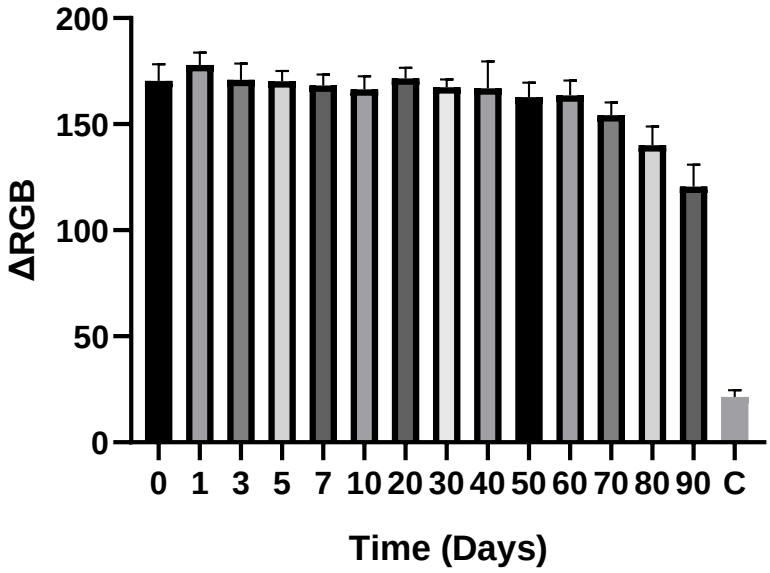

Figure S3.8. Long-Term Stability Assessment. The Ab@NHS@MF membranes were prepared by using 10% sucrose as a stabilizer followed by freeze-drying. They were stored at a consistent temperature of 4°C and assessed over a period of 90 days. Data are presented as mean ± SD, with n = 3 independent experiments. *C = Control group

Chapter 4. Versatility and Stability of Melamine Foam-Based Biosensors (f-ELISA) Using Antibodies, Nanobodies, and Peptides as Sensing Probes

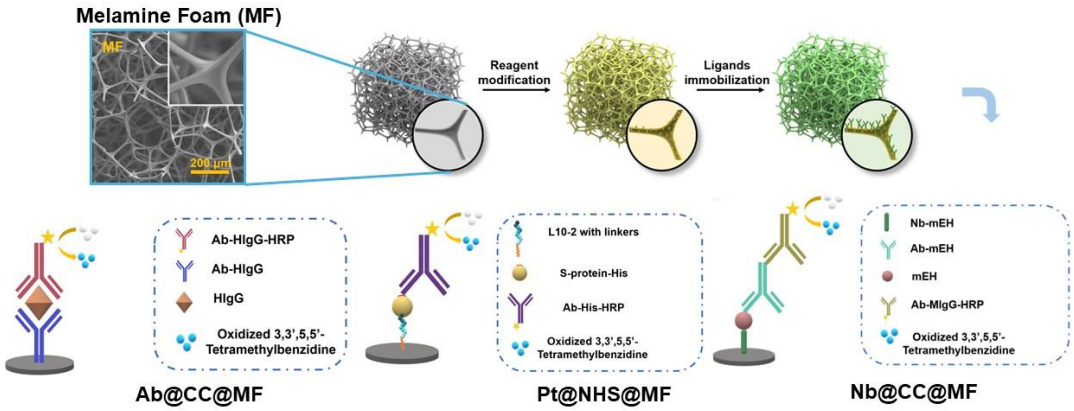

Abstract

Macroporous three-dimensional (3D) framework structured melamine foam-based Enzyme-Linked Immunosorbent Assay (f-ELISA) biosensors were developed for rapid, reliable, sensitive, and on-site detection of trace amount of biomolecules and chemicals. Various ligands can be chemically immobilized onto the melamine foam, which brings in the possibility of working with antibodies, nanobodies, and peptides, respectively, as affinity probes for f-ELISA biosensors with improved stability. Different chemical reagents can be used to modify the foam materials, resulting in varied reactivities with antibodies, nanobodies, and peptides. As a result, the f-ELISA sensors produced from these modified foams exhibit varying levels of sensitivity and performance. This study demonstrated that the chemical reagents used for immobilizing antibodies, nanobodies, and peptides could affect the sensitivities of the f-ELISA sensors, and their storage stabilities under different temperatures varied depending on the sensing probes used, with f-ELISA sensors employing nanobodies as probes exhibiting the highest stability. This study not only showcases the versatility of the f-ELISA system but also opens new avenues for developing cost-effective, portable, and user-friendly diagnostic tools with optimized sensitivity and stability.

4.1 Introduction

Enzyme-linked immunosorbent Assay (ELISA) has long been a gold standard method for selective and sensitive detection of biomolecules in medical diagnostics and monitoring environmental pollutants[1,2,3]. However, the use of professional lab

equipment and operation, together with relatively lengthy and complicated procedures, and limited adaptability and scalability, affects the personal and on-site applications of the method[4,5]. In response to these challenges, paper-based ELISA (p-ELISA) emerged as a more portable and user-friendly alternative[6]. By simplifying the operational complexity, they opened the door to field applications, especially in resource-limited settings[7,8]. Despite these advancements, p-ELISAs still face significant drawbacks, including compromised sensitivity and difficulties in quantifying results accurately[9]. The observed limitations of the p-ELISA are partly attributed to its inherent layered fiber mat structure, which leads to heterogeneity in the sensor media, particularly in the vertical direction of the media[10]. This inconsistency restricts the penetration of larger biomolecules through the matrix, resulting in a lower incorporation rate of biomolecules on the internal fibers than on the external surfaces[11,12]. Although often described as three-dimensional, the internal parts of these materials are not fully utilized in practice[13].

A foam-based ELISA (f-ELISA) using macroporous framework melamine foams (MF) as a platform was developed to overcome the constraints of paper-based systems[14,15]. This platform of the f-ELISA matrix features a macroporous, reticulated, three-dimensional framework structure, enabling free movement of biomolecules in varied sizes in every direction inside. Besides, this interconnected framework promotes chaotic and vortex mixing, thereby increasing the frequency of contacts between biomolecules and surfaces of the framework media, leading to improved efficiency and effectiveness in the detection of target molecules. The f-ELISA has shown effectiveness

in rapid and sensitive detection for various targets, such as SARS-CoV-2 spike protein, chloramphenicol, and pathogens, using different ELISA techniques like direct, competitive, and sandwich assays[14,15]. Additionally, the f-ELISA system uses covalent bonding to immobilize sensing probes instead of using other intermolecular interactions. This strategy ensures a more stable and permanent attachment of small or large proteins to the platform, significantly enhancing coating efficiency and overcoming the limitations of the physical adsorption of smaller molecules.

However, there are several challenging questions on this system to be answered, including the chemical immobilization process, which may lead to varied interactions and activities with the proteins in different sizes serving as probes, and stability of the f-ELISA biosensors, especially the storage stability.

In the ELISA system, antibodies, as the classical choice, are well-established as indispensable reagents[16,17,18]. Their remarkable specificity and affinity for target antigens make them ideal for capturing and detecting specific molecules in complex samples[19]. Furthermore, antibodies can be easily conjugated to enzymes or fluorescence tags, enabling the quantification of target analytes with precision[20,21]. On the other hand, variable heavy (VHH) single domain antibodies, or nanobodies, sourced from *Camelidae* family, offer distinct advantages in assay development[22,23,24]. They are simpler to produce and standardize compared to traditional monoclonal or polyclonal antibodies, contributing to more consistent and reliable assays[25]. Their smaller size, about one-tenth that of conventional antibodies, does not compromise their affinity[26,27].

Additionally, nanobodies exhibit enhanced stability and are more easily modified, making them increasingly popular as therapeutics and analytical reagents[28,29,30]. Another sensing probe, peptide, a short chain of amino acids, offers a unique set of advantages in ELISA applications[31,32,33]. Custom-designed peptides can mimic specific epitopes, facilitating the development of highly specific assays[34]. Moreover, peptides are cost-effective and can be easily synthesized, making them an attractive economical option[35,36,37].

In this context, use of different chemical modification methods and different sensing probes with varied structural and bioconjugation features in f-ELISA system were investigated in this study, which can reveal the versatility of the f-ELISA matrix. By preparing the performance of f-ELISA biosensors made from using different chemical reactions and varied probes, we can compare the f-ELISA biosensor's adaptability and stability of storage, making it a versatile and effective tool in diagnostics, offering broader applications, and improving detection processes in various fields. Additionally, with the successful incorporation of nanobodies and peptides, the biosensors could also demonstrate the robustness of the f-ELISA matrix for potentially broadened commercial applications.

4.2 Experimental Section

4.2.1 Materials

N, N'-disuccinimidyl carbonate (DSC), cyanuric chloride (CC), 1,1'-Carbonyldiimidazole (CDI), triethylamine (TEA), 1,4-dioxane, acetone, phosphate-

buffered saline (PBS), 3,3′,5,5′-Tetramethylbenzidine (TMB), goat anti-Mouse IgG secondary antibody with HRP, 6x-His Tag Monoclonal Antibody (HIS.H8) HRP (Ab-His-HRP), Pierce™ BCA Protein Assay Kit, and 96-well plates were purchased from ThermoFisher Scientific (Pittsburgh, PA). The SARS-CoV-2 spike protein active trimer with His tag (S-protein-His) (CatalogNo. SPN-C52H) was purchased from ACRO Biosystems (Newark, DE). Anti-Human IgG (Fab specific) antibody (Ab-HIgG) and Human IgG (HIgG) were purchased from Sigma-Aldrich (Milwaukee, WI). Goat anti-human IgG (Fc) antibody with HRP (Ab-HIgG-HRP) was purchased from Bio-Rad Laboratories (Hercules, CA). All Fmoc-protected amino acids were purchased from P3 Biosystems (Louisville, KY) and Chem-Impex International, Inc. (Wood Dale, IL). Melamine foams were purchased from Swisstek (Swisstek Manufacturer). The preparation of microsomal epoxide hydrolase (mEH), anti-mEH nanobodies (Nb-mEH), and anti-human mEH monoclonal antibodies (Ab-mEH) was described in the previous works[38].

4.2.2 Chemical modifications of melamine foam

The modification of melamine foam using DSC was illustrated in a previous publication[15]. For the modification using CC, the process is described below: 0.5 g of MF samples of 1 mm thickness and 5 mm diameter were first immersed in a 3 mol/L NaOH solution at 5°C for 30 minutes. Following this, they were washed with deionized water and then immersed in a 0.1 g/mL CC solution (prepared by dissolving 5 g of CC in 50 mL of 1,4-dioxane) at room temperature for 2 hours. After the treatment, the

samples were thoroughly rinsed with water and acetone, and then vacuum dried. To modify MF using CDI, the samples (0.5 g, 1 mm thickness, 5 mm diameter) were immersed in 0.1 g/mL CDI solution (prepared by dissolving 5 g of CDI in 50 mL of DMF). After 6 h incubation under room temperature, the resulting samples were thoroughly washed with N, N-dimethylformamide (DMF), and acetone, and subsequently dried under vacuum conditions.

4.2.3 Characterizations

The morphology of the modified MF samples was examined using a scanning electron microscope (Quattro ESEM, Thermo Scientific). This allowed for detailed observation of the structural changes resulting from the different modification processes applied to the membranes. The chemical structures of MF, DSC-modified MF membranes (NHS@MF), CC-modified MF membranes (CC@MF), and CDI-modified MF membranes (CDI@MF) samples were characterized by using FTIR spectrometer (Nicolet 8700, Thermo Nicolet Co., USA) at a wavenumber range (4000 cm^{-1}- 500 cm^{-1}). The water contact angles of the membranes were measured when a small droplet of water came into contact with the surface, and the images were captured by a Dino-Lite camera (Dunwell Tech. Inc., USA). This procedure helps in assessing the hydrophobic or hydrophilic nature of the membranes before and after the modifications.

4.2.4 Peptide synthesis

The L10-2 peptides were synthesized by solid phase peptide synthesis through Fmoc chemistry[39]. In general, Rink Amide MBHA Resin (~0.5 mmol/g, P3 BioSystems,

Louisville, KY) was soaked in DMF for 2 hours before usage. In DMF, the peptides were synthesized by a CEM Liberty Blue microwave peptide synthesizer using ethyl cyanohydroxyiminoacetate (Oxyma) and diisopropylmethanediimine (DIC) as coupling reagents and 4-methylpiperdine for Fmoc deprotection. After the peptide coupling, global deprotection and cleavage were performed by TFA cocktail (TFA : Water : Triisopropylsilane = 95% : 2.5% : 2.5%, v/v) for 2 hours at room temperature. The TFA cocktail was drained and concentrated, and the peptides were precipitated by cold ether. The crude peptides were purified by C-18 HPLC (LC-20AR liquid chromatograph suite, Shimadzu). We also synthesized variants of the L10-2 peptides, namely L10-2a, L10-2b, and L10-2c, by incorporating one, two, or three 8-amino-3,6-dioxaoctanoic acid (AEEA) spacers, respectively, at the N-terminus of each peptide.

4.2.5 Immobilization and optimization of immunoprobes

Immobilization of Antibodies: The modified MF membranes (NHS@MF, CC@MF and CDI@MF) were immersed in a 100 μL solution of antibody (Ab-HRP) with a concentration of 100 mg/L. This incubation was carried out for 30 minutes. Following incubation, the membranes were washed using PBS buffer in preparation for subsequent measurements, as detailed in the colorimetric data analysis section of the study. The amount of the immobilized antibodies on these membranes was determined by the bicinchoninic acid (BCA) protein assay via a micro-plate reader and the calibration curve of antibody concentration versus absorbance response was shown in the supporting information (Figure S4.1a).

Immobilization of nanobodies: The chemically modified MF membranes were immersed in a 100 μL solution of biotinylated nanobody (Bt-Nb) with a concentration of 100 mg/L. This incubation was carried out for 30 minutes. Following incubation, the membranes were washed using PBS and then immersed in 100 μL streptavidin HRP conjugate (SA-HRP) solution with a concentration of 1 mg/L and incubated for 30 minutes under mild shaking. Lastly, the membranes were washed again using PBS buffer in preparation for subsequent measurements, as detailed in the following colorimetric data analysis section. The amount of the immobilized nanobodies was also determined by the bicinchoninic acid (BCA) protein assay with the calibration curve shown in Figure S4.1b.

Immobilization of peptides: The chemically modified MF membranes were immersed in a 100 μL solution of biotinylated L10-2 peptide (Bt-L10-2, 0.1%) for 30 minutes with mild shaking and then washed with PBS buffer. Subsequently, the membranes were immersed in 100 μL Streptavidin Alexa Fluor™ 647 conjugate solution (1 mg/L) and incubated for 30 minutes with mild shaking. Afterward, the membranes were washed again using PBS buffer and then their fluorescent intensities were measured by a microplate reader at the wavelength of 647 nm. The amounts of immobilized peptides were determined using a pierce quantitative fluorometric peptide assay following the protocol[40], with the calibration curve shown in Figure S4.1c.

4.2.6 Assay procedures of foam-based ELISA

Antibody Assay: A volume of 100 μL of Ab-HIgG solution with a concentration of 5

mg/L was added onto the CC@MF membranes and left to incubate for 30 minutes at room temperature under gentle agitation. After the antibody was immobilized, the membranes were treated with 200 μL of 3% skim milk (SKM) as a blocking agent and incubated for 30 minutes to block any unbound active sites. Following the steps of immobilization and blocking, the resulting membranes were designated as Ab@CC@MF. Then, 100 μL of HIgG at various concentrations (0 to 50 mg/L) was added to Ab@CC@MF membranes and incubated for 30 minutes with mild agitation. Following this, 100 μL of 1 mg/L Ab-His-HRP was applied to each of the Ab@CC@MF membranes. The incubation of the membranes with Ab-His-HRP lasted for 20 minutes. After the incubation, the membranes were first washed with 0.05% tween-20 and then with PBS buffer in preparation for subsequent measurements, as detailed in the colorimetric data analysis section of the study.

Nanobody Assay: A volume of 100 μL of Nb-mEH solution with a concentration of 2 mg/L was added onto the CC@MF membranes and left to incubate for 30 minutes at room temperature under gentle agitation. After the nanobody was immobilized, the membranes were blocked using 200 μL of 3% skim milk (SKM) and incubated for 30 minutes to block any unbound active sites. Following the steps of immobilization and blocking, the resulting membranes were defined as Nb@CC@MF. Then, 100 μL of mEH at various concentrations (0 to 50 mg/L) was added to the Nb@CC@MF membranes and incubated for 30 minutes with mild agitation. Afterward, 100 μL of 1 mg/L Ab-mEH was applied to each membrane. The incubation with Ab-His-HRP lasted for 20 minutes. Following this incubation, the membranes were then immersed into 100

μL Ab-MIgG-HRP solution at the concentration of 1 mg/L for 20 minutes. Lastly, the membranes were sequentially washed with 0.05% tween-20 and then with PBS buffer in preparation for subsequent measurements, as detailed in the colorimetric data analysis section of the study.

Peptide Assay: A volume of 100 μL of L10-2c peptide solution (0.1% in PBS buffer) was added onto the NHS@MF membranes and left to incubate for 30 minutes at room temperature under gentle agitation. Afterward, the residual active sites on the membranes were blocked by using 200 μL of 3% skim milk (SKM) and incubated for 30 minutes. Following the steps of immobilization and blocking, the resulting membranes were designated as Pt@NHS@MF. Then, 100 μL of S-protein-His at various concentrations (0 to 50 mg/L) was added to the Pt@NHS@MF membranes and incubated for 30 minutes with mild agitation. Following this, 100 μL of 1 mg/L Ab-His-HRP was applied to the membrane and allowed for 20 minutes of incubation. Afterward, the membranes were washed with 0.05% tween-20 and then with PBS buffer in sequence for subsequent measurements of the colorimetric data analysis. The procedure for immobilizing different peptides with varied linker lengths onto the membranes remains the same, with the only variation being the substitution of L10-2c by other peptides (L10-2, L10-2a, or L10-2b) as the target-recognizing ligands. This adaptation allows for the assessment of peptides with different lengths while maintaining the same overall experimental approach.

4.2.7 Colorimetric data analysis

Upon the addition of TMB to the membranes at the last step of the assays, they were placed in a lightbox with an LED lightbox (from E mart) and on a light panel (5”×4”, LP-100N). The images were captured using a smartphone camera (iPhone 14pro max) positioned at 50 cm above the samples. The change of color intensity (ΔRGB) was analyzed using the red channel value (R-value) from the RGB color model, as measured by the Photoshop software. ΔRGB value was calculated by the R-value difference between the white background and the membrane, following the equation:

$$\Delta RGB = RGB_{background} - RGB_{membranes} \quad (1)$$

$RGB_{background}$ denotes the R-value of the white background (without the presence of HRP), and $RGB_{membranes}$ refers to the R-value of the sample membranes.

4.2.8 Storage stability test

To assess the long-term efficacy and consistency of the f-ELISA using various sensing probes, we investigated the activity of f-ELISA biosensors made with antibodies and nanobodies on the CC modified MF, and the biosensors made with peptides on DSC modified MF after stored under two conditions for a duration of up to 30 days. The membranes underwent lyophilization and were then divided into two equal portions. One portion was kept at a steady temperature of 4°C, while the other was maintained under room temperature (~25°C). The membranes were subsequently evaluated over a 30-day period. At specific time points, samples were collected and employed in the f-

ELISA assay to identify corresponding targets of HIgG, mEH, or S-protein-His, respectively, following the same protocols. After the addition of TMB substrate, the colorimetric signal intensity was calculated by the following equation:

$$\text{Signal}(\%) = \frac{\Delta\text{RGB of x day}}{\Delta\text{RGB of 0 day}}$$

4.2.9 Statistical analysis

For this study, each assay was conducted three times. The data are presented as mean ± standard deviations (SD). Differences between groups were evaluated using the two-tailed Student's t-test, with significance levels defined as *P < 0.05, **P < 0.01, and ***P < 0.001. A P-value of less than 0.05 was considered statistically significant. The correlation between the observed and predicted values was determined by the correlation coefficient (R). The limit of detection (LOD) was determined using the formula 3.3 σ/S, where σ represents the standard deviation of the response and S is the slope derived from the calibration curve. All statistical analyses were performed using GraphPad Prism software.

4.3 Results and Discussion

4.3.1 Chemical modifications of melamine foam

In this study, we applied three distinct chemical modification approaches to melamine foam (MF) membranes with a thickness of 1 mm and diameter of 5 mm (Figure 4.1a) to create reactive sites for biomolecules with free amino groups (Figure 4.1b). These modifications involve the activation of secondary amine groups on the MF (Figure S4.2)

using reagents of DSC, CDI, and CC, which introduced N-hydroxysuccinimide (NHS), 2-acetylimidazole, and chloro-1,3-triazine functional groups onto the material. This process yielded three intermediates, NHS@MF, CDI@MF, and CC@MF, each capable of reacting with amino groups in proteins or peptides, as shown in Figure 4.1c. ATR-FTIR analysis validated the successful incorporation of reactive groups to MF, evidenced by specific spectral peaks, including NHS@MF's carbonate peak at 1707 cm^{-1}, CDI@MF's amide peak at 1728 cm^{-1}, and CC@MF's carbon-chloride peak at 794 cm^{-1}, as shown in Figure 4.1d. The SEM images presented in Figure 4.1e demonstrate that the MF samples retain their morphology of framework structures intact after the chemical modifications. The images reveal a consistent pore size of approximately 150 μm and a fiber diameter of around 7 μm within the MF framework. This consistency indicates that the modification processes could not significantly damage or change the reticulated, macroporous, and 3D structure of the MF material but only altered the surface chemical structures and properties, such as hydrophilicity of the material surfaces, as depicted in Figure 4.1f. The CC@MF membrane exhibited the highest hydrophobicity, attributed to the less-polar nature of the triazine ring, while NHS@MF showed greater hydrophilicity compared to both CC@MF and CDI@MF, due to the presence of the ester group connection to succinimide ring (Figure 4.1c). For platforms using fiber-based membranes, high hydrophobicity of the material can cause inhomogeneous colorimetric signals and inefficient use of the internal surface area, due to the hydrophobic surface repelling the aqueous solution[9,41]. However, the unique foam-like, reticulated, and macroporous structure of the MF enables aqueous solutions

to permeate the 3D matrix even with a hydrophobic surface, overcoming the surface tension. Once biomolecules are immobilized on the MF surface, the materials are uniformly hydrophilic. Therefore, the MF material here with high hydrophobicity does not impede aqueous molecule movement within the structure, overcoming a common limitation seen in fiber-based systems[15,16].

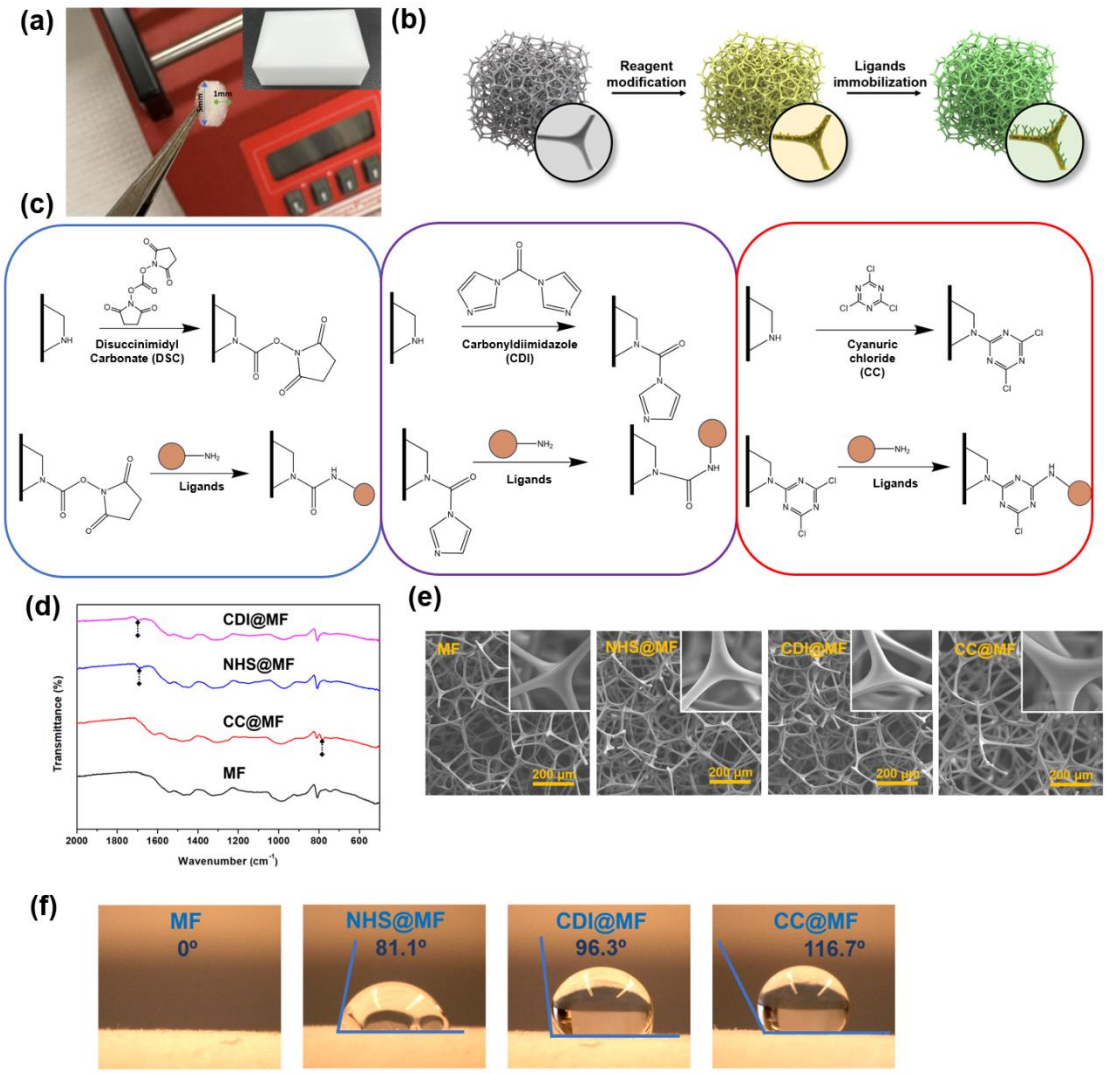

Figure 4.1. (a) Optical view of a commercial MF and standardized membranes with a thickness of 1 mm and diameter of 5 mm. (b) Schematic illustration of the reagent modification and the following ligand immobilization. (c) Reaction of MF with DSC,

CDI, and CC, and ligands with free amino group. (d) ATR-FTIR results of MF after different modifications. (e) SEM images of MF, NHS@MF, CDI@MF, and CC@MF. (f) Water contact angle results of MF, NHS@MF, CDI@MF, and CC@MF.

4.3.2 Antibody immobilization

The three differently modified membranes were used for antibody immobilization, employing Ab-HRP as an indicator to qualitatively assess the number of the molecules immobilized. The intensity of the colorimetric signals served as an indicator after the addition of TMB substrate, with darker blue colors indicating a higher quantity of immobilized antibodies. Among all, the CC@MF membranes demonstrated the most intense colorimetric signal under identical experimental conditions, a difference that was visually discernible in the optical images of each membrane, as presented in Figure 4.2a. To accurately quantify the immobilized antibodies, a BCA assay kit was conducted on each membrane, which was incubated with 100 mg/L of the human antibody solution for 30 minutes at room temperature, facilitating the antibody immobilization for subsequent quantitative analysis. The amount of antibodies immobilized on each membrane was determined using the calibration curve provided in Figure S4.1a. The CC@MF membrane demonstrated the highest amount of the antibody immobilization (Figure 4.2b), aligning well with the results of the qualitative analysis previously mentioned. The higher immobilization amounts of antibodies on the CC@MF membranes can be attributed to its more hydrophobic nature, which enhances hydrophobic interactions between the CC@MF surface and the antibodies

and consequently increases the probability of molecules contacting the surface, thereby enhancing the efficiency of covalent bond formation between the ligands and the membranes. Additionally, the chemical structure of CC@MF, as shown in the reaction scheme, provides two active sites per secondary amine, compared to the single active site in the other two modifications, which also likely contribute to the increased antibody binding on the CC@MF membranes. Besides, the CC@MF framework structure morphology was intact after the immobilization of the antibody (Figure S4.3a). Hence, for the subsequent f-ELISA experiments utilizing antibodies as the target recognizing ligand, CC@MF has been chosen as the preferred platform.

4.3.3 Performance of antibody based f-ELISA

The CC@MF membranes immobilized with antibodies were employed in sandwich f-ELISA to detect targets. In this case, Ab-HIgG was first immobilized on the membranes and then the antigen HIgG was added, which can be specifically captured by Ab-HIgG. Subsequently, Ab-HIgG-HRP was introduced to bind with the captured HIgG, resulting in colorimetric signals generated by the reaction of HRP with the TMB substrate, as depicted in Figure 4.2c. To confirm the specificity of the assay, various control experiments were performed. The results indicated that in the absence of the HRP enzyme or the Ab-HIgG, there was either no color development or a very minimal color response (Figure S4.4). This outcome demonstrates the specificity of the assay, particularly highlighting the negligible color change in negative control setups where key components were omitted.

To assess the sensitivity of the f-ELISA in detecting targets, an assay using varied HIgG concentrations (0 to 5 mg/L) was performed, and the visually discernible blue color signals corresponding to different concentrations of the HIgG are shown in Figure 4.2d. The color intensities were analyzed using the Photoshop software, and from this analysis, a linear equation for the colorimetric assay was fitted as $y=460.60x + 7.83$ ($R^2=0.98$) within the range of 0 to 0.1 mg/L. The results of the assay demonstrate that the detection of HIgG by the naked eye was feasible at a concentration as low as 0.02 mg/L, with the limit of detection (LOD) determined to be 0.013 mg/L, aided by a smartphone camera and subsequent Photoshop analysis.

In addition, the selectivity of this f-ELISA biosensing platform was tested using various similar proteins, including mouse antibody (MIgG), rabbit antibody (RIgG), goat antibody (GIgG), and human serum albumin (HSA). Notably, only HIgG showed a significant colorimetric response, as shown in Figure 4.2e. The absence of a response from other proteins, including antibodies from other species highlights the selectivity of this f-ELISA sensor. The selectivity in distinguishing HIgG demonstrates the potential of this f-ELISA biosensor for accurate HIgG detection in medical diagnostics, unaffected by the presence of these tested proteins.

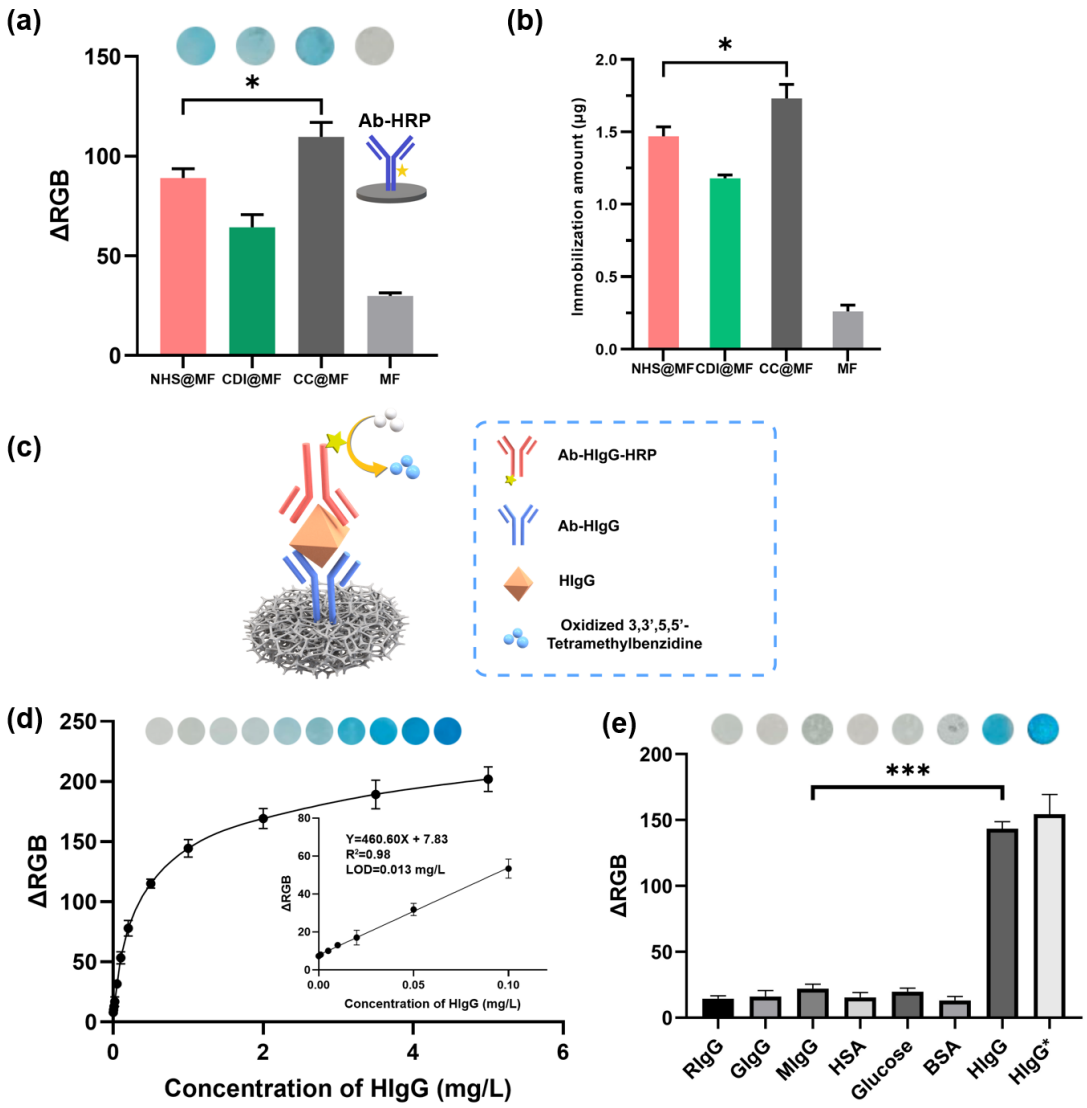

Figure 4.2. (a) Schematic illustration of Ab-HRP immobilization; optical images and colorimetric comparison results among different MF membranes. (b) Quantification of antibodies immobilized on different MF membranes via BCA assay kit. (c) A diagram of the antibodies as immunoprobes in f-ELISA for human IgG. (d) Optical images and the calibration curve of f-ELISA by using Ab-HIgG as the capture antibody. (e) Selectivity of f-ELISA toward HIgG detection in comparison with rabbit IgG (RIgG), goat IgG (GIgG), mouse IgG (MIgG), and Human serum albumin (HSA). The concentration of each protein used in the selectivity assay is 1 mg/L. The data are

presented as the mean ± standard deviation (SD) from three independent experiments. Statistical significance was determined using a two-tailed Student's t-test.*P < 0.05, ***P < 0.001. *LOD = limit of detection.

4.3.4 Nanobody immobilization

The chemically modified membranes were initially immersed in a solution containing biotinylated nanobodies (Bt-Nb). Following this, streptavidin-horseradish peroxidase (SA-HRP) was used as an indicator to qualitatively determine the amount of nanobodies immobilized on each membrane, with darker colors indicating a higher quantity of immobilized nanobodies (Figure 4.3a). Among all, the CC@MF membranes demonstrated the most intense colorimetric signal under identical experimental conditions. This difference was visually discernible in the optical images of each membrane, as presented in Figure 4.3b. The same BCA assay was conducted to quantify the amount of nanobodies immobilized on each membrane. The amount of nanobodies immobilized on each membrane was determined using a calibration curve provided in Figure S4.1b. The CC@MF membrane still demonstrated the highest amount of immobilization of the nanobody (Figure 4.3c). The higher immobilization of the nanobodies on the CC@MF membranes can be attributed to the same reason as the immobilization of the antibodies mentioned above since even though the size of the nanobody is ten times smaller than the antibodies, it is still considered a single-domain antibody. Besides, the CC@MF retains the framework structure morphology and the nature after the process of the nanobody immobilization (Figure S4.3b). Therefore, the

CC@MF was employed in the subsequent f-ELISA experiments utilizing nanobodies as the sensing probes.

4.3.5 Performance of nanobody based f-ELISA

In this study, nanobodies targeting human microsomal epoxide hydrolase (Nb-mEH), an enzyme found in plasma that has been unveiled to have a significant association with the metastasis of Kaposi's sarcoma to the liver, were utilized in this case[42]. These nanobodies possess the specific capture ability to the human microsomal epoxide hydrolase (mEH) and were prepared according to the methods described previously[38] as sensing probes and immobilized on the CC@MF membranes. Subsequently, anti-human mEH monoclonal antibodies (Ab-mEH) were applied as detection antibodies once the mEH was specifically captured on the membranes. Following this, anti-mouse antibodies conjugated with horseradish peroxidase (Ab-MIgG-HRP) were introduced as secondary antibodies to interact with Ab-mEH. This setup generated colorimetric signals through the reaction between HRP and TMB substrate, as illustrated in Figure 4.3d. To assess the sensitivity of the nanobody-based f-ELISA in detecting targets, an assay using varied mEH concentrations (0 to 10 mg/L) was performed, and the visually discernible blue color signals corresponding to varied concentrations of the mEH are shown in Figure 4.3e. The color intensities were analyzed using the Photoshop software, and from this analysis, a linear equation for the colorimetric assay was fitted as $y=47.67x + 25.41$ ($R^2=0.97$) within the range of 0.02 mg/L to 1 mg/L. The results of the assay demonstrate that the detection of the mEH by the naked eye was feasible at a

concentration as low as 0.5 mg/L, with the limit of detection (LOD) determined to be 0.33 mg/L, aided by a smartphone camera and subsequent software analysis. The selectivity test of the nanobody-based f-ELISA was also conducted. Figure 4.3f revealed that only the human mEH could be visually identified, while other enzymes did not exhibit chromogenic reactions. The assay demonstrated high specificity for the human mEH, with minimal cross-reactivity to human soluble epoxide hydrolase (sEH), epoxide hydrolase 3 (EH3), epoxide hydrolase 4 (EH4), and denatured human mEH. Notably, it did not exhibit cross-reactivity with rat mEH, given the 80% similarity in gene sequences between the human mEH and rat mEH. These results highlight the strong specificity and selectivity of the nanobody-based sandwich f-ELISA for targeting human mEH.

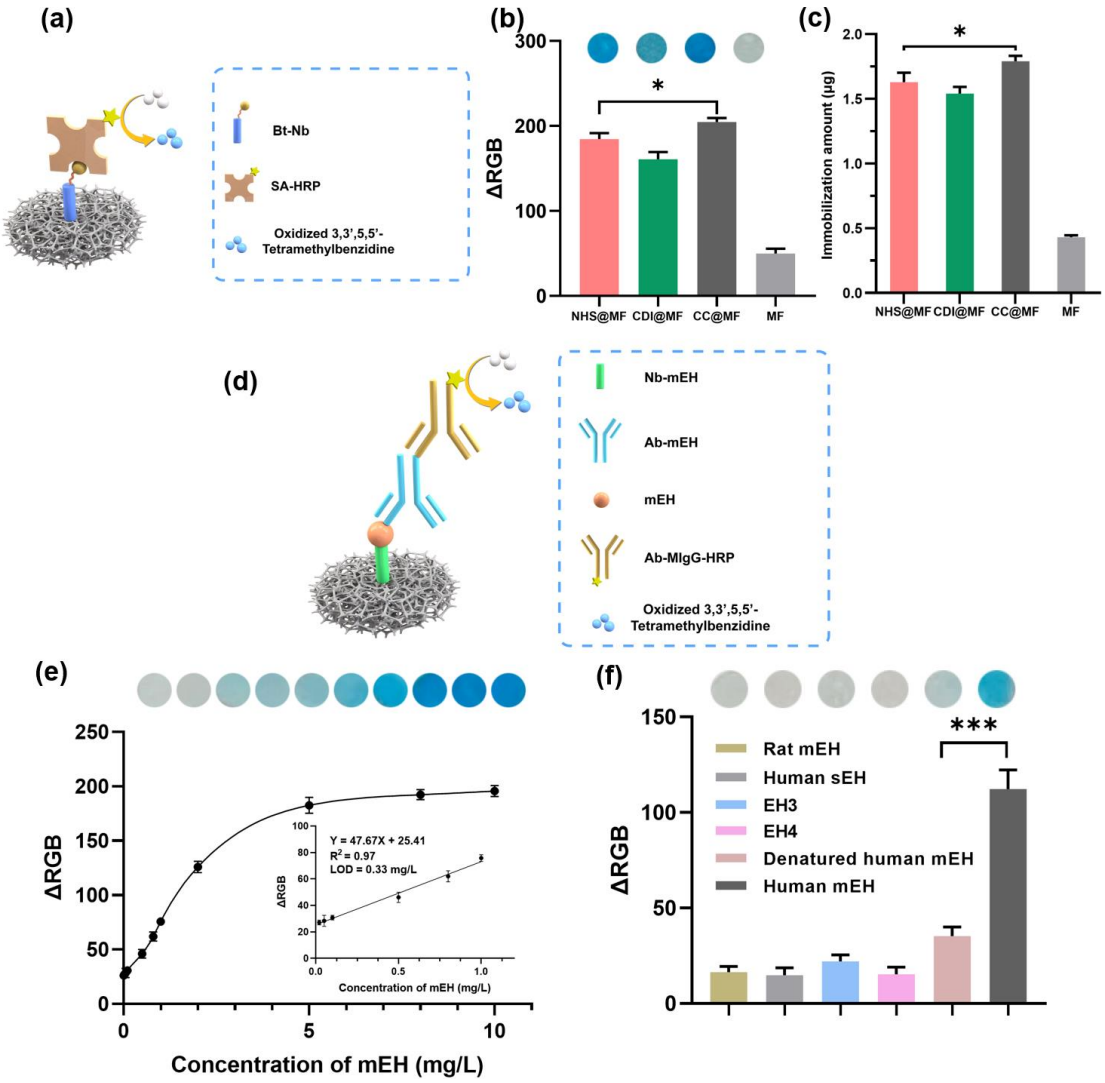

Figure 4.3. (a) Schematic illustration of biotinylated nanobody (Bt-Nb) immobilization and the use of SA-HRP as the signal development tracer. (b) Optical images and colorimetric comparison results among different MF membranes. (c) Quantification of nanobodies immobilized on different MF membranes via BCA assay kit. (d) A diagram of the nanobodies as immunoprobes in f-ELISA for human mEH. (e) Optical images and the calibration curve of f-ELISA by using Nb-mEH as the capture ligand. (f) Selectivity of f-ELISA toward human mEH detection in comparison with rat mEH, human sEH, EH3, EH4, and denatured human mEH. The concentration of each epoxide hydrolase used in the selectivity assay is 1 mg/L. The data are presented as the mean ±

standard deviation (SD) from three independent experiments. Statistical significance was determined using a two-tailed Student's t-test.*P < 0.05, ***P < 0.001. *LOD = limit of detection.

4.3.6 Peptide immobilization

The same modified MF membranes were initially immersed in a solution containing biotinylated peptides (Bt-L10-2). Afterward, streptavidin-horseradish peroxidase (SA-Alexa 647) was used as an indicator to qualitatively determine the amount of peptides immobilized on each membrane, with higher fluorescent intensity indicating a higher quantity of immobilized peptides (Figure 4.4a). Different from antibodies or nanobodies, the CC@MF membranes demonstrated the lowest fluorescent signals under identical experimental conditions, while NHS@MF showed the highest intensity among these membranes, a difference of each membrane that was visually discernible in the optical images captured under the Bio-Rad imaging system, as presented in Figure 4.4b. To accurately quantify the immobilized peptides, a Pierce fluorescent quantitative peptide assay was conducted on each membrane, which was incubated with a 0.1% peptide solution for 30 minutes at room temperature. The amount of the peptides immobilized on each membrane was determined using the calibration curve provided in Figure. S1c. The NHS@MF membrane showed the highest amount of the peptide immobilization (Figure 4.4c), consistent with the results of the qualitative analysis.

In comparison, distinct binding behaviors were observed for small peptides (10 AAs, ~1800 Da) and larger proteins like antibodies (~150 kDa) and nanobodies (~15 kDa)

on surfaces of MFs in varied hydrophilicities. This phenomenon can be attributed to the nature of these biomolecules and their interactions with the surface of the modified MF membranes. Hydrophilic surfaces, due to their polar or charged groups, are more conducive to immobilizing small peptides, which typically have fewer hydrophobic regions. Conversely, the complex structures of larger proteins, possessing multiple hydrophobic regions, tend to bind more efficiently with hydrophobic surfaces due to hydrophobic interactions, increasing the probability of contact between large biomolecules with the reactive sites on the surfaces. This distinction in binding efficiency is crucial, especially considering the structural and size-related differences between small peptides and large proteins, influencing their interactions with different surface chemistries. Besides, the morphology of NHS@MF framework structure was unchanged as well after the process of peptide immobilization (Figure S4.3c). Therefore, based on the results, the NHS@MF was employed as the matrix to immobilize peptides as the target recognizing reagents for the subsequent f-ELISA experiments.

4.3.7 Performance of peptide based f-ELISA

In this study, L10-2 peptides with a nanomolar binding affinity toward the SARS-CoV-2 spike protein (S-protein)[33], were used as a capture reagent immobilized on NHS@MF membranes. Here, anti-His antibodies-HRP conjugates (Ab-His-HRP) were utilized as the detection antibody to quantify the captured His-tagged spike protein active trimer (S-protein-His) through colorimetric signals generated from the HRP-TMB substrate reaction, as shown in Figure 4.4d. When assessing the sensitivity of this peptide-based

f-ELISA biosensor, we observed unexpectedly low colorimetric signals, as indicated in Figure 4.4f. Such a result could be caused by potential steric hindrance of the solid material surfaces, as the L10-2 tightly linked to the surfaces and its refrained conformation limiting the ability to bind to the spike protein. To address this issue, we added a different number of AEEA linkers at the N-terminus as the spacers to push the binding peptides away from the NHS@MF surface, minimizing the interference brought by the close distance between the material surface and the peptide. The resulting L10-2 analogs (Figure 4.4e, Figure S4.5-S4.8), named L10-2a-c by the increasing length of spacers, were immobilized on the NHS@MF membranes through the same chemistry. Compared to the original version of L10-2, stronger signal intensities were observed at both 5 and 50 mg/L concentrations of S-protein His with these L10-2 analogs. More importantly, the signal intensity was also affected by the spacer length, as longer AEEA spacers resulted in stronger detection signals for samples with the same concentrations (Figure 4.4f). Besides, the trend in signal enhancement was also visually discernable in the optical images of each membrane, as illustrated in Figure 4.4f. This correlation between the increased linker length and signal strength highlights the impact of the spacer on the sensitivity of f-ELISA biosensors and the solid surface interference to the bioactivity and bioconjugation of the immobilized peptides. Such improvement has little to do with the differences in immobilization capacity, as all peptide analogs showed similar immobilization amounts (Figure S4.9). The key factor enhancing signal strength is the extended spatial separation provided by the longer linkers, which effectively mitigates steric hindrance. Therefore, L10-2c was

used as the target recognizing ligand in the following experiments.

To assess the sensitivity of the peptide-based f-ELISA in detecting targets, an assay using varied S-protein-His concentrations (0 to 50 mg/L) was performed, and the visually discernible blue color signals corresponding to varied concentrations of the S-protein-His are shown in Figure 4.4g. The color intensities were analyzed using Photoshop software. From this analysis, a linear equation for the colorimetric assay was fitted as $y=52.72x + 26.10$ ($R^2=0.95$) within the range of 0 mg/L to 1 mg/L. The results of the assay demonstrate that the detection of S-protein-HRP by the naked eye was feasible at a concentration as low as 0.5 mg/L, with the limit of detection (LOD) determined to be 0.38 mg/L, aided by a smartphone camera and subsequent software analysis.

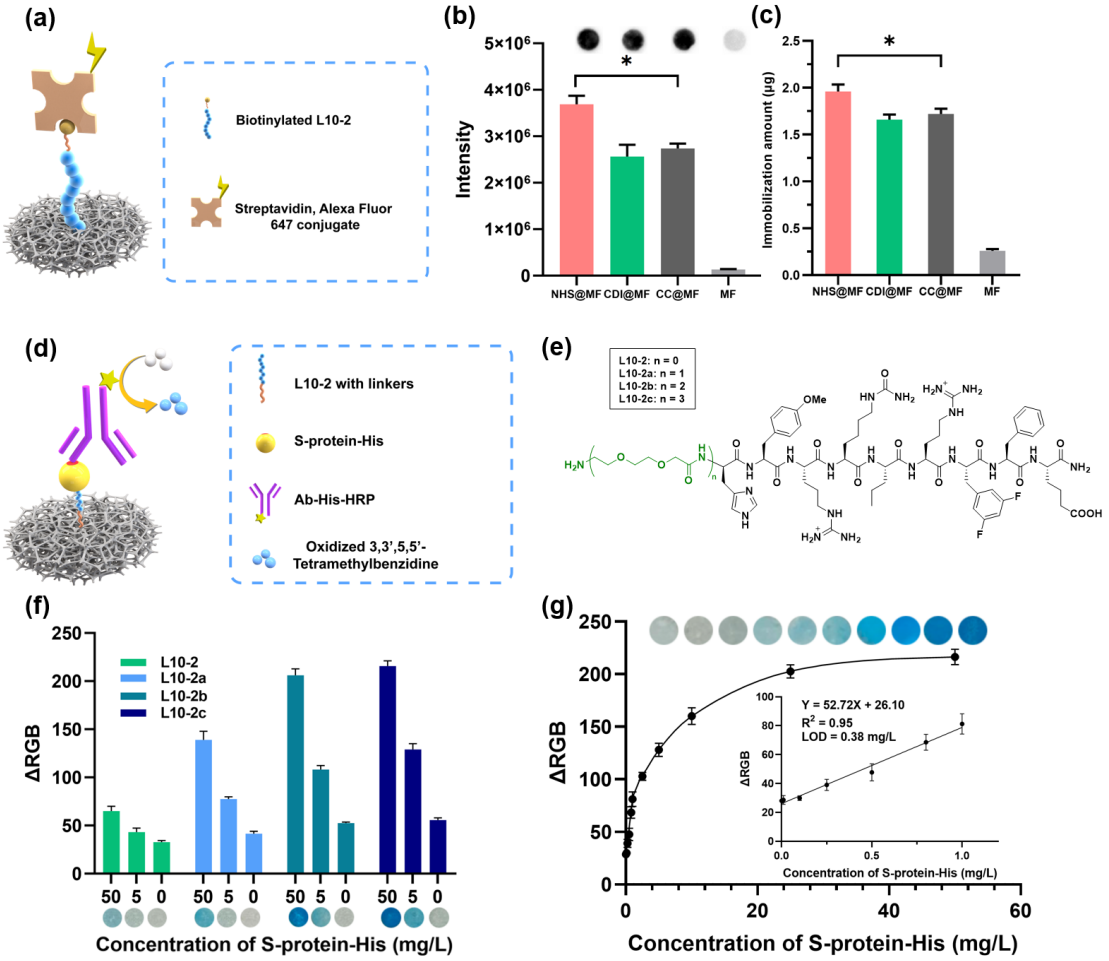

Figure 4.4. (a) Schematic illustration of biotinylated L10-2 peptide (Bt-L10-2) immobilization and the use of streptavidin with Alexa 647 conjugation as the signal development tracer. (b) Optical images captured from Bio-Rad imaging system and fluorescence results among different MF membranes. (c) Quantification of peptides immobilized on different MF membranes via pierce quantitative fluorometric peptide assay. (d) A diagram of the peptides as immunoprobes in f-ELISA for SARS-CoV-2 spike protein with His tag (S-protein-His). (e) Schematic illustration of L10-2 and peptides with 1-3 AEEA linkers. One AEEA linker was added to the N-terminus of L10-2a, two with L10-2b, and three with L10-2c. (f) Optical images and the colorimetric results of f-ELISA by using peptides with different numbers of linkers as illustrated

above. (g) Optical images and the calibration curve of f-ELISA by using L10-2c peptide as the capture antibody. The data are presented as the mean ± standard deviation (SD) from three independent experiments. Statistical significance was determined using a two-tailed Student's t-test.*P < 0.05. *LOD = limit of detection.

4.3.8 Storage stability evaluation for f-ELISA

All biosensors face a challenge of stability for prolonged storage under conditions of low or room temperature, which is critical for broad applications of the biosensor products. The stability difference of sensing probes of antibodies, nanobodies, and peptides on the f-ELISA biosensors could provide a clue for a potential solution, which was the main focus of the study. To compare the long-term storage stabilities of the f-ELISA biosensors, Ab@CC@MF, Nb@CC@MF, and Pt@NHS@MF membranes were prepared according to the immobilization protocol described in the experimental section. The membranes were then freeze-dried and stored under two different conditions: 4°C and room temperature, for a duration of 30 days. At specific time points, samples were collected and employed in the f-ELISA assay to identify HIgG (5 mg/L), mEH (5 mg/L), or S-protein-His (5 mg/L), respectively, following the same protocols. As shown in Figure 4.5a, under storage condition at 4°C, the activity of the Ab@CC@MF declined the fastest among all three biosensing platforms, dropping to 80% after one week, while the immobilized peptide on the Pt@NHS@MF lost approximately 20% of its activity after about 15 days of storage. The Nb@CC@MF showed the best storage stability under 4°C and maintained over 90% of the

colorimetric signal when detecting 5 mg/L mEH after 30 days. At the same time, Ab@CC@MF and Pt@NHS@MF still retain good stability with close to 70% of the original colorimetric signal in detecting 5 mg/L HIgG and S-protein-His, respectively. When these biosensing platforms were stored at room temperature, as depicted in Figure 4.5b, the colorimetric signal intensities decreased more significantly compared to those stored at 4°C. The Ab@CC@MF only retained 50% of the activity after 5 days and can be considered inactive after 20 days. Pt@NHS@MF showed better stability, but the activity still dropped below 50% of the original colorimetric signal after 10 days. In contrast, Nb@CC@MF displayed the best stability among three f-ELISA biosensors with the colorimetric signal maintained above 70% of the original intensity after stored for 30 days under room temperature, indicating that the immobilized nanobody on the foam was more stable than other two probes. The results indicate that the lower temperature storage condition could prolong the stability of the f-ELISA biosensors, and Nb@CC@MF is the best one for long-term storage under both 4°C and room temperature.

The superior stability of nanobodies compared to antibodies and peptides on the surfaces of the foams can be attributed to their unique structural properties. Nanobodies are single-domain antibody fragments that are lack of the light chain and the first constant domain of the heavy chain found in conventional antibodies. This compact structure makes nanobodies more resistant to denaturation and aggregation, which are common causes of protein instability[43]. In contrast, the larger size and more complex structure of antibodies make them more susceptible to degradation, especially at room

temperature[44]. Peptides, although smaller than nanobodies, exhibit better stability than antibodies due to their simpler structure. However, peptides are still less stable than nanobodies because they lack a well-defined tertiary structure, which makes them more prone to oxidation and other chemical modifications that can lead to a loss of activity[45]. Peptides are short chains of amino acids that do not possess complex folding and have less stabilizing disulfide bonds. This lack of structural complexity and stability makes peptides more susceptible to degradation than nanobodies, particularly under harsh conditions such as elevated temperatures or prolonged storage. Therefore, by successfully incorporating nanobodies into the biosensing platform, we achieved enhanced storage stability compared to platforms utilizing antibodies or peptides. This improved stability of the nanobody-based biosensing platform is crucial for maintaining the efficacy and reliability of the f-ELISA system, making it a promising tool for various diagnostic and research applications.

Besides, compared to p-ELISA, in which the sensing probes were immobilized on the matrix through physical adsorption and the activity of the fixed antibody without adding any stabilizer dropped to 50% after just one day of storage at 4°C and dropped to lower than 20% after two days under room temperature [46], the f-ELISA biosensors demonstrated significantly improved storage stability due to the covalent bond between the matrix and probes. This enhanced stability can be attributed to the several advantages offered by covalent bonding over physical adsorption for immobilized antibodies, such as stronger attachment, specific orientation, reduced denaturation, and resistance to environmental factors. In conclusion, the superior storage stability of f-

ELISA biosensors, achieved through covalent immobilization of sensing probes, makes them a more reliable and practical choice for point-of-use applications compared to traditional p-ELISA systems.

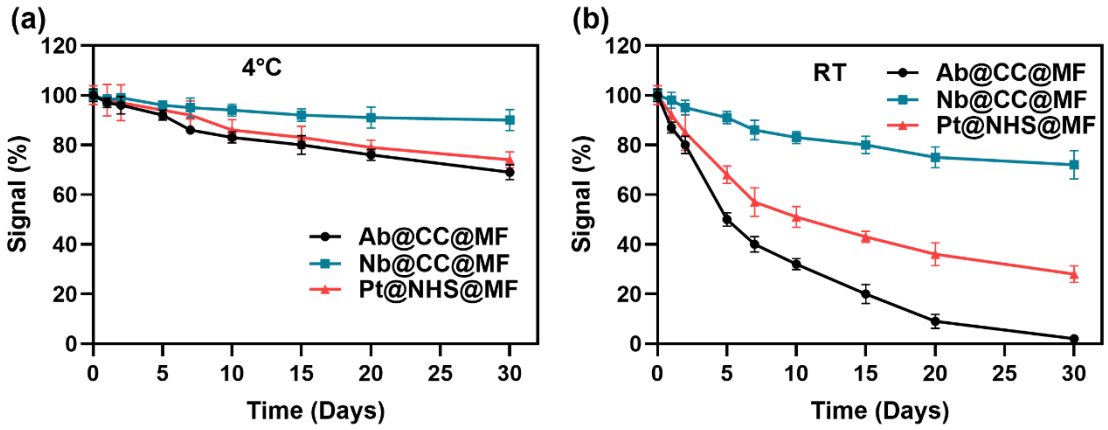

Figure 4.5. Comparison of the colorimetric signal (%) of Ab@CC@MF, Nb@CC@MF, and Pt@NHS@MF over a 30-day storage period at different storage temperatures: (a) 4°C and (b) 25°C (room temperature, RT). The membranes were used to detect HIgG (5 mg/L), mEH (5 mg/L), and S-protein-His (5 mg/L), respectively, using the f-ELISA assay at specific time points during the storage period. The colorimetric signal (%) represents the percentage of the initial signal intensity retained at each time point. The data are presented as the mean ± standard deviation (SD) from three independent experiments.

4.4 Conclusion

The macroporous framework melamine foam could be chemically modified with three different reagents, and the resulted foam materials demonstrated good reactivity to immobilize antibodies, nanobodies and peptides to produce foam-based Enzyme-

Linked Immunosorbent Assay (f-ELISA) biosensors. Among them, the CC@MF could work better with antibodies and nanobodies, while NHS@MF revealed better reactivity with peptides. Solid surfaces could inhibit interactions and activities of peptides as sensing probes on the foams. The f-ELISA biosensors made from using antibodies, nanobodies, and peptides, with sizes ranging from 1800 to 150,000 Daltons, all demonstrated excellent selectivity and sensitivity to the corresponding targets. Additionally, the f-ELISA biosensor (Nb@CC@MF) made of using nanobodies as sensing probes, demonstrated best storage stability versus the other two biosensors using antibodies and peptides as probes. The results offer valuable insights for the application of f-ELISA biosensors as point-of-use devices. Overall, by exploring different functionalization methods and sensing probes on this innovative biosensing platform, various types of f-ELISA system can be developed, establishing a library that enables a wide range of applications.

4.5 Reference

1. Clark, M. F., Lister, R. M., & Bar-Joseph, M. (1986). ELISA techniques. In *Methods in enzymology* (Vol. 118, pp. 742-766). Academic Press.

2. Tighe, P. J., Ryder, R. R., Todd, I., & Fairclough, L. C. (2015). ELISA in the multiplex era: potentials and pitfalls. *PROTEOMICS–Clinical Applications*, *9*(3-4), 406-422.

3. Shah, K., & Maghsoudlou, P. (2016). Enzyme-linked immunosorbent assay (ELISA): the basics. *British journal of hospital medicine*, *77*(7), C98-C101.

4. Hosseini, S., Vázquez-Villegas, P., Rito-Palomares, M., & Martinez-Chapa, S.

O. (2018). Advantages, disadvantages and modifications of conventional ELISA. *Enzyme-Linked Immunosorbent Assay (ELISA) from A to Z*, 67-115.

5. Yolken, R. H. (1982). Enzyme immunoassays for the detection of infectious antigens in body fluids: current limitations and future prospects. *Reviews of infectious diseases*, *4*(1), 35-68.

6. Cheng, Chao-Min, Andres W. Martinez, Jinlong Gong, Charles R. Mace, Scott T. Phillips, Emanuel Carrilho, Katherine A. Mirica, and George M. Whitesides. 2010. "Paper-Based ELISA." *Angewandte Chemie 122* (28) (May 28): 4881–4884. doi:10.1002/ange.201001005.

7. Hu, J., Wang, S., Wang, L., Li, F., Pingguan-Murphy, B., Lu, T. J., & Xu, F. (2014). Advances in paper-based point-of-care diagnostics. *Biosensors and Bioelectronics*, *54*, 585-597.

8. Mabey, D., Peeling, R. W., Ustianowski, A., & Perkins, M. D. (2004). Diagnostics for the developing world. *Nature Reviews Microbiology*, *2*(3), 231-240.

9. Zhao, C., Si, Y., Pan, B., Taha, A. Y., Pan, T., & Sun, G. (2020). Design and fabrication of a highly sensitive and naked-eye distinguishable colorimetric biosensor for chloramphenicol detection by using ELISA on nanofibrous membranes. *Talanta*, *217*, 121054.

10. Zhao, C., Si, Y., Zhu, S., Bradley, K., Taha, A. Y., Pan, T., & Sun, G. (2021). Diffusion of protein molecules through microporous nanofibrous polyacrylonitrile membranes. *ACS applied polymer materials*, *3*(3), 1618-1627.

11. Cannell, D. S., & Rondelez, F. (1980). Diffusion of polystyrenes through microporous membranes. *Macromolecules*, *13*(6), 1599-1602.

12. Davidson, M. G., & Deen, W. M. (1988). Hindered diffusion of water-soluble macromolecules in membranes. *Macromolecules*, *21*(12), 3474-3481.

13. Zhao, C., Pan, B., Wang, M., Si, Y., Taha, A. Y., Liu, G., Pan, T., & Sun, G. (2022). Improving the Sensitivity of Nanofibrous Membrane-Based ELISA for On-Site Antibiotics Detection. *ACS sensors*, *7*(5), 1458-1466.

14. Pan, B.; Zhao, C.; Norwood, M.; Wang, M.; Liu, G.; Sun, G. Highly Sensitive Naked Eye Detectable Colorimetric Biosensors Made from Macroporous Framework Melamine Foams for Onsite and Simultaneous Detection of Multiple Environmental Hazards in Flowing Through Sensing Systems. *Advanced Sensor Research* 2023, *3*(1), 2300080.

15. Pan, B., El-Moghazy, A. Y., Norwood, M., Nitin Nitin, & Sun, G. (2024). Rapid and Ultrasensitive Colorimetric Biosensors for Onsite Detection of *Escherichia coli* O157:H7 in Fluids. *ACS Sensors*, *9*(2), 912–922.

16. Butler, J. E., Feldbush, T. L., McGivern, P. L., & Stewart, N. (1978). The enzyme-linked immunosorbent assay (ELISA): a measure of antibody concentration or affinity? *Immunochemistry*, *15*(2), 131-136.

17. Reen, D. J. (1994). Enzyme-linked immunosorbent assay (ELISA). *Basic Protein and Peptide Protocols*, 461-466.

18. Tiller, K. E., & Tessier, P. M. (2015). Advances in antibody design. *Annual review of biomedical engineering*, *17*, 191-216.

19. Davies, D. R., Padlan, E. A., & Sheriff, S. (1990). Antibody-antigen complexes. *Annual review of biochemistry*, *59*(1), 439-473.

20. Boorsma, D. M., & Kalsbeek, G. L. (1975). A comparative study of horseradish peroxidase conjugates prepared with a one-step and a two-step method. *Journal of Histochemistry & Cytochemistry*, *23*(3), 200-207.

21. Ta, H. T., Peter, K., & Hagemeyer, C. E. (2012). Enzymatic antibody tagging: toward a universal biocompatible targeting tool. *Trends in cardiovascular*

medicine, *22*(4), 105-111.

22. De Meyer, T., Muyldermans, S., & Depicker, A. (2014). Nanobody-based products as research and diagnostic tools. *Trends in biotechnology*, *32*(5), 263-270.

23. Muyldermans, S., Baral, T. N., Retamozzo, V. C., De Baetselier, P., De Genst, E., Kinne, J., Leonhardt, H., Magez, S., Nguyen, V. K., Revets, H., Rothbauer, U., Stijlemans, B., Tillib, S., Wernery, U., Wyns, L., Hassanzadeh-Ghassabeh, G., & Saerens, D. (2009). Camelid immunoglobulins and nanobody technology. *Veterinary Immunology and Immunopathology, 128*(3-4), 178-183.

24. Zhao, H., Ren, J., Wu, S., Guo, H., Du, Y., Wan, B., Ji, P., Wu, Y., Zhuang, G., Zhang, A., & Zhang, G. (2022). HRP-conjugated-nanobody-based cELISA for rapid and sensitive clinical detection of ASFV antibodies. *Applied Microbiology and Biotechnology*, *106*(11), 4269-4285.

25. Li, D., Cui, Y., Morisseau, C., Wagner, K. M., Cho, Y. S., & Hammock, B. D. (2020). Development of a Highly Sensitive Enzyme-Linked Immunosorbent Assay for Mouse Soluble Epoxide Hydrolase Detection by Combining a Polyclonal Capture Antibody with a Nanobody Tracer. *Analytical chemistry*, *92*(17), 11654-11663.

26. Liu, M.; Li, L.; Jin, D.; Liu, Y. Nanobody-A versatile tool for cancer diagnosis and therapeutics. Wiley Interdiscip. Rev. Nanomed. Nanobiotechnol. 2020, 13, e1697.

27. Zhu, M., Gong, X., Hu, Y., Ou, W., & Wan, Y. (2014). Streptavidin-biotin-based directional double Nanobody sandwich ELISA for clinical rapid and sensitive detection of influenza H5N1. *Journal of translational medicine*, *12*(1), 1-10.

28. Salvador, J. P., Vilaplana, L., & Marco, M. P. (2019). Nanobody: outstanding features for diagnostic and therapeutic applications. *Analytical and bioanalytical chemistry*, *411*, 1703-1713.

29. Liu, X., Tang, Z., Duan, Z., He, Z., Shu, M., Wang, X., J. Gee, Hammock, B. D.,

& Xu, Y. (2017). Nanobody-based enzyme immunoassay for ochratoxin A in cereal with high resistance to matrix interference. *Talanta*, *164*, 154-158.

30. He, Q., McCoy, M. R., Yang, H., Lin, M., Cui, X., Zhao, S., Morisseau, C., Li, D., & Hammock, B. D. (2023). Mix-and-Read Nanobody-Based Sandwich Homogeneous Split-Luciferase Assay for the Rapid Detection of Human Soluble Epoxide Hydrolase. *Analytical Chemistry*, *95*(14), 6038-6045.

31. Velumani, S., Ho, H. T., He, F., Musthaq, S., Prabakaran, M., & Kwang, J. (2011). A novel peptide ELISA for universal detection of antibodies to human H5N1 influenza viruses. *PloS one*, *6*(6), e20737.

32. Blasco, H., Lalmanach, G., Godat, E., Maurel, M. C., Canepa, S., Belghazi, M., Paintaud, G., Degenne, D., Chatelut, E., Cartron, G., & Le Guellec, C. (2007). Evaluation of a peptide ELISA for the detection of rituximab in serum. *Journal of Immunological Methods, 325*(1-2), 127-139.

33. Yu, X., Pan, B., Zhao, C., Shorty, D., Solano, L. N., Sun, G., Liu, R., & Lam, K. S. (2023). Discovery of Peptidic Ligands against the SARS-CoV-2 Spike Protein and Their Use in the Development of a Highly Sensitive Personal Use Colorimetric COVID-19 Biosensor. *ACS sensors*. *8* (6), 2159-2168

34. Bidart, J. M., Troalen, F., Ghillani, P., Rouas, N., Razafindratsita, A., Bohuon, C., & Bellet, D. (1990). Peptide immunogen mimicry of a protein-specific structural epitope on human choriogonadotropin. *Science*, *248*(4956), 736-739.

35. Bodanszky, M. (2012). *Principles of peptide synthesis* (Vol. 16). Springer Science & Business Media.

36. Lam, K. S., Salmon, S. E., Hersh, E. M., Hruby, V. J., Kazmierski, W. M., & Knapp, R. J. (1991). A new type of synthetic peptide library for identifying ligand-binding activity. *Nature*, *354*(6348), 82-84.

37. Yu, X., Ruan, M., Wang, Y., Nguyen, A., Xiao, W., Ajena, Y., Solano, L. N., Liu, R., & Lam, K. S. (2022). Site-Specific Albumin-Selective Ligation to Human Serum Albumin under Physiological Conditions. *Bioconjugate Chemistry*, *33*(12), 2332-2340.

38. He, Q., McCoy, M. R., Qi, M., Morisseau, C., Yang, H., Xu, C., Shey, R., Goodman, M. C., Zhao, S., & Hammock, B. D. (2023). The Generation of a Nanobody-Based ELISA for Human Microsomal Epoxide Hydrolase. *International Journal of Molecular Sciences, 24*(19), 14698.

39. Behrendt, R., White, P., & Offer, J. (2016). Advances in Fmoc solid-phase peptide synthesis. *Journal of Peptide Science*, *22*(1), 4-27.

40. Creane, S., Joyce, M., MacLoughlin, R., Weldon, S., Dalton, J. P., & Taggart, C. C. (2023). In vitro evaluation of the potential use of snake-derived peptides in the treatment of respiratory infections using inhalation therapy: A proof of concept study. *European Journal of Pharmaceutical Sciences*, *183*, 106398.

41. Zhu, X., Xiong, S., Zhang, J., Zhang, X., Tong, X., & Kong, S. (2018). Improving paper-based ELISA performance through covalent immobilization of antibodies. *Sensors and Actuators B: Chemical*, *255*, 598-604.

42. Hammock, B. D., Loury, D. N., Moody, D. E., Ruebner, B., Baselt, R., Milam, K. M., Volberding, P., Ketterman, A., & Talcott, R. (1984). A methodology for the analysis of the preneoplastic antigen. *Carcinogenesis*, *5*(11), 1467–1473.

43. Joyce, A. M., Kelly, A. L., & O'Mahony, J. A. (2018). Controlling denaturation and aggregation of whey proteins during thermal processing by modifying temperature and calcium concentration. *International Journal of Dairy Technology*, *71*(2), 446-453.

44. Kunz, P., Zinner, K., Mücke, N., Bartoschik, T., Muyldermans, S., & Hoheisel,

J. D. (2018). The structural basis of nanobody unfolding reversibility and thermoresistance. *Scientific reports*, *8*(1), 7934.

45. Bell, L. N. (1997). Peptide stability in solids and solutions. *Biotechnology progress*, *13*(4), 342-346.

46. Chen, C. A., Yeh, W. S., Tsai, T. T., & Chen, C. F. (2019). Three-dimensional origami paper-based device for portable immunoassay applications. *Lab on a Chip*, *19*(4), 598-607.

4.6 Supporting Information

4.6.1 Calibration curves for antibodies, nanobodies, and peptides

(a)

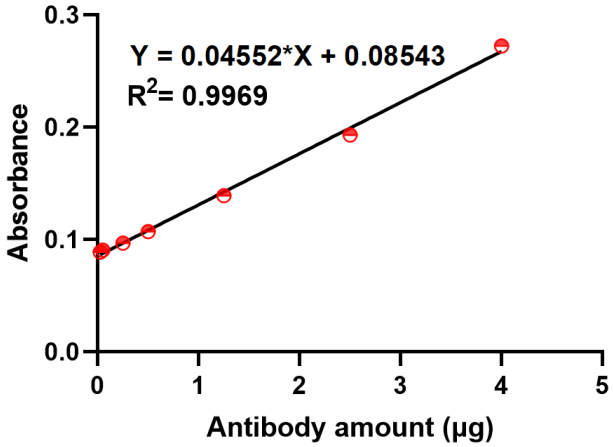

(b)

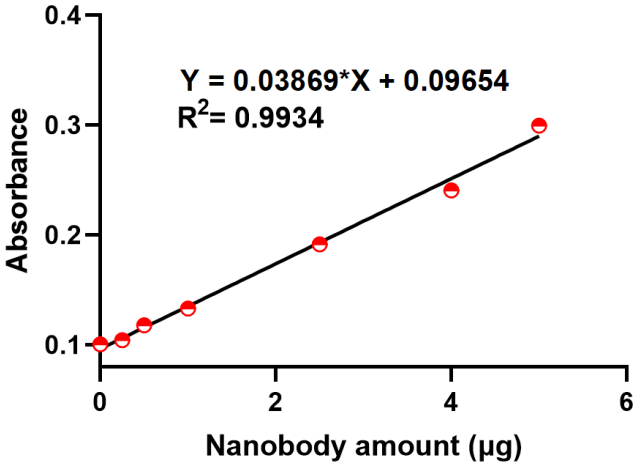

(c)

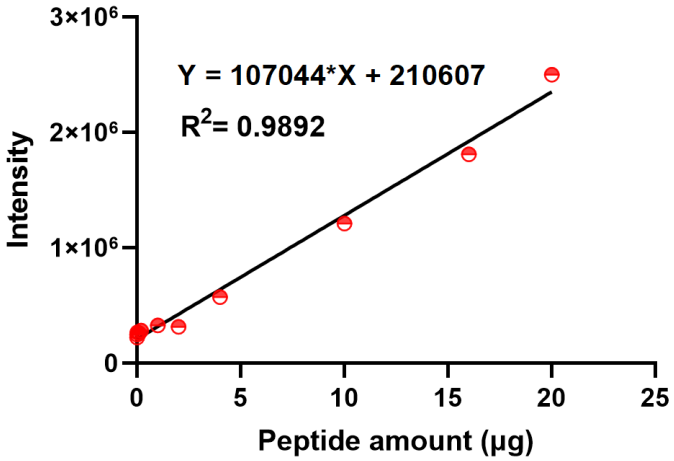

Figure S4.1. Calibration curves for (a) antibody, (b) nanobody, and (c) peptide.

4.6.2 Chemical structure of melamine foam

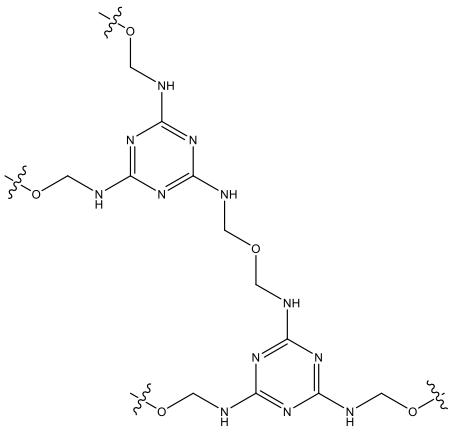

Figure S4.2. Chemical structure of the melamine foam.

4.6.3 SEM images of MF membranes with the immobilized ligands

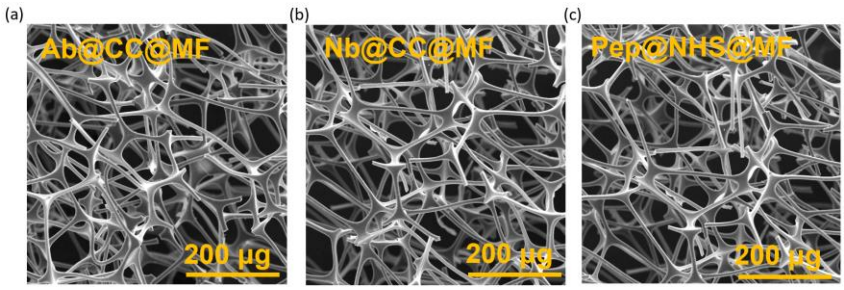

Figure S4.3. SEM images of (a) antibodies-immobilized CC@MF (Ab@CC@MF), (b) nanobodies-immobilized CC@MF (Nb@CC@MF), and (c) peptides-immobilized NHS@MF (Pt@NHS@MF).

4.6.4 Specificity of the assay

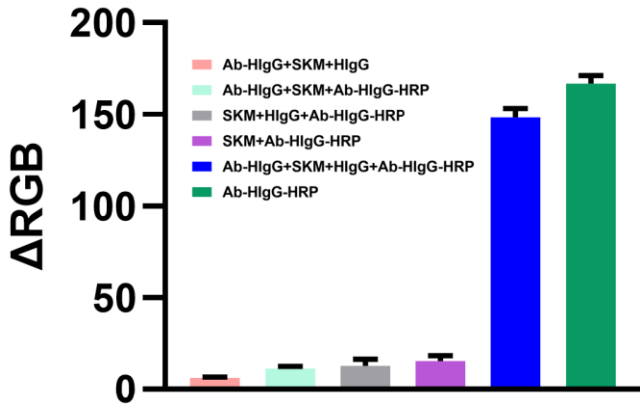

Figure S4.4. Specificity of the assay. Images of the NHS@MF membranes with different treatments after adding TMB substrate: 100 μL Ab-HIgG (5 mg/L), 200 μL skimmed milk (SKM) (3%), 200 μL HIgG (1 mg/L), and 100 μL Ab-HIgG-HRP (1 mg/L) were used accordingly. The bar diagram for the ΔRGB was observed from the images. Data are presented as mean ± SD, with n = 3 independent experiments.

4.6.5 Chemical structure and mass spectrometry of peptides

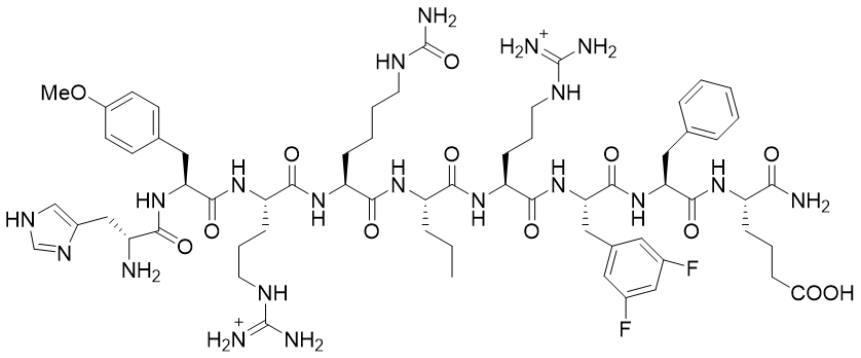

L10-2

Exact Mass: 1388.73

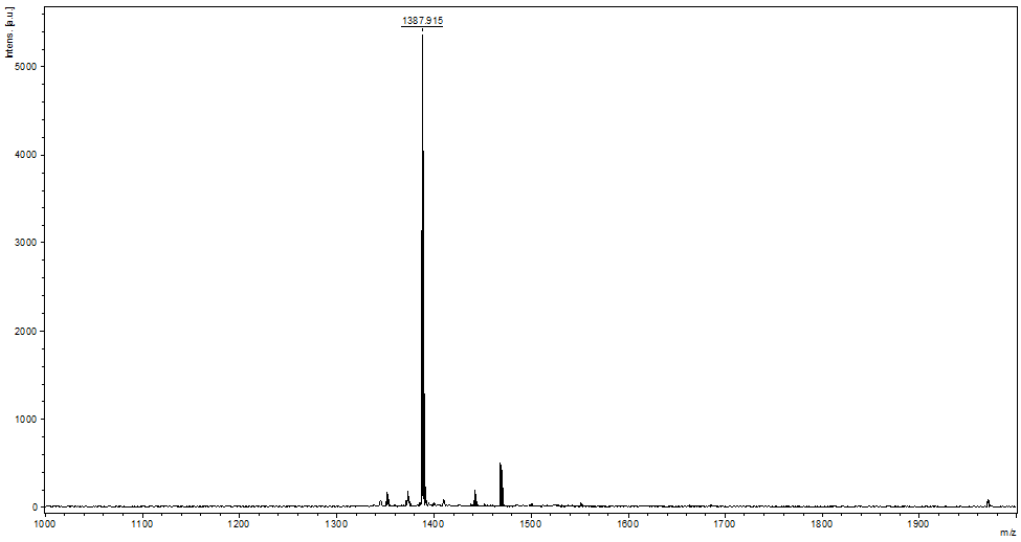

Figure S4.5. Chemical structure and mass spectrometry of L10-2.

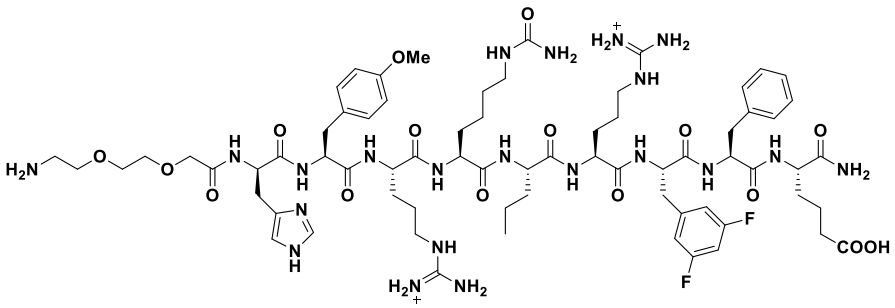

L10-2a

Exact Mass: 1533.17

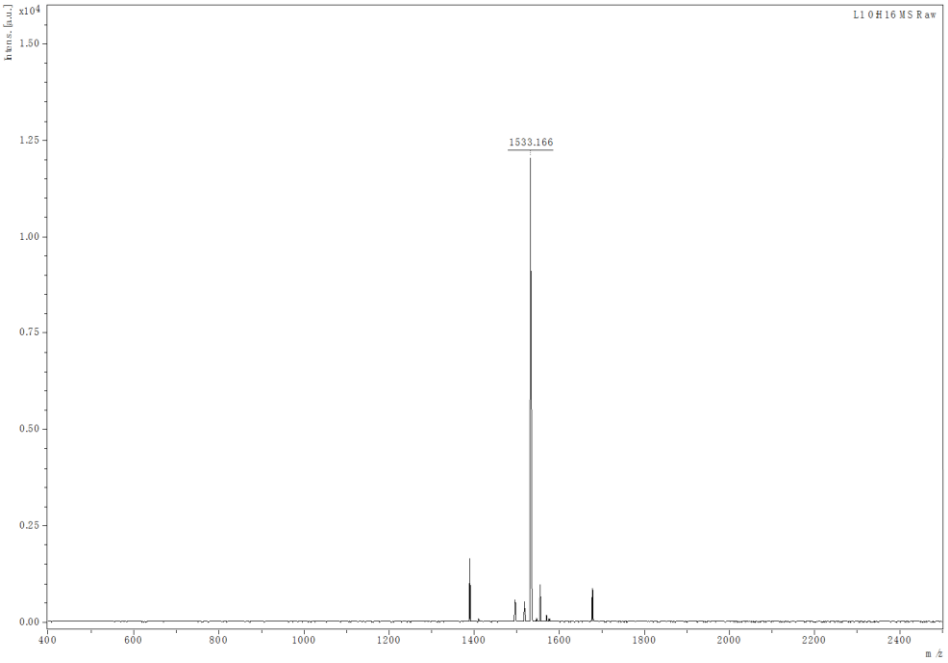

Figure S4.6. Chemical structure and mass spectrometry of L10-2a.

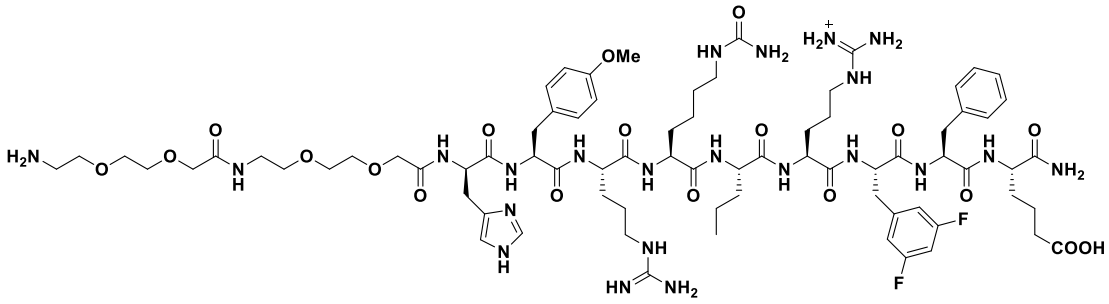

L10-2b

Exact Mass: 1678.30

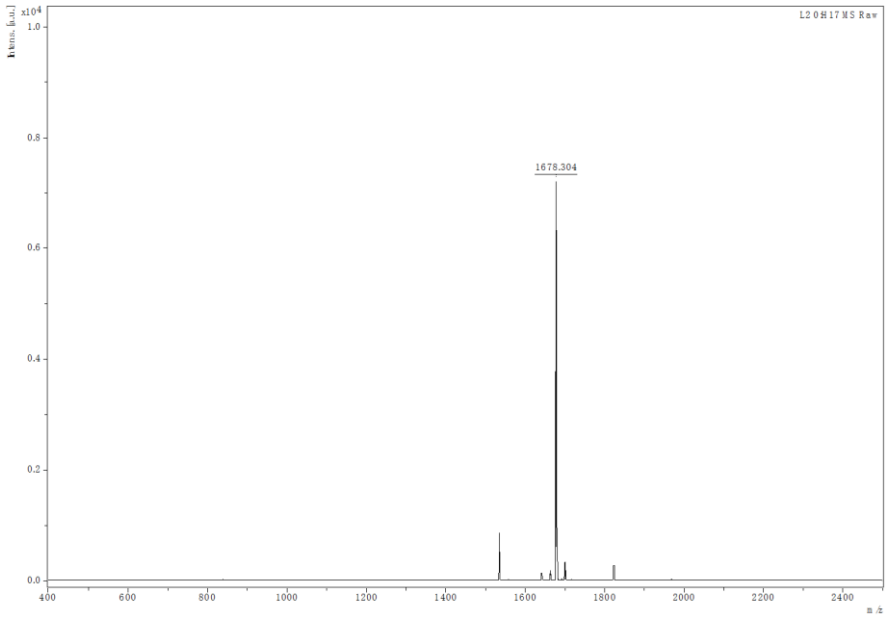

Figure S4.7. Chemical structure and mass spectrometry of L10-2b.

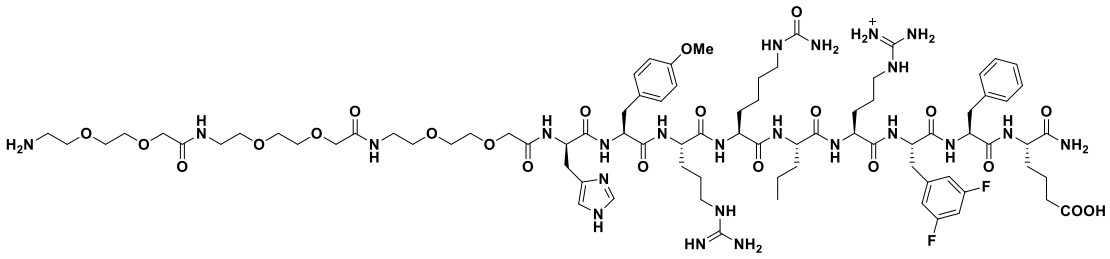

L10-2c

Exact Mass: 1823.45

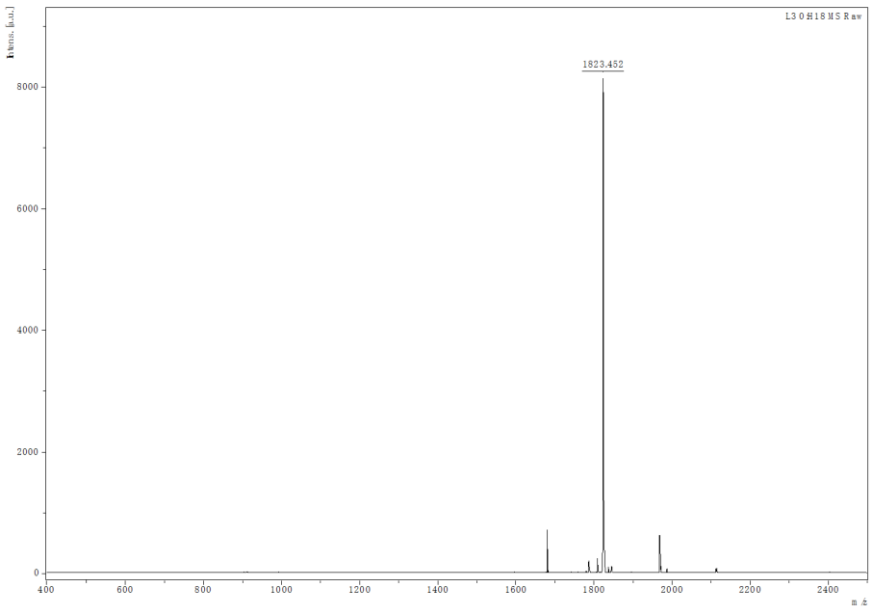

Figure S4.8. Chemical structure and mass spectrometry of L10-2c.

4.6.6 Immobilization number of varied peptides on modified MFs

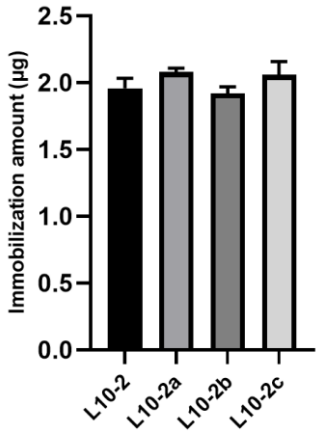

Figure S4.9. Quantification of varied peptides immobilized on NHS@MF membranes via pierce quantitative fluorometric peptide assay.

Chapter 5. Executive Conclusion

The development of the foam-based ELISA (f-ELISA) system, utilizing chemically modified melamine foam (MF) as a biosensing platform, has been the primary focus of this dissertation. The unique 3D macroporous reticulated structure of the MF allows for rapid mass transfer of large biomolecules and even bacteria cells through the framework in all directions. This structural feature ensures excellent accessibility of the entire active binding sites on the framework to the target molecules, resulting in significantly increased sensitivity and volume-responsive detection capabilities.

In Chapter 2, unique rapid, sensitive, additive, and volume responsive colorimetric sensor materials were fabricated from using chemically modified framework melamine foam (MF), which can be applied in competitive, direct, and sandwich ELISA biosensors. The MF sensor materials demonstrated promising detection sensitivity to a SARS-CoV-2 spike protein with histidine tag (SP-RBD-His), a transmembrane protein of the SARS-CoV-2 virus, and chloramphenicol (CAP), often used as an antibiotic. Naked eye recognizable SP-RBD-His reached 1 mg/L level with a limit of detection (LOD) at 0.52 mg/L when supplemented by a smartphone for the direct ELISA sensor. In the case of the sandwich ELISA sensor, it's capable of detecting SP-RBD-His at a concentration of 0.1 mg/L by the naked eye and can reduce the LOD to as low as 0.047 mg/L with the help of a smartphone. In addition, using a competitive ELISA, chloramphenicol (CAP) can be detected at 1 ng/mL level with the naked eye and at 0.096 ng/mL with the help of a smartphone. Moreover, due to the excellent mechanical

properties and framework structure of the MF, diffusion of the analyte through the different membrane layers is fast and homogeneous in all directions, making the MF suitable for the simultaneous detection of trace amounts of two or more targets in samples with large volumes in one integrated system. The successful fabrication of such sensor materials is expected to improve the sensitivity and broaden the applications of ELISA sensors for onsite and personal uses. The foam-based ELISA (f-ELISA) platform was first introduced in this chapter.

Chapter 3 described the application of the f-ELISA system in the development of a novel biosensor for the detection of *E. coli* O157:H7. Building upon the advantages of f-ELISA using melamine foam (MF) as a medium, which were demonstrated in Chapter 2, this chapter explored the suitability of f-ELISA for detecting *E. coli* O157:H7. Given the larger size of bacterial cells compared to chemical compounds and proteins, the application of f-ELISA in this context could fully showcase the benefits of the macroporous features offered by the chemically modified MF. In contrast to conventional ELISA (c-ELISA), which is restricted by the limited surface area of a 96-well plate, and other p-ELISA methods, bacteria as antigens can move freely in every direction within this macroporous 3D matrix. This enhanced freedom of movement facilitates an amplified interaction between the immobilized antibodies and antigens, leading to substantial enrichment and heightened sensitivity in colorimetric detection. The testing process needs less than 1.5 h to complete both preparation and detection, and the results indicated that the sensors made of the modified MF materials can detect *E. coli* O157:H7 at a level of 10 CFU/mL by the naked eye with a limit of detection

(LOD) at 5 CFU/mL when supplemented by a smartphone. Following a brief enrichment period of 1 h, the sensitivity was further amplified to 2 CFU/mL, which is considered to be ultrasensitive for bacteria detection. In essence, using *E. coli* O157:H7 as a proof of concept, this work not only paves the way for improved bacterial detection in environmental and food samples but also introduces f-ELISA as a new model that could be adapted for other pathogens and contaminants.

Chapter 4 investigated the versatility and stability of chemically modified MF as a general platform for preparing f-ELISA biosensors using different sensing agents, including antibodies, nanobodies, and peptides. The study revealed that the MF could be chemically modified with three different reagents: DSC, CDI, and CC. Among them, CC@MF worked better with antibodies and nanobodies, while NHS@MF showed better reactivity with peptides. The f-ELISA biosensors made using antibodies, nanobodies, and peptides, with sizes ranging from 1800 to 150,000 Daltons, all demonstrated excellent selectivity and sensitivity to their corresponding targets. However, solid surfaces could inhibit interactions and activities of peptides as sensing probes on the foams, which could be overcome by introducing spacers between the peptides and the MF surface. Additionally, the f-ELISA biosensor (Nb@CC@MF) made using nanobodies as sensing probes demonstrated the best storage stability compared to the other two biosensors using antibodies and peptides as probes. The superior stability of nanobodies was attributed to their unique structural properties, making them more resistant to denaturation and aggregation. Incorporating varied ligands expands the f-ELISA system's adaptability and functionality, making it a

versatile and effective diagnostic tool with broader applications and improved detection processes across various fields. The successful use of nanobodies and peptides also demonstrates the biosensors' enhanced storage stability.

In conclusion, the f-ELISA platform developed in this dissertation offers a rapid, sensitive, selective, versatile, and robust biosensing solution for the detection of a wide range of targets, from small molecules to proteins and bacteria. The platform's unique structural features and adaptability to various sensing probes make it a promising tool for diverse applications in environmental monitoring, food safety, and medical diagnostics.